AN EXPERIMENTAL SET UP TO INVESTIGATE NON-INVASIVE DETECTION OF HIP PROSTHESIS LOOSENING

M. Sc. Eng. Ayman Eshra

geboren am 04.07.1967, in Demmiette/ Ägypten

2004

Referent: Prof. Dr.-Ing. E. Reithmeier
Korreferent: Prof. Dr.-Ing. C. Hartung

Vorsitz der Prüfungskommission: Prof. Dr.-Ing. H. Louis

Tag der Promotion: 15.12.2004

ACKNOWLEDGEMENTS

ABSTRACT

Total hip replacement is one of the most successful operations world wide. However, the number of reoperations and revisions increases each year. Usually, the reason for a revision is aseptic loosening of the prosthesis[1]. The market prise of the hip prostheses is in range $ 2,200 - 3,000. The surgical revision cost range of $ 20,000 – 30,000 including anesthesia, surgical procedure, and hospital stay. The costs are of increasing concern to surgeons, hospitals and insurers[2]. In USA about 541,245 of hip and knee prosthesis were implanted in 1999 [3]. Also, the trend of implantation of shoulder prosthesis is increased. In Germany about 150,000 hip and knee prosthesis are implanted per year [4].

The loosening of the hip prosthesis may be from the cement-bone interface or cement-prosthesis interface or the destruction of the cement mantel. However , the air bubbles in the cement mantel may be caused a fatigue fracture of the mantel.

Ultrasonic have been used successfully in medicine. It has a great roll in medicine. It is a non-invasive method for diagnostic. No one know its side effects. Ultrasound is an unlimited and repeatable method in comparison with the other methods such as X-ray method which has a side effect on the patient and embryo.

Non-invasive diagnostic of the hip prosthesis is a dream for patients and surgeons. The aim of this work is to introduce a novel non-invasive method for determination the loosening of the hip prosthesis. It details the development of a novel vibroacoustical (VA) diagnostic technique to monitor the internal state of the hip prosthesis in the femur through an appropriate processing of measured vibrational signal. The state of the prosthesis in-vitro will be determined. The thigh model with a secured hip prosthesis will be excited by an acoustic exciter. The resulted transfer function will be consider as the base line or the reference vector, which will be stored for the analysis. The prosthesis will be pulled out without destruction the cement mantel and returned again to its initial position (artificial loosening). Again the same measurement will be carried out for the loosed prosthesis. The dynamic characteristics of the system will be examined in frequency domain through the comparison between the base vector (secure case) and the fault vector (loose case) to indicate the effect of the loosening on the system dynamic.

The detection of loosening of the hip prosthesis based on the fundamental through-thickness resonance (1st resonance) frequency. The loosening produce a reduction of 40%-60% in the vibration energy of the 1st resonance frequency.

Nyquist plot was found to be a very important diagnostic tool for prosthesis loosening. The changes in the Nyquist plot for secure and loose cases indicates the presence of the loosening in the system.

The novel in this study, is the approximation of the real system (Thigh) by using a FIR-Filter. The measured FRF of the real system will be used to design the required FIR-Filter. This technique provides a useful information on the internal state of the prosthesis. This novel FIR-Filter technique is developed for discrimination between the vibroacoustical signals from both intact and loosed prosthesis. The FIR-Filter impulse response and coefficients at loosening wear found to be lower than that for the healthy case.

Keywords
Hip prosthesis, loosening, vibration, acoustic, transfer function, natural frequencies, Nyquist plot, FIR-filter approximation

Zusammenfassung

Die Implantation von Hüftgelenkprothesen ist eine der erfolgreichsten Operation weltweit. Jedes Jahr nimmt die Zahl an Nachsorgeuntersuchungen und -operationen zu. Die Hauptursache für Nachsorgeoperationen ist die Hüftgelenkprothesenlockerung. Der Marktpreis einer Hüftgelenkprothese beträgt ca. 2.200 - 3.000 US $. Der chirurgische Eingriff kostet ca. 20.000 - 30.000 US $ einschließlich der Anästhesie, des chirurgischen Verfahrens und des Krankenhausaufenthalts. Die Kosten verursachen wachsende Besorgnis bei den Chirurgen, den Krankenhäusern und den Krankenversicherungen [2]. In den USA wurden 1999 über 541.245 Hüftgelenk- und Knieprothese eingepflanzt [3]. Auch die Tendenz der Implantation von Schulterprothese steigt. In Deutschland werden pro Jahr über 150.000 Hüftgelenk- und Knieprothesen eingepflanzt [4].

Die Lockerung der Hüftgelenkprothese kann von der Knochenzement-Knochen-Schnittstelle oder von der Knochenzement-Prothese-Schnittstelle oder von der Zerstörung des Knochenzementsmantel herrühren. Dabei kann durch Luftblasen im Knochenzementmantel ein Ermüdungsbruch des Knochenzementsmantel verursacht werden.

Ultraschall spielt eine große Rolle in der Medizin. Es ist eine nicht-invasive Methode der Diagnostik. Es sind keine Nebenwirkungen bekannt. Ultraschall ist eine unbegrenzt und wiederholbar anwendbare Methode im Gegensatz zu anderen Methoden wie der Röntgenstrahlmethode, die Nebenwirkungen auf den Patienten und Embryonen hat. Nicht-invasive Diagnostik von Hüftgelenkprothesen ist ein Traum für Patienten und Chirurgen.

Das Ziel dieser Arbeit ist es, ein neues nicht-invasives Verfahren zur Ermittlung der Lockerung von Hüftgelenkprothesen vorzustellen. Es wird die Entwicklung einer neuen vibroakustischen (VA) Diagnosetechnik geschildert, um den internen Zustand der Hüftgelenkprothese im Oberschenkel durch eine passende Verarbeitung des gemessenen Schwingungssignals zu überwachen.

Der Zustand der Prothese wird in vitro festgestellt. Das Schenkelmodell mit einer gesicherten Hüftgelenkprothese wird von einem akustischen Erreger angeregt. Die resultierte Übertragungsfunktion ist als die Grundlinie oder der Bezugsvektor zu betrachten, die für die Analyse gespeichert wird. Die Prothese wird ohne Zerstörung des Knochenzementmantels herausgezogen und wieder in ihre Ausgangsposition zurückgebracht (künstliches Lockerung). Wieder wird die gleiche Messung für die gelöste Prothese durchgeführt.

Die dynamischen Eigenschaften des Systems werden im Frequenzgang durch den Vergleich zwischen dem Bezugsvektor (sicherer Fall) und dem Störungsvektor (lockerer Fall) überprüft, um den Effekt der Lockerung auf das dynamische System anzuzeigen.

Die Detektion der Lockerung der Hüftgelenkprothese basiert auf der Resonanzfrequenz (1. Resonanz). Die Lockerung erzeugt eine Verminderung von 40 % - 60 % der Schwingungsenergie der 1. Resonanzfrequenz.

Es wurde herausgefunden, dass das Nyquist Diagramm ein sehr wichtiges Diagnosewerkzeug zur Feststellung der Prothesenlockerung ist. Die Änderungen im Nyquist Diagramm für sichere und gelockerte Fälle zeigen das Vorhandensein von Lockerung im System an.

Die Neuheit in dieser Studie ist die Approximation des realen Systems (Schenkel) mittels FIR-Filter. Die gemessene Frequenzantwort des realen Systems wird verwendet, um das FIR-Filter zu entwerfen. Diese Technik stellt nützliche Informationen über den internen Zustand der Prothese zur Verfügung. Diese neue FIR-Filtertechnik wurde zur Unterscheidung zwischen den vibroakustischen Signalen von intakten und gelockerten Prothesen entwickelt. Die Impulsantwort und Filterkoeffizienten des FIR-Filter bei gelockerter Prothese sind niedriger als im intakten Fall.

CONTENTS

LIST OF FIGURES

NOMENCLATURE

A, B	Pressure amplitude of plan wave.
b_i	FIR-Filter Coefficients.
c	Propagation velocity.
C_g	Group velocity.
d	layer thickness.
[D]	Damping matrix.
E_T	Transmitted Acoustic Energy.
E_R	Reflected Acoustic Energy.
$f(t)$	Input force.
$F(\omega)$	Fourier Transform of $f(t)$.
$h(t)$	System Impulse Response.
$h(n)$	Unit-sample Response.
$H(\omega)$	System transfer function.
$[H(\omega)]$	FRF matrix of the system.
j	$\sqrt{-1}$
k	Wave number in i direction of propagation.
[K]	Stiffness matrix.
L	Distance between receiver and transmitter.
[M]	Mass matrix.
M	FIR-Filter degree.
N	Number of degrees of Freedom.
n	Number of layers, Integer
$P\#i$	Measuring point i ($i = 1, 2, \ldots\ldots 11$)
p	Acoustic pressure.
P	Instantaneous pressure.
p_o	Hydrostatic pressure.
s	Laplace operator.
t	Time.
u	Particle velocity.
V_p	Compression wave velocity.
V_s	Shear wave velocity.
V_R	Surface wave velocity " Rayleigh wave velocity ".
x	Wave propagation direction.
$x(t)$	System displacement.
$X(\omega)$	Fourier transform of $x(t)$.
$\dot{x}(t)$	System velocity.
$\ddot{x}(t)$	System acceleration.
Z_i	Acoustic impedance in medium i.
$\bar{z}$	Specific acoustic impedance.
ξ	Particle displacement.

ρ_o	Mean density of the medium.
λ	Wavelength.
ω	Angular frequency(Radian/s).

Abbreviation

DOF	Degree of freedom.
IRF	Impulse Response Function.
FIR	Finite Impulse Response.
FFT	Fast Fourier Transformation.
FRF	Frequency Response Function.
FRF$_{ij}$	Frequency response function (measured at point i for excitation at point j).
SUT	Sytem Under Testing.
NVH	Noise, Vibration and Harshness analysis
IRF	Impulse Response Function.
THA	Total Hip Arthroplasty.
Re.	Real part of FRF.
Im.	Imaginary Part of FRF.

Dedication

This thesis is dedicated to my family, which has been very supportive of my work over the years. Special recognition is given to my wife Amal Sakr and my three daughters Esraa, Tasnieem and Khadija. Also with deep appreciation, I must acknowledge my mother and father for their support and encouragement.

M. Sc. Eng. Ayman Eshra

CHAPTER 1

DIAGNOSIS OF HIP PROSTHESIS LOOSENING

Total hip arthroplasty (THA) is often performed to replace a diseased and damaged articulating surface. The intramedullary stem portion of a femoral prosthesis is necessary to hold the replacement articulating surface in its anatomical location and this fixation must be durable and generally pain-free over the long term [1]. Artificial-Joint replacement has become one of the major surgical advances of the last century. The rate of operations is 600,000 per year. It is a second invasive treatment of body ailments after the dental reconstruction treatment [2]. It is an effective treatment of serious forms of osteoarthritis and for disabling effects of rheumatoid arthritis, congenital deformities, and Particular kinds of posttraumatic conditions. Osteoarthritis (OA) is the most frequent indication for joint replacement. It is responsible for the majority of cases involving musculo-skeletal discomfort and, second to cardio vascular conditions, is an important causes for complete or partial disabilities [3].

1.1 Development of Artificial Joint Replacement

The development and application of artificial-joint replacement, particularly THA and total knee arthroplasty (TKA), has achieved a tremendous reduction in disabilities, particularly in the older segment of the population. The economic effects of this surgical treatment on society as a whole in terms of saving in medical care, drugs, and disability aids, and the sickness level of absence from jobs are significant. The personal effects on the happiness and life fulfilment of patients are overwhelming. The majority of the estimated 400,000 patients receiving THA annually can hardly walk at all and suffer serious continuous pain, day and night. A few weeks after the operation they will, with few exceptions, be pain free, able to function normally, and resume jobs and sometimes even active sports. Complication problems will usually not recur until after 10 to 20 years. When they do, due to eventual wear or loosening, revision surgery is possible. At least 90% of the patients live normal, pain free live for at least 10 years after the operation [4].

1.2 Hip Joint Replacement (Hip Arthroplasty)

Hip replacement, or arthroplasty, is a surgical procedure in which the diseased parts of the hip joint are removed and replaced with new, artificial parts. These artificial parts are called the prosthesis. The goals of hip replacement surgery are to improve mobility by relieving pain and improve function of the hip joint.

1.2.1 Description

The hip joint is located where the upper end of the femur meets the acetabulum. The femur, or thigh bone, looks like a long stem with a ball on the end. The acetabulum is a socket or cup-like structure in the pelvis, or hip bone. This "ball and socket" arrangement allows a wide range of motion, including sitting, standing, walking, and other daily activities, as shown in Fig. 1.1.

Cartilage   Synovial membrane
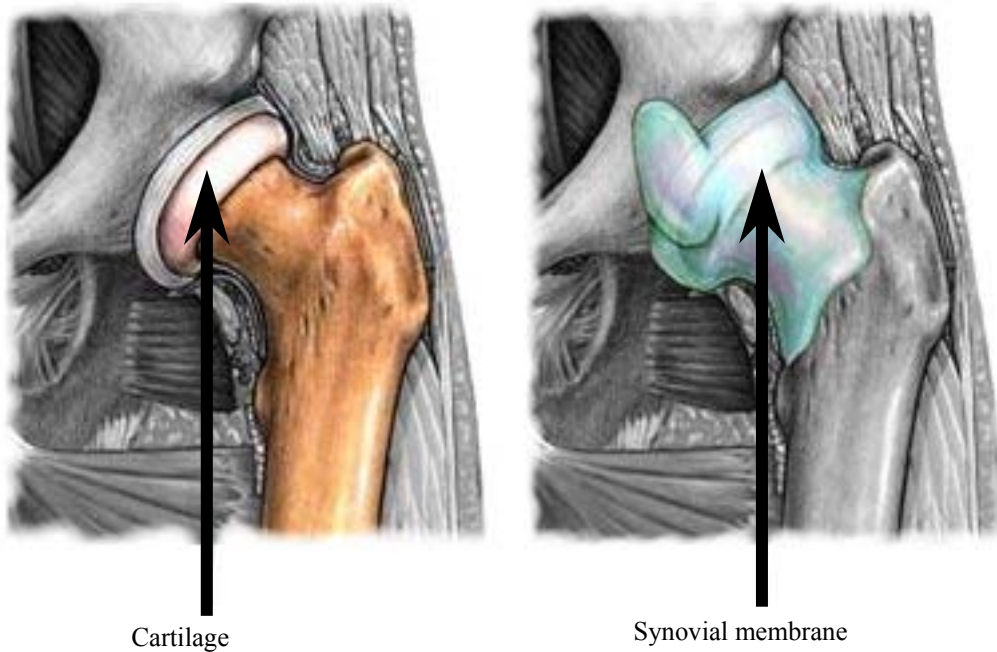
Fig. 1.1 Hip joint anatomy, from [5].

A total hip prosthesis is surgically implanted to replace the damaged bone within the hip joint. Figure 1.2 shows the diseased hip joint anatomy.

The total hip prosthesis consists of three parts:

1. A cup that replaces the hip socket. The cup is usually plastic or ceramic and metal.
2. A metal or ceramic ball that will replace the fractured head of the femur, as shown in Fig. 1.3.
3. A metal stem that is attached to the shaft of the bone to add stability to the prosthesis, as shown in Fig. 1.4.
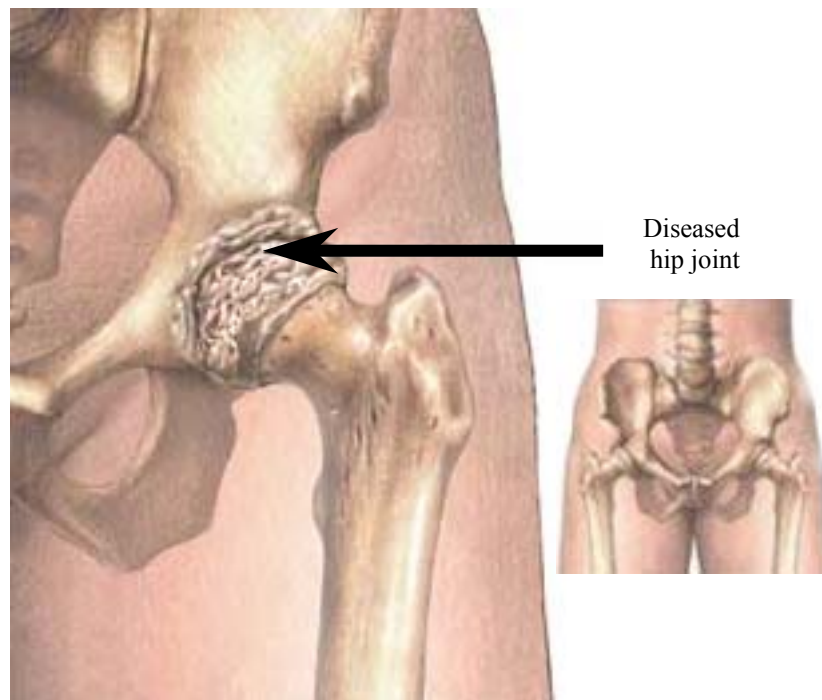
Fig. 1.2   Diseased hip joint anatomy, from [5].

Fig. 1.3   Photograph of the acetabular components of a contemporary total hip replacement. The shell is usually made out of metal, and the liner may be ceramic, metal, or ultra-high-molecular weight polyethylene, from [6].

Fig. 1.4   Photograph of femoral stem and femoral head. The head may be made out of metal or ceramic, and the finish of the head may vary, from [6].

During hip replacement, the orthopaedic surgeon makes an incision, often over the buttocks, to expose the hip joint. The head of the femur is cut out and removed as shown in Fig 1.5.
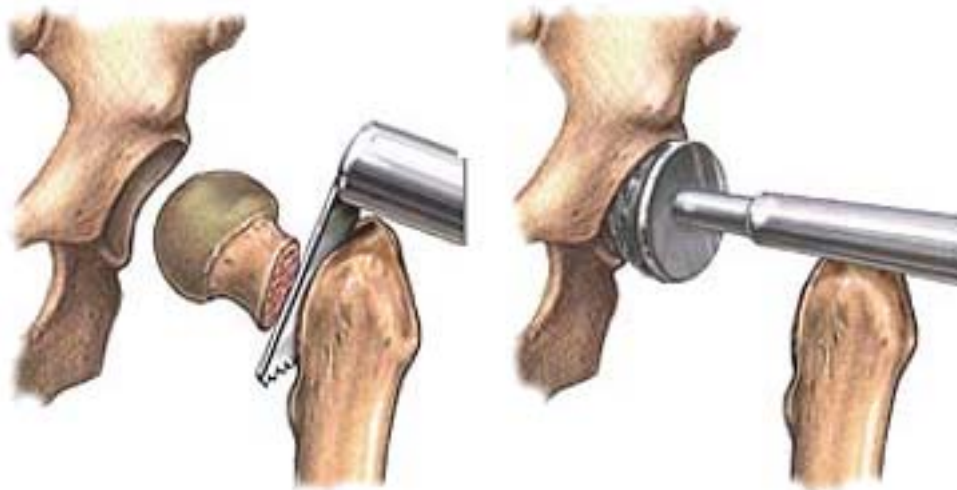
Fig. 1.5   Removing the head of the femur and a layer of the hip socket, from [5].

Then, the hip socket is cleaned out by a reamer to remove all of the remaining cartilage and arthritic bone.

The new socket is implanted, after which the metal stem is inserted into the femur. The artificial components are fixed in place, sometimes with a special cement, as shown in Fig.1.6 and Fig. 1.7.
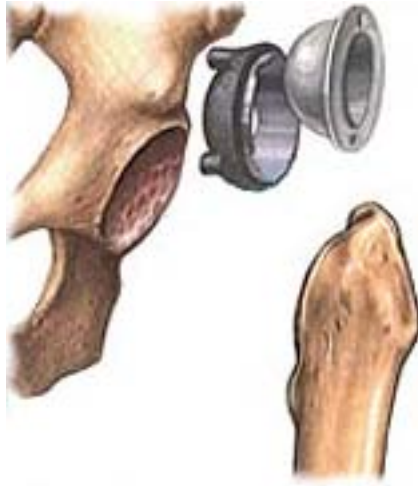
Fig. 1.6   Placing the plastic socket in the enlarged pelvis cup, from [5].

Fig. 1.7   Inserting the metal ball and stem in the femur, from [5].

The muscles and tendons are then replaced against the bones and the incision is closed.

The pain should gradually decrease, and by the third day after surgery, oral analgesic medications may be sufficient to control the pain.

Results with a hip prosthesis have been excellent. The operation relieves pain and stiffness symptoms, and most patients (over 80%) need no help walking. With time, loosening of the artificial joint has been observed due to the limited properties of the cement used to attach the artificial parts to the bones. After surgery, the patient stays in the hospital for 5 to 8 days. However, some people may need further rehabilitation and assistance after hip replacement surgery. Fig. 1.8 shows the hip joint before and after replacement operation [5].

Fig. 1.8   Hip joint before and after replacement operation, from [5].

The successful application of artificial-joint replacement on a large scale, which essentially evolved during the last four decades, is an accomplishment of scientific and technological development in orthopaedic surgery and bioengineering, in particular form the scientific specialties of biomaterials and biomechanics. The proliferation of application, again mostly of THA, started around 1960, with the introduction of two inventions by sir John Charnley. One was the adoption of the low-friction principle, whereby a relativity small femoral head was made to against a polyethylene acetabular cup. Another was the use of acrylic cement (PMMA) as a filling material to accommodate uniform load transfer between the smoothly shaped prosthesis and the irregular interdigitates with the bone and cures to form a solid but relatively flexible mantle between bone and prosthesis as shown in Fig. 1.9 [7,8].

The success of THA has also triggered developments of other joint replacements, such as the knee joint, the application frequency and results of which are beginning to approach those of the hip. Replacements of the finger, shoulder, elbow, wrist, and ankle joints are much less frequent [9].

acetabulum

Proximal
,

Distal

Lateral,   medial

Cortical bone

Spangeous bone

Acrylic cement

Polyethylene

Metal
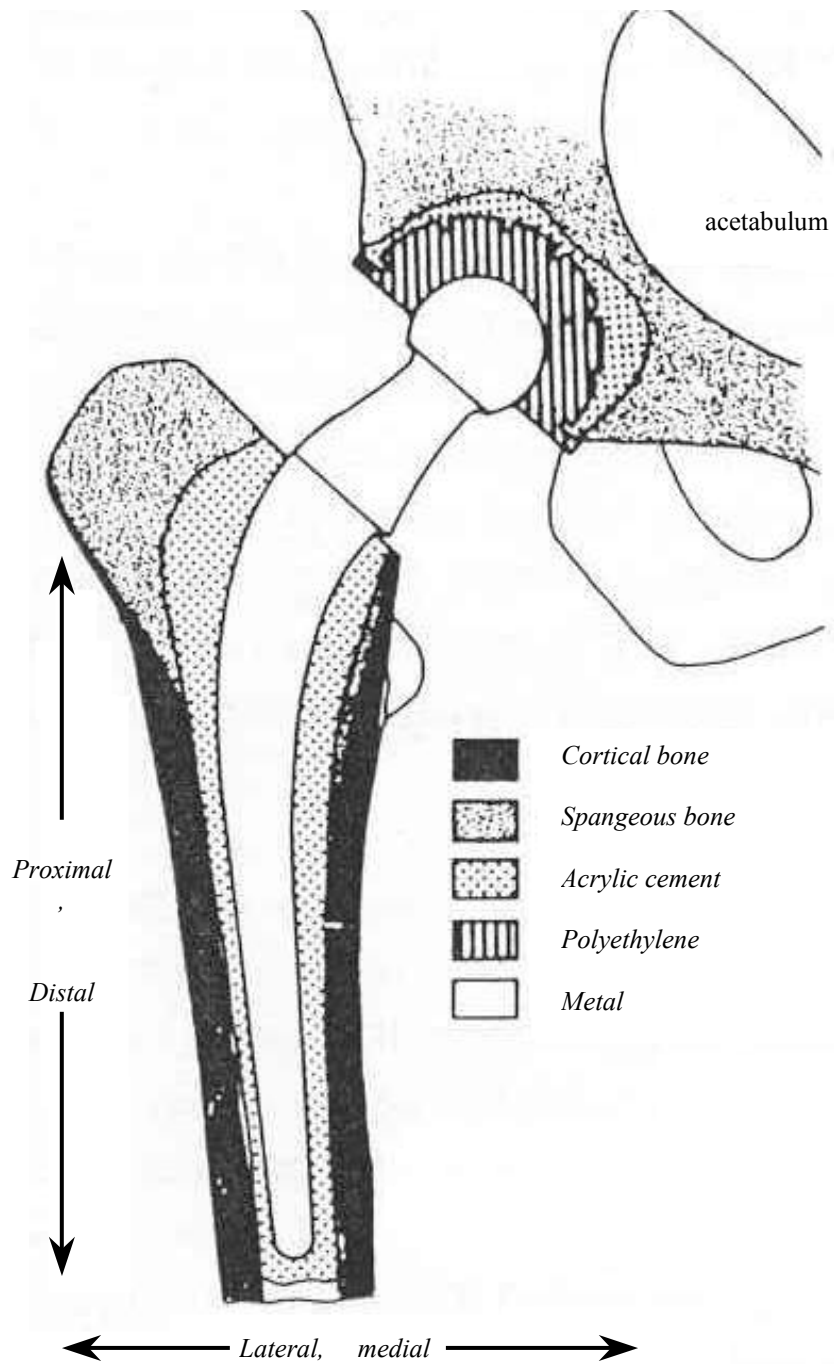
Fig.1.9 Schematic section of a cemented Charnley Prosthesis, from [7].

1.3 Problem Statement

The quality of a joint replacement depends on such clinical factors as medical complications the patient may suffer, presence of residual pain, and functional demands on and endurance of the prosthetic device. The latter conditions depend on the quality of the fixation of the prosthesis to the bone. Although the precise relationships are not always evident, the quality is basically determined by prosthetic design factors (materials, prosthetic shape, fixation concept, and surgical instruments), surgical factors (surgical skills and experience, including patient and device selection, age, weight, and level of physical activity).

During the last 40 years are vast amount of bio-mechanics research has been devoted to a better understanding of the relationships between quality and factors that might cause prosthesis failure (e.g., severe pain, loosening, fracture removal). Many technological improvements have been introduced to prolong clinically acceptable prosthesis function.

These efforts were directed at understanding and postponing aseptic loosening of the fixation. This long-term complication is by far the most frequent one, and is the limiting factor for the functional life span of the bone-prosthesis structure.

A painful total hip or knee prosthesis suggests the possibility of loosening of one or both components. Routine radiographs may be helpful in determining the presence of loosening but are frequently normal [10]. The patient who have an initially or partial loosening suffer from pains during walking on a loosened implant. The pain resulted from kicking, stretching, shaking or rotating of the patient's leg during the clinical examination of the prostheses is an indication to loosening [11].

The clinical objective of a stable fixation in joint replacement can be restated in terms of the load transfer from prosthesis to bone. In a prosthetic femoral stem, physiological loads are applied through the head of the prosthesis and distally, below the stem, these forces are fully supported by the cortical femoral bone, as shown in Fig. 1.10.
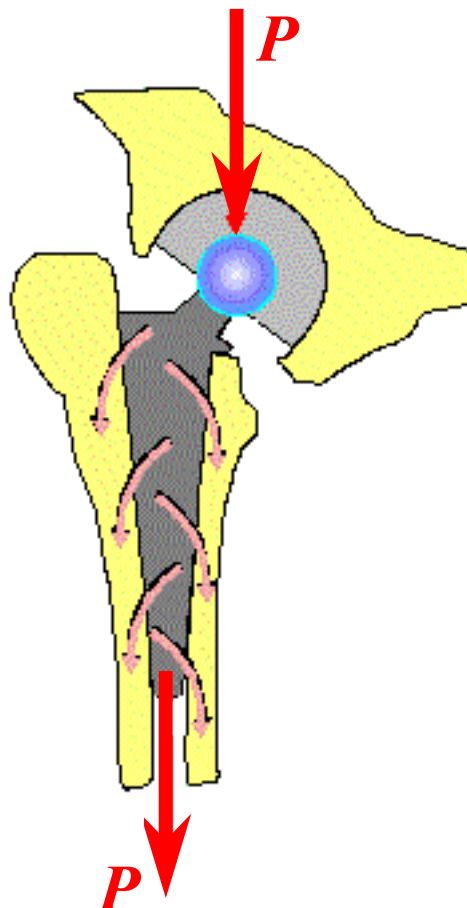
Fig. 1.10   The pattern of load transfer.

The applied force must therefore be transferred from prosthesis to bone across their common interface, and a stable and pain-free transfer of these physiological forces is synonymous with the goal of a clinically satisfactory fixation [1]. Figure 1.11 shows the prosthesis-bone interface.
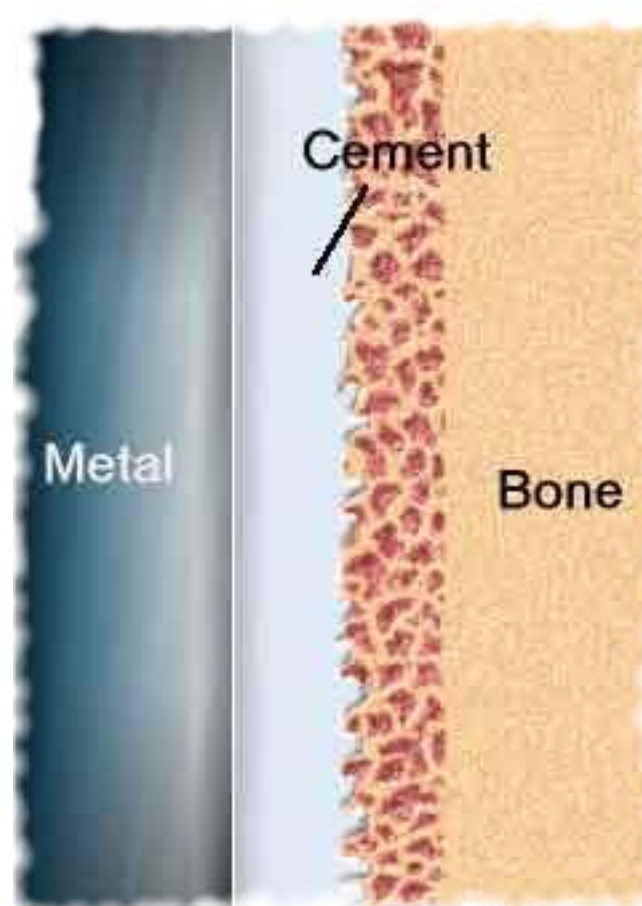
Fig. 1.11   Prosthesis-bone interface.

Studies of the mechanical properties of prosthesis in bone have usually concentrated on the strength of the fixation. Typically, push-out studies have been used to monitor the strength of bone ingrowths or bonding [12, 13]. The bond does exist between the cement and the metal surface and the tensile pull-off strength between bone cement and the metal surface of grit-blasted femoral prostheses is approximately 5 MPa [14-16]. However, The tensile pull-off strength of cement bond to a polished cement surface was only 0.6 MPa [14]. This means that, the exists bond has a weakly resistance to loosening mechanism, therefore the loosening of hip prosthesis must be occur at any time of the patient life. However, it is not the fixation strength that determines the pattern of load transfer to bone. Generally, the stiffer parts of any structure will carry most loads when this load is shared across components of different stiffness. Strength and stiffness are not the same and indeed my be conflicting requirements. A highly mineralised bone has high stiffness but this is achieved with loos of the strength that is derived more from its organic collagenous constituents [17].

Aseptic loosening is a gradual process [18-21] where by the mechanical integrity of the implant/ bone interface is lost and a fibrous tissue is formed between the two surfaces. A gradual increase of tissue thickness occurs with time. As a result, patient suffers from pain and functional restrictions. It is likely that, the occurrence of interface loosening is unavoidable. The space between implant and bone causes a mechanical disturbance, which leads at the end to loosening of the prosthesis [11]. The relative (micro) motion between implant and bone as a result of different modules of elasticity of implant and cement mantel at the boundary layer produces a cement wear particles [22,23]. The wear particles activate the

osteoclast process at the film between bone and cement. The bone breakdown process accelerated until destruction of the bearing bone layer i.e. loosening.

The precise mechanism of the loosening of cemented prosthesis is not entirely known, but it is likely that the process is initiated by mechanical failure of the acrylic cement and / or Cement bone interface [24–28]. Hence, the life span limits would depend on the (fatigue) strength of the cement and the interface relative to the stresses generated in these regions caused by the load-transfer mechanism. If cement and/or interface fixation failure occur, repetitive relative (micro) motion between the implant and bone would develop. This micro-motion is known to cause the bone to resorb [29].

The bending impacts, which occur during normal and stairs walking and jogging may already be stressed the interface (implant-bone) by axial torsional loads. The amplitude of the axial rotations of the cortical bone were small in comparison to the ones of the prosthesis head, indicating that axial rotational vibrations following femur bending vibrations mainly stresses the spongiosa and the cement layer [30-32]. These vibration produced dynamic torsional loads on the implant mounting system. Such torsional loads lead to the axial rotational micro-movements deemed chiefly responsible for aseptic loosening of the implant [33, 34]. The biological mechanism will accelerate the propagation of mechanical cracks and thus it increases the failure of the prosthetics device. As a result of the bone resorption, a fibrous interface membrane fills the gap. This membrane is seen clinically as the radiolucent line on X-ray. Thus, loosening of the prosthesis-bone interface is a biomechanical phenomenon that could have resulted from chronic mechanical overloading [28].

The first phase of loosening can not be determined clinically or radiologically because of the lack of information. It is very important to know the first stage of loosening of implant because the increasing in destruction process of bone make the change process of implant very complicated [11]. Since the progressing of the loosening process leads to a destruction of the bearing bone [35-37].

The variables which may be the possible causes of femoral component loosening are (1) prosthesis type; (2) body weight; (3) femoral component position; (4) prior femoral head replacement prosthesis; (5) activity level; (6) abductor/body weight moment arm ratios; (7) amount of preoperative osteoporosis [38].

Other factors that may contribute to prosthesis-bone loosening are:-

(a) Thermal damage to bone due to the heat generated from curing of the cement in situ which leads to bone necrosis [9, 18, 39],
(b) Cytotoxic effects from residual methacrylate monomers in the cement [40],
(c) Migration of cement and polyethylene wear particles in the cement-bone interface [41], and
(d) The physiological process of endosteal bone resorption and intramedullary canal widening in the femur [42].

There is evidence that the cement-implant interface porosity results in biomechanical weakening and diminished longevity of cemented hip arthroplasties [43]. The consistent and significant finding from long-term follow-up studies and revision surgery studies suggests that chronic overloading of the cement and interfaces is a dominant factor in prosthesis loosening [44-46].

10

1.4 The State of the Art

X-ray radiation has an important place in modern medicine. Since its discovery its use in medical diagnosis has been extended dramatically, and in highly developed nations half of the population are likely to undergo an X-ray diagnostic examination [47]. The biological effects of radiation are essentially due to the chemical changes induce in body cells as a result of ionisation, excitation, dissociation and atomic displacement. A number of factors must be taken into account in assessing the effects of radiation on living organisms, whether from external radiation or from ingested or inhaled radioactive materials. These include the density of ionisation, the dose rate, the localisation effect and the rates of administration and elimination of radioactive material. In spite of its usefulness in medicine and agriculture, radiation has some deleterious effects. The effects can be somatic or genetic, and there is no threshold dose below which there are no somatic or genetic effects of radiation. [48, 49].

A painful total hip or knee prosthesis suggests the possibility of loosening of one or both components. Routine radiographs may be helpful in determining the presence of loosening but are frequently normal. However, plain films did not help in demonstrating loosening. The radiographical features of femoral component loosening consist of either medial tilting, longitudinal settling, a combination of these, or gross scalloping. Femoral component loosening is better determined by the radionuclide study, because of in adequate visualization of the methacrylate-bone interface of the femoral component on the antero-posterior subtraction view [10]. A painful total joint can be a difficult diagnostic problem. Many modalities have been used to investigate painful total hip prostheses, including clinical evaluation, haematology, plain radiographs, fluoroscopic manipulation, needle aspiration, and arthrography [50]. Figure 1.12 shows the bone imaging pattern.
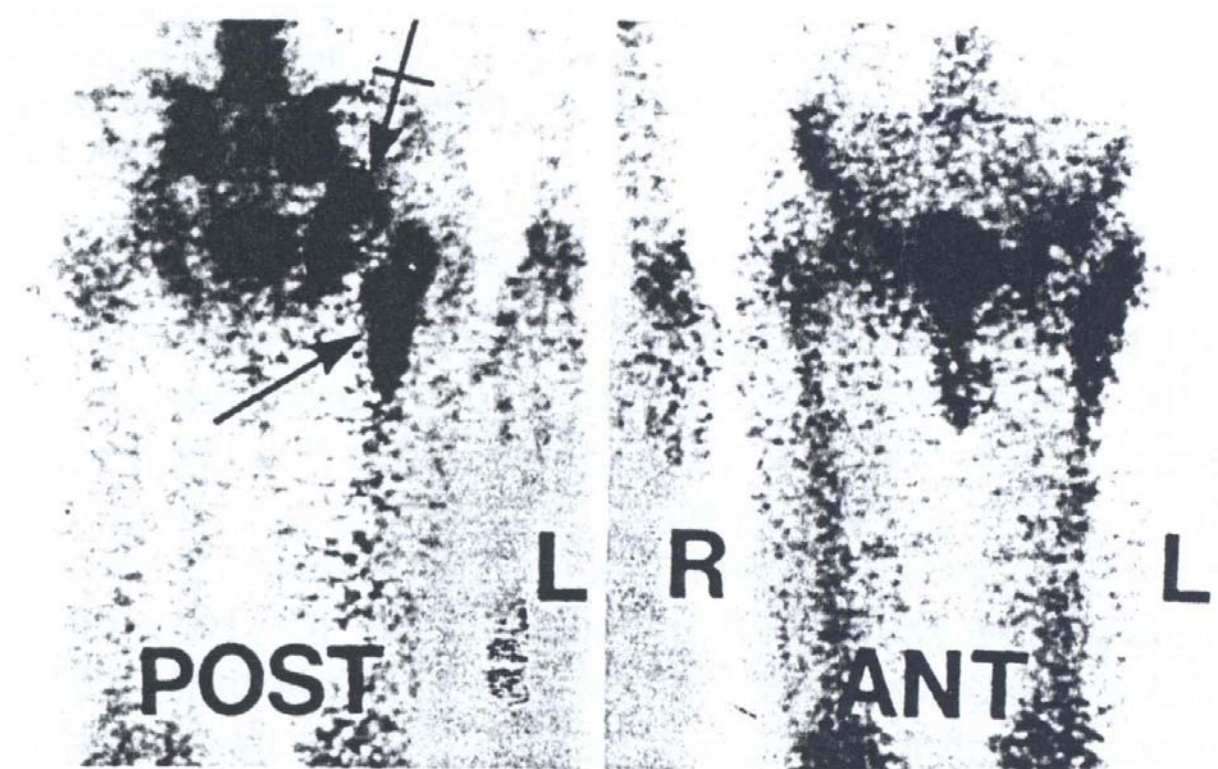
Fig. 1.12   A combination of diffuse femoral (→) and acetabular (←+) activity, shown on the left in this patient, was seen in both patients with infected prostheses and in one patient with combined loosening of femoral and acetabular components, from [50].

A serial radiographic evaluation with the use of reproducible high-contrast X-rays was used to assess the mechanical and biological performance of the cemented stem-type femoral component. The object of identification and assessment of the modes of failure of cemented stem-type femoral components by using the radiographic analysis of loosening is threefold:

(1) Early radiographic diagnosis of mechanical changes and forecast of future response,
(2) Identify patients with high risks for stem fracture and loosening and provide proper advice and guidance to the patient during subsequent activity, and
(3) Provide recommendations for improved surgical and cement technique, and information for design and material selection for femoral components and their long-term fixation [25].

Bone imaging has received some attention, initially with early scanning agents [51-53]. The scanning agent were used to scan the prostheses e.g., ^{99m}Tc-phosphate agents [52, 54-57], as shown in Fig. 1.13. The imaging has been performed by using 15.0 mCi (555 MBq) of ^{99m}Tc-methylene diphosphonate (MDP) and Cleon imager. However, bone imaging is extremely useful, the differentiation between infection and loosening can not be made using this technique, as both conditions may cause increased activity. The images consider abnormal if increased activity is present [58]. Many authors believed that the abnormal bone image is usually associated with significant disease. The loosening and infection can not be differentiated by bone images. If the image is normal, major disease is unlikely; but if it is abnormal pattern is focal, loosening is probable. If the abnormal pattern is diffuse, and
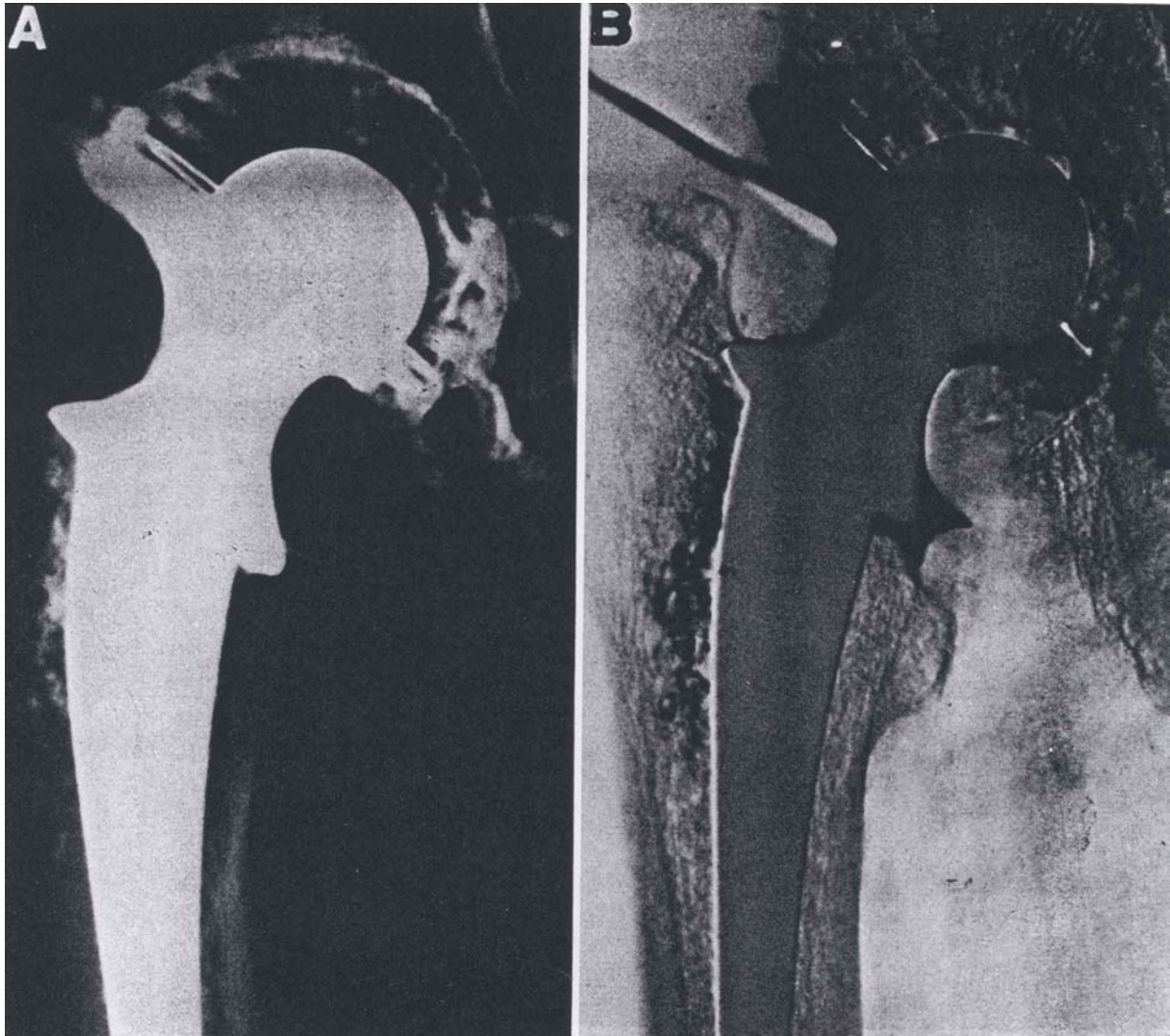
Fig. 1.13 A and B. An arthrogram utilizing subtraction technique confirms loosening of both components and delineates fistulous in the region of the acetabulum, from [55].

particularly if it is surrounds both prosthetic components, infection needs to be seriously considered [56, 58], as shown in Fig. 1.14.

The patient may be underwent imaging with 87mSr or 18F or ^{99m}Tc-phosphate [8]. The Gallium radioisotope scanning may be used because of the affinity of Gallium for white blood cells [59]. The patients received twenty millicuries of technetium pyrophosphate intravenously or three millicuries of Gallium-67 citrate. An interior and posterior rectilinear scans of the joint has been made by using a picker Magna Scanner four hours after injection [60]. The radionuclide image was interpreted as abnormal and consistent with loosening if increased radioactivity was observed at the cement-bone interface of either the acetabular or femoral component of the knee prosthesis. Increased radioactivity was determined by comparison with contralateral side. The subtraction arthrogram was interpreted as indicating loosening if contrast was present at the cement-bone interface of any of the prosthetic components or at the metal-cement interface of the femoral component of the total hip prosthesis. Radionuclide imaging utilizing a ^{99m}Tc phosphate complex is an effective
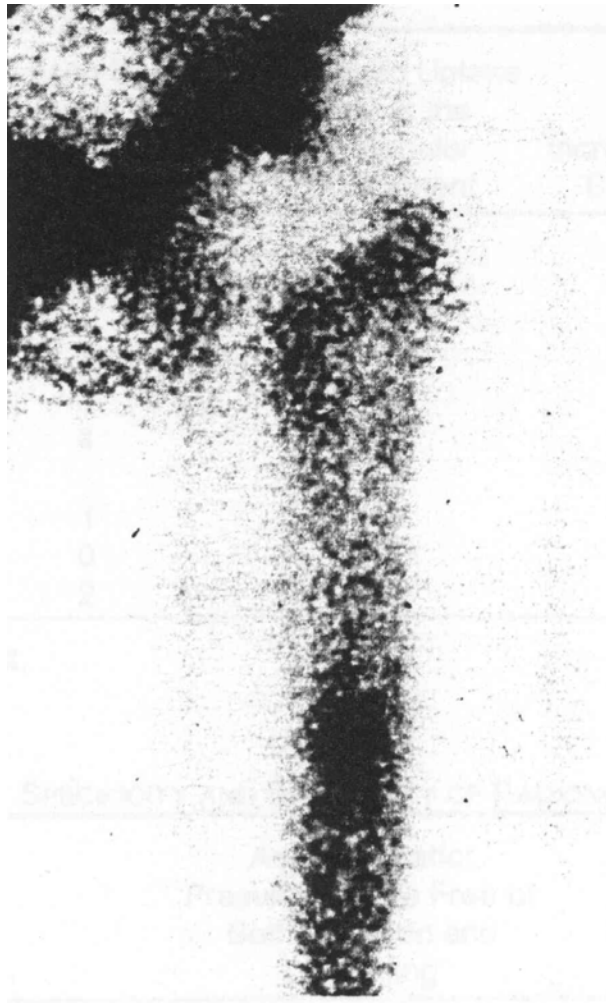
Fig. 1.14 The marked focally increased uptake at the tip of the femoral prosthetic component is pathognomonic of loosening and/or infection, from [58].

screening procedure to determine the presence of loosening as well as other complications. If the image is abnormal or equivocal, it should be followed by arthrography. Arthrography will confirm the presence of loosening or demonstrate other possible causes of a positive image, some of which do not require surgical intervention [10].

The limitation of plain film radiography and routine arthrography in the evaluation of painful total joint replacement may make digital subtraction arthrography a suitable alternative for conventional subtraction techniques. The technique of subtraction arthrography has been long used in the diagnosis of contrast-material tracking in total joints. While digital subtraction radiography has been utilized primarily in the evaluation of vascular diseases [61, 62]. Digital subtraction arthrography was performed using either a pulsed radiographic unit utilizing a fixed mask subtraction technique (Diasonics) or a continuous fluoroscopic unit utilizing the recursive filtration technique (aster Medical). Both unit acquire the display information in a in a 512 X 512 X 8 bit matrix [63].

The technique of digital subtraction arthrography was explained in many literatures [63-68]. Ginai et al. has been performed an arthrography exam on a Philips DVI system (14-inch image intensifier, 512×512 image matrix) [64]. Where, the leg of the patient on the side of the examination was immobilized using a strap over the knee and the thigh regisons. To avoid puncturing the femoral artery its position was marked on the skin with an indelible

14

marker. The puncture area was cleaned and draped with sterile covers. About 10 ml of 1% nonbacteriostatic xylocaine was used as local anaesthetic. A 12.5 cm long spinal puncture needle (20 gauge) was then introduced parallel to the table top and directed slightly cranially for a lateral puncture route [65, 66]. When the pseudocapsule around the hip prosthesis is punctured and the tip of the needle touches the metallic neck of the femoral component, the position is usually correct and is confirmed fluoroscopically. An attempt was made to aspirate joint fluid before contrast injection. In cases where no fluid could be aspirated, a few millilitres of nonbacterio-static physiological saline were injected into the joint and reaspirated.

The aspirate was saved and sent for bacteriological analysis and culture. The patient was positioned so that both components were fully visible for evaluation before contrast injection. A scout view was obtained and the nonionic contrast medium Iohexol 300 (Omnipaque) injected using a connecting tube and hand injection. The amount of contrast medium varied between 10 and 40 ml (mostly 20 ml) according to the size of the capsule and presence of bursae or cavities around the prosthesis. Digital subtraction views were obtained at a speed of 1 per second with a maximum of 20 views [64]. The criterion used to define loosening of the femoral component consisted of any contrast leakage at the prosthesis-cement interface up to or beyond the intertrochanteric level (zones 1 or 7; Figs. 1.15 and 1.16)
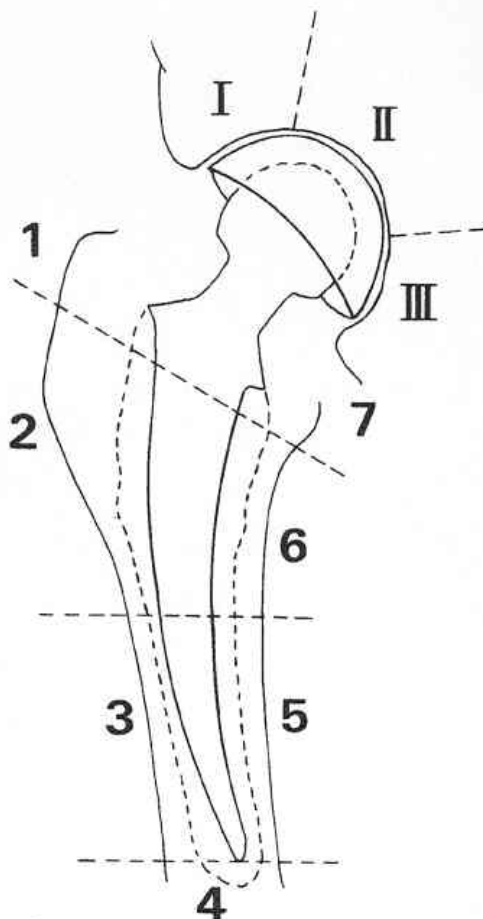
Fig. 1.15   A diagrammatic representation of the various zones used in defining loosening of the femoral and acetabular components of hip arthroplasty, from [64, 68].

at the cement-bone interface. In the case of the acetabular component, contrast leakage at the bone-cement interface had to be in at least two zones or around the whole of the component in

order for it to be considered loose (Figs. 1.15 and 1.17). These criteria are similar to those described by others [67, 68].
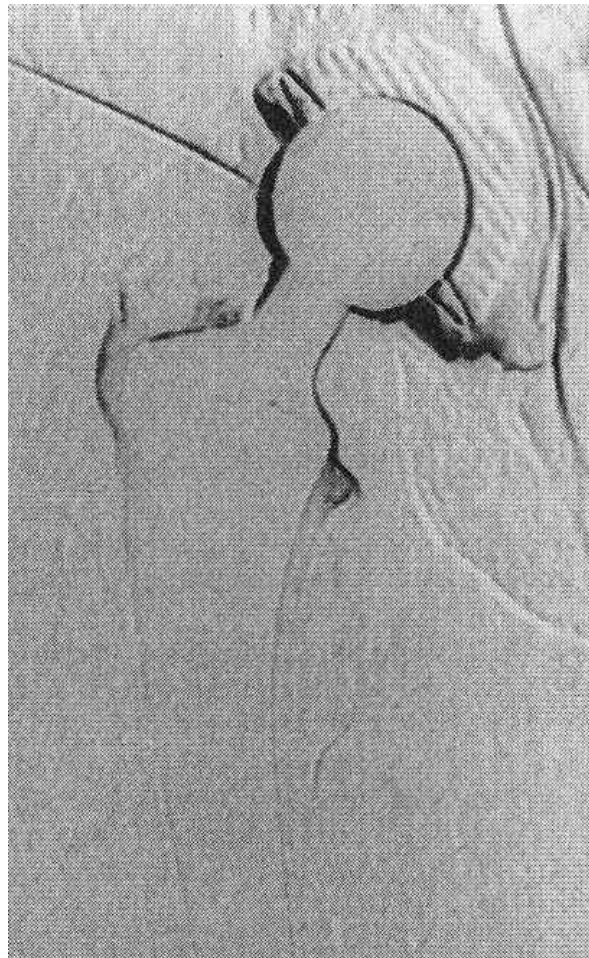
Fig. 1.16 Subtraction arthrogram showing contrast in zones 1 and 7 (see Fig. 1.15) at the cement-bone interface, graded as a loose femoral component. The component was also found to be loose at surgery, from [64].

The plain film criteria for femoral component loosening include a lucent zone at the metal-cement or bone-cement interface was reported by greater than 2 mm wide. Migration and/or subsidence of the femoral component into the femoral shaft are accepted as a definite indication of prosthetic loosening. Cracks in the cement and radiolucency are indirect signs that the prosthesis has moved [69]. For indicating acetabular component loosening, radiolucency of more than 2 mm between cement and bone around almost the whole of the component on the anteroposterior view or any change in position such as tilting or migration are similar to the criteria used by other authors [70, 71]. For the femoral component any contrast leakage between metal-cement interface beyond or at least up to the intertrochanteric line in the cement-bone interface was considered to indicate loosening of the component (Figs. 1.15 and 1.16). In femoral component loosening many authors have described accumulation of contrast medium at the tip of the stem [72].

16
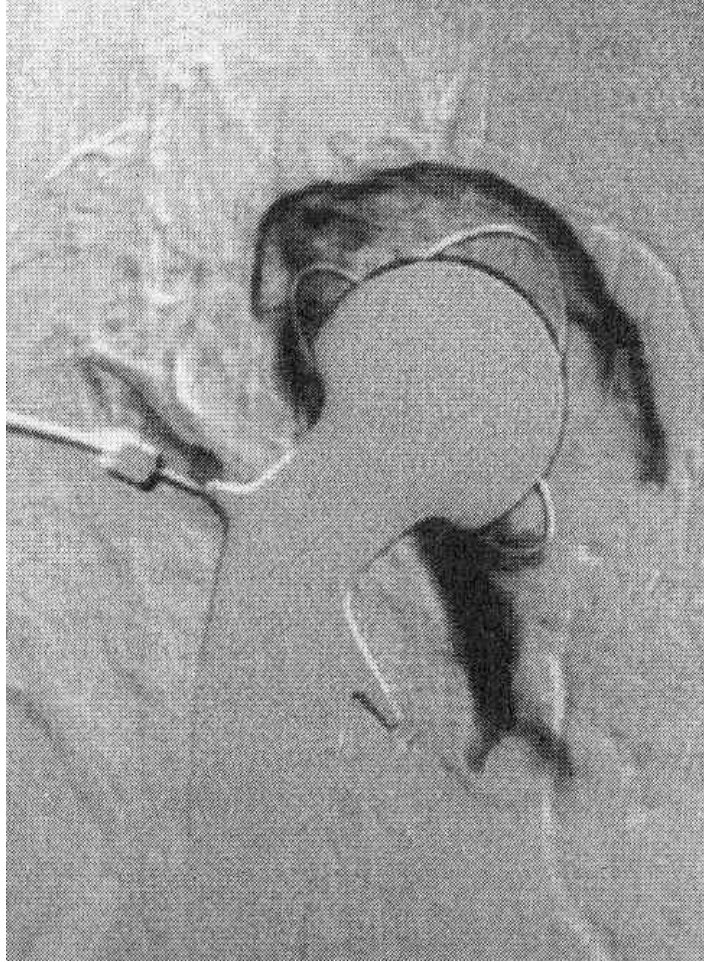
Fig. 1.17 Subtraction arthrogram showing a loose acetabular component with contrast in zones I, II and part of zone III at the cement-bone interface. The femoral component shows no signs of loosening, from [64].

Bone scintigraphy was performed after intravenous injection of 370 MBq ^{99m}Tc-labelled methylene diphosphonate. The first image was taken 2–6 min after injection in an anteroposterior position with counts obtained for 2 min. Increased uptake of isotope indicates hyperaemia, and can be a sign of infection. After 2 h anteroposterior, posteroanterior and, if necessary, oblique images were taken by collecting 400000 counts to detect increased uptake along the acetabular or femoral components which was indicative of loosening [64]. Bone scintigraphy is a sensitive indicator of bone turnover but does not distinguish infection from loosening. Increased isotope uptake may be due to loosening and infection but could also be due to heterotopic ossification, stress fracture, tumour, Paget's disease or reflex sympathetic dystrophy syndrome [73].

Joint fluid aspiration and culture was used as the definitive criterion for the diagnosis of infection. Prosthetic loosening caused by infection may account for 7–56% of the total number of loose prostheses [70]. Joint fluid may obtain at arthrography or at surgery for bacteriological analysis. The positive culture of the joint fluid was an indication for infection. Where 8 patients had positive cultures and the results of the surgical specimens were similar to the joint aspirates obtained at arthrography [64].

A comparison between plain radiographs, scintigraphy and the digital subtraction arthrography was made to evaluate each of them [64]. On plain radiographs a diagnosis of loose acetabular component was made in 50% of patients. At surgery the percentage of loose acetabular components was 70% in this group. Of the 50% of components considered solid on plain radiographs, 52% (P=0.20) were found to be loose at surgery. On scintigraphy a loose acetabular component was diagnosed in 52% of patients and at surgery 76% of these components were found to be loose. Of the 48% considered solid on scintigraphy, 43% (P=0.01) were found to be loose at surgery. On digital subtraction arthrography a loose acetabular component was diagnosed in 67% of patients and 84% of these components were found to be loose at surgery. Of the 33% considered solid on digital subtraction arthrography, 14% (P<0.001) were found to be loose at surgery.

As a result of high pressure within the small pseudocapsule a leakage of contrast may take place at the bone-cement interface [68]. Which led to false positive radiographic abnormalities "true loosening", where contrast was definitely seen at the bone-cement interface but at surgery the prosthesis was found not to be loose [64]. Some of the false negative results on arthrography are explainable on the basis of interpositional soft tissue (such as granulation tissue, fibrous tissue or pus) blocking passage of contrast into the metal-cement or cement-bone interface [74]. Another reason for false negative results can be large bursae or cavities around the prosthesis, which may hinder filling of the bone-cement or cement-metal interface due to reduced injection pressure.

Recent studies have shown a high rate of false positive scintigraphy related to increased activity, probably due to endosteal remodelling around the prosthesis and cement [75]. The decision to operate must be based on both clinical signs and symptoms and the results of the imaging studies. The macroscopic loosening of the prosthetic components, which will be done by, the orthopaedic surgeon must be by means of traction and rotation of the prosthesis at surgery [64].

It has been shown that digital subtraction arthrography is equal to or better than manual subtraction technique [76]. The results are immediately available as the technique allows real time review of injection dynamics. Data manipulation by pixel shift after the examination is often necessary despite immobilization of the leg with a strap and Polythene blocks. The enhanced contrast resolution of this technique also allows detection of even tiny amounts of contrast at the cement-bone or cement-prosthesis interfaces.

Ginai et. al. [64], was found that, the digital subtraction arthrography of the hip gives the best results in predicting loosening of acetabular and femoral components in the preoperative evaluation of patients with painful hip arthroplasty. Where it was quick and easy to perform, and causes little discomfort to the patient. The ability to view the subtraction images in real time and to manipulate the digital images after the arthrography was clear advantages of this method of examination. The disadvantage was a relatively long injection time, which necessitate prolonged patient immobilization. The background structures were subtracted from injected contrast material, and accurate imaging becomes virtually impossible [63].

Geiman et al. found signs of loosening in a plain film include widening of the zone of radiolucency, which frequently develops at the cement-bone interface. This zone was normally not wider than 1 to 2 mm and smooth in contour. In addition to widening, scalloping of the lucent zone as well as the development of a lucent zone at the prosthesis-cement interface may indicate a loosened component [10].

18

Another methods for evaluation the painful THA were Erythrocyte sedimentation rates and the white blood-cell counts [60].

Not all scanning methods tell us the true situation of the implant. However, the patient had a negative scan by Gallium, he had a positive technetium scan, and in both a loose prosthesis was found at the time of surgical exploration [60]. This mean that a false negative Gallium Scan.

A non-destructive detecting of bonded and debonded cement-metal interface of femoral prostheses cemented into fiberglass femur and femurs from human cadaver has been examined [77]. The time domain analysis of the reflected wave from the bonded surfaces, cement bonded to metal, exhibited a characteristic W-shaped reflection. Conversely, for debonded surfaces an opposite phase M-shaped waves were showed. However, if fluid is present between the cement and metal, the debonded interface appears bonded [77].

There are many invasive modalities have been used to investigate painful total hip prostheses, including clinical evaluation, haematology, plain radiographs, fluoroscopic manipulation, needle aspiration, and conventional arthrography, digital subtraction arthrography and radionuclide bone imaging [11, 50, 78-80]. There is not an invasive method for determination the loosening of hip prosthesis.

1.5 Objective and Structure of the Work

The aim of this work is to introduce a novel non-invasive method for determination the loosening of the hip prosthesis. Using an acoustic exciter the state of the prosthesis in vitro will be determined through its transfer function. Determination of the more sensitive resonance frequency to the loosening is one of our goals. Also, The simulation of the system by FIR-filter to extract the loosening conditions has been formulated.

The thesis is divided into the following parts:

Chapter 2 presents the theoretical background of the interaction between the acoustic waves and the multi-layered media. Also, damage detection in structures will be reviewed. The signal processing techniques in dynamic testing will be described. The description of the FIR filter technique and its impulse response will be presented.

Chapter 3 will describe the experimental set-up. Also, the construction of the thigh model, the coupling of acoustic waves and the capturing of output signal will be showed.

Chapter 4 presents the results of the dynamic testing of the model for secured and loosed prosthesis. It will be a discussion about the results to get the evaluation of the work. The frequency response function and its components will be examined for secure and loose cases of prosthesis. The effect of loosening on the resonance frequencies of the system will be studied. The using of Nyquist plot to extract the loosening conditions will be mentioned. The application of FIR-filter to approximate the real system and extract the loosening conditions will be reported.

Chapter 5 presents the main conclusions of this work.

CHAPTER 2

THEORETICAL BACKGROUND

Acoustics is a science that nowadays appears in a large number of domains. Really developed in town planning (for all audible noises), it also deals with domains which are much more disparate such as the biomedical domain (imaging processes), solid mechanics (characterisation of material properties), the sorting process on production lines, the military domain (sonar, radar), non destructive testing in general (which can cover a wide range of structures, from hull of a ship to a soldered spot on a printed circuit). It is however obvious that all those applications do not use the same working frequencies since one can go from the hertz (Hz) range in the building domain up to the tera-hertz (10^{12} Hz) range in electronics for example. The frequency range used in this thesis will vary from 0 Hz up to 25 kHz.

2.1 Ultrasonic Technique

Ultrasonic methods have been used for assessing comparative strength of materials, detecting flaws such as voids or cracks, and estimating member thickness. The inspection of materials by ultrasonic methods is well documented. Ultrasonic techniques involve the propagation and detection of mechanical vibrations that have interacted in some way with the structure under test. When the surface of a semi-infinite solid is excited by a time varying mechanical force, energy is radiated from the source as three distinct types of elastic wave propagation. The fastest of these waves has particle displacements in the direction of travel of the disturbance and is called the longitudinal, compression or P-wave. The compression wave velocity V_P is a function of the dynamic Young's modulus E, the Poisson's ratio ν, and the mass density ρ [81], and is given by:

$$V_p = \sqrt{\frac{E(1-\nu)}{\rho(1+\nu)(1-2\nu)}} \qquad (2.1).$$

The second fastest is the shear, transverse or S-wave, which has particle displacements perpendicular to the propagation direction. The shear wave velocity V_S is a function of the dynamic shear modulus G and ρ,

$$V_s = \sqrt{\frac{G}{\rho}} \qquad (2.2)$$

Young's and the shear moduli are related by

$$E = 2G(1+\nu) \qquad (2.3)$$

Compression and shear wave velocities are theoretically interrelated by Poisson's ratio ν, which can be expressed as

$$v = \frac{0.5 - (V_s / V_p)^2}{0.1 - (V_s / V_p)^2}$$ (2.4)

The compression and shear waves propagate throughout the material in all directions. The third type of wave motion produced travels along the surface and has elliptical particle motion, where the component of displacement normal to the surface is greater than the component in the direction of wave propagation. The velocity, V_R, of this surface wave, known as the Rayleigh wave, in simplified form is given by

$$V_R = A V_s$$ (2.5)

where A is a function of v and V_S. The ratio of V_R / V_S increases as Poisson 's ratio increases.

Ultrasonic inspection of materials is basically the evaluation of one or more of these wave velocities. Since wave velocity is a direct indication of stiffness of the material, a higher wave velocity is associated with higher stiffness. When an ultrasonic wave is incident on a plane boundary between two media, some of the ultrasonic energy is transmitted through the boundary and some is reflected. The percentages of energy transmitted and reflected depend on the specific acoustic impedance, Z,

$$Z = \rho V$$ (2.6)

where ρ is the density of the material and V is the velocity of the wave. For two materials of different acoustic impedances Z_1 and Z_2 the percentage energy transmitted (E$_T$) is given by E_T [82] as:

$$E_T = \frac{4Z_1 Z_2}{(Z_1 + Z_2)} X 100$$ (2.7)

and the reflected energy E_R, by:

$$E_R = \left\{ \frac{Z_1 - Z_2}{Z_1 + Z_2} \right\}^2 X 100$$ (2.8)

For amplitude values the square root of the above equations are taken. The equations are valid for both compression and transverse waves, but as a transverse wave cannot be sustained in a liquid, a transverse wave at normal incidence is always completely reflected at a solid/liquid or solid/gas interface. As acoustic energy spreads out into a medium so the magnitude of the disturbance at the wave front decreases by some function to satisfy the principle of energy conservation.

2.1.1 Pulse Velocity

Ultrasonic inspection technique involves the generation of a pulse, transmitting this to the medium, receiving and amplifying the pulse and measuring and displaying the time taken. In general, repetitive pulses are generated electronically and transmitted into mechanical wave energy by a piezoelectric transducer. Due to the attenuation effects of material, through-transmission utilising narrow band (minimal damping) transducers are preferred, so as to

maximise the received signal. Good acoustic coupling (maximised transfer coefficient) between material surface and transmitting transducer is provided by a suitable medium such as ultrasonic's gel. A similar receiving transducer is coupled a known distance d away from the transmitter, and upon reception, the mechanical energy is converted back into electric pulses. An electrical timing device measures the interval between onset of excitation and reception and displays the signal transit time t .The velocity V_L is then calculated from the relationship

$$V_L = \frac{d}{t}$$
(2.9).

2.1.2 Acoustic Wave Propagation In Multi-Layered Media

2.1.2.1 Wave Parameters

The fundamental feature of waves is their capability of carrying energy and information over long distances. The velocities, which are of interest, are the phase velocity, the group velocity and the energy velocity. The phase velocity is the velocity at which the wave fronts or crests travel. The group velocity is the derivative of the frequency wave-number dispersion relation, $V_g = \partial \omega / \partial k_x$ (where ω is the angular frequency, and k_x is the wave-number in the direction of propagation) and the energy velocity is the velocity at which the wave carries its potential and kinetic energy along the structure.

The main equations of the linear acoustic theory are presented [83-85] and the particle displacement field, the polarizations and the dispersion equations of such waves are examined. Multilayered plates such as adhesive joints and diffusion bonded joints are of great interest in nondestructive testing, and Lamb wave properties could potentially be used to detect defects including poor cohesion and poor adhesion, as considered by a number of authors [85].

Ultrasonic testing is particularly attractive due to its relatively low cost, rapid inspection and that it is non-destructive [86]. One being that a viscous couplant must be applied to the faces of the transducers to achieve good acoustic coupling.

The propagation of an acoustic wave through a medium can be characterized by certain parameters, which periodically vary with both space and time [87]. The propagation of acoustic wave in a multi-layered medium can be studied by solving the wave equation with the appropriate boundary conditions [85, 88-89], using of input impedance approach, analogous to transmission line theory or considering the multiple reflections which occur at each interface [85]. The transfer and longitudinal waves appear at each interface of the multi-layered medium if the acoustic wave incident at an oblique angel [90]. Other wave modes may also be produced, such as lamb waves, which have a different wave velocities and different rates of absorption in the layers. Testing may take place at normal incidence and in fact this arrangement is favoured due to the ease of practical implementation. Particle displacement, ξ, is the amount of displacement of a particle from its mean position within the medium under the action of an acoustic pressure. Acoustic pressure,p, is the change of pressure from the mean value and is equal to the difference between the instantaneous pressure,P, and the hydrostatic pressure,p_o.

Particle velocity, u, is the velocity of a particle in the medium and is given by the time derivative of the particle displacement

$$u = \frac{d\xi}{dt}$$ (2.10)

The propagation velocity, c, is the velocity with which the acoustic wave passes through the medium, and is related to the mechanical constants of the medium. The characteristic property of a plane wave is that parameters such as acoustic pressure and particle displacement have common phases and amplitudes at all points on any given perpendicular to the direction of propagation of the wave. If the acoustic pressure is independent of the y- and z-directions, the general wave equation reduces to

$$\frac{\partial^2 p}{\partial^2 t} = c^2 \frac{\partial^2 p}{\partial^2 x}$$ (2.11)

This equation has a general solution of the form

$$p = F_1(ct - x) + F_2(ct + x)$$ (2.12)

which represents two plane acoustic disturbances travelling in the positive and negative x-directions respectively, each with a velocity, c.

The simple harmonic form of the solution to Eq. (2.12) can be written

$$p = A e^{j(\omega t - kx)} + B e^{j(\omega t + kx)}$$ (2.13)

For non-linear responses real parts of Eq. (2.13) must be used

$$p = A \cos(\omega t - kx) + B \cos(\omega t + kx)$$ (2.14)

where A and B represent the pressure amplitudes of two plan waves of angular frequency, ω, travelling in opposite directions and the wave number k is defined as

$$k = \frac{\omega}{c} = \frac{2\pi}{\lambda}$$ (2.15)

The relationship between pressure and the particle velocity of the plan wave can be expressed as

$$\frac{-\partial p}{\partial x} = \rho_o \frac{\partial u}{\partial t}$$ (2.16)

where ρ_o is the mean density of the medium.

Integrating the expression $\partial u / \partial t$ with respect to the time yields the particle velocity

$$u = \int \frac{\partial u}{\partial t} dt = \frac{-1}{\rho_o} \int \frac{\partial p}{\partial x} dt$$ (2.17)

24

and enable the coefficients A and B to be determined

$$\int \frac{\partial p}{\partial x}\, dt = \frac{-K}{\omega} A\, e^{j(\omega t - kx)} + \frac{K}{\omega} B\, e^{j(\omega t + kx)} \tag{2.18}$$

The instantaneous particle velocity is then

$$u = \frac{A}{\rho_o c}\, e^{j(\omega t - kx)} - \frac{B}{\rho_o c}\, e^{j(\omega t + kx)} \tag{2.19}$$

Finally it is a useful to define a quantity termed the 'specific acoustic impedance'

$$\bar{z} = \bar{p}/\bar{u} \tag{2.20}$$

Where $\bar{p}$ and $\bar{u}$ are not in the same phase, Thus from Eq. (2.20)

$$\bar{z} = \rho_o c \left\{ \frac{A\, e^{-jkx} + B\, e^{jkx}}{A\, e^{-jkx} - B\, e^{jkx}} \right\} \tag{2.21}$$

For the plan progressive waves, the phase of p and u is identical and

$$z = \rho_o c \tag{2.22}$$

The product $\rho_o c$ is generally given the units of kg/m^{2}s and called the 'characteristic acoustic impedance'.

2.1.2.2 Solution of the Wave Equation

If a weave is incident on a multi-layered medium consisting of $(n-1)$ layers, as shown in Fig. 2.1, then at the first interface (between Z_1 and Z_2) it will be partially reflected and transmitted. The transmitted wave will give rise to multiple reflections in the first layer, which in turn gives rise to multiple reflections in the following $(n-2)$ layers. After a steady state condition has been reached, it is sufficient to suppose that there is only one wave in each direction in each layer and only one wave in the final medium, Z_{n+1}.

All the waves will have the same frequency, but as a result of the difference between the velocities in each layer, the values of the wave numbers, k, will be different. For only one layer, as shown in Fig. 2.2, the system of five waves may be written

$$p_1 = A_1\, e^{j(\omega t - k_1 x)} + B_1\, e^{j(\omega t + k_1 x)}$$

medium1

$$u_1 = \left\{ A_1\, e^{j(\omega t - k_1 x)} - B_1\, e^{j(\omega t + k_1 x)} \right\} \bigg/ Z_1$$
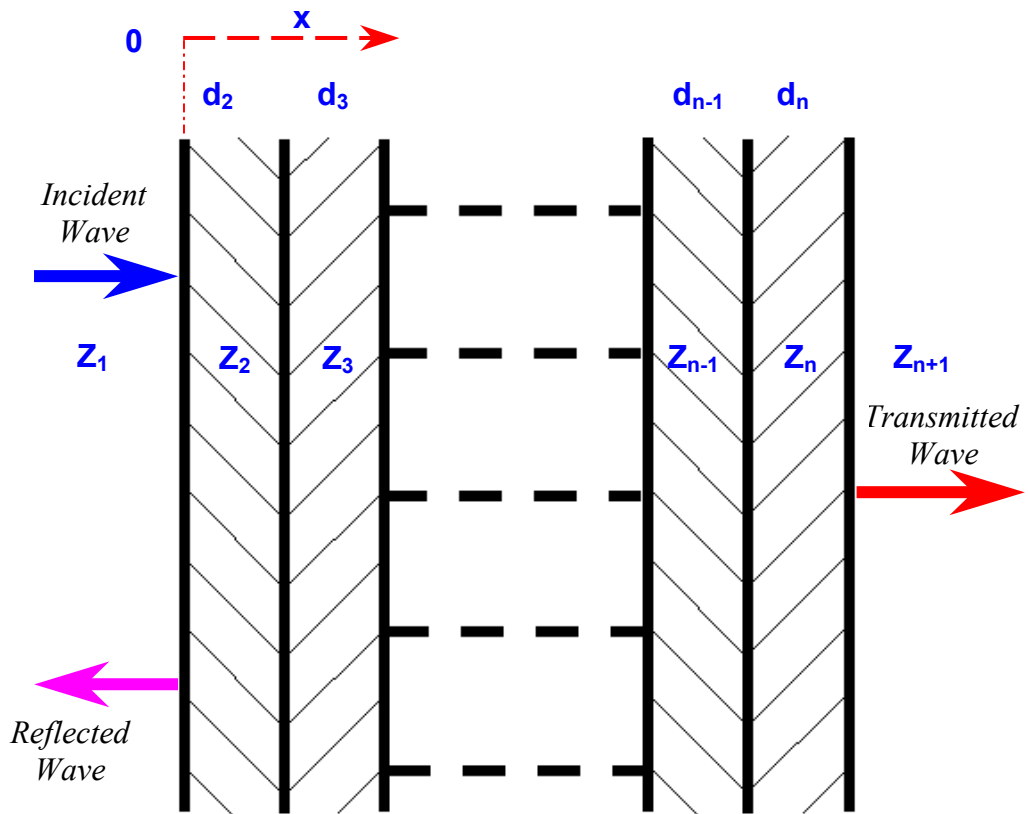
Fig. 2.1   Wave propagation in a multi-layered medium.
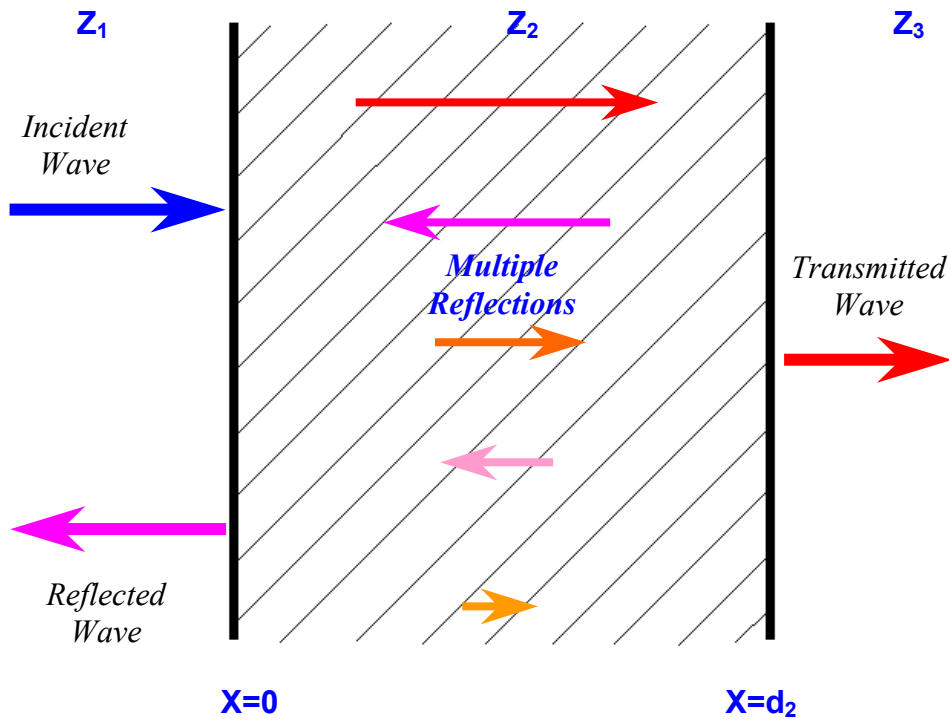
Fig. 2.2   Wave propagation in a single layer.

26

$$p_2 = A_2\, e^{j(\omega t - k_2 x)} + B_2\, e^{j(\omega t + k_2 x)}$$

medium2 (2.23)

$$u_2 = \left\{ A_2\, e^{j(\omega t - k_2 x)} - B_2\, e^{j(\omega t + k_2 x)} \right\} \Big/ Z_2$$

$$p_3 = A_3\, e^{j(\omega t - k_3(x - d_2))}$$

medium3

$$u_3 = \left\{ A_3\, e^{j(\omega t - k_3(x - d_2))} \right\} \Big/ Z_3$$

The conditions on pressure and particle velocity must now be satisfied at both boundaries, so, at $x = 0$, continuity of pressure gives

$$A_1 + B_1 = A_2 + B_2 \tag{2.24}$$

And continuity particle velocity gives

$$\left\{ A_1 - B_1 \right\} / Z_1 = \left\{ A_2 - B_2 \right\} \Big/ Z_2 \tag{2.25}$$

In a similar manner, for $x = d_2$,

$$A_3 = A_2\, e^{-jk_2 d_2} + B_2\, e^{jk_2 d_2}$$

(2.26)

$$A_3 / Z_3 = \left\{ A_2 e^{-jk_2 d_2} + B_2 e^{jk_2 d_2} \right\} \Big/ Z_2$$

Equation (2.26) can then be solved to give any of the waves in terms of the incident wave. The writing of the wave conditions in the first layer (Eq. (2.23)) in matrix form produces the expression.

$$\begin{bmatrix} p_2 \\ u_2 \end{bmatrix} = \begin{bmatrix} e^{-jk_2 x} & e^{jk_2 x} \\ e^{-jk_2 x}/Z_2 & -e^{jk_2 x}/Z_2 \end{bmatrix} \begin{bmatrix} A_2\, e^{j\omega t} \\ B_2\, e^{j\omega t} \end{bmatrix} \tag{2.27}$$

Pressure and particle velocity are continuous at the boundaries and the specific values for the single layer can be found by substituting the values $x = 0$ and $x = d_2$ into the general matrix equation. So, at $x = 0$,

$$\begin{bmatrix} p_0 \\ u_0 \end{bmatrix} = \begin{bmatrix} 1 & 1 \\ 1/Z_2 & -1/Z_2 \end{bmatrix} \begin{bmatrix} A_2 e^{j\omega t} \\ B_2 e^{j\omega t} \end{bmatrix} \tag{2.28}$$

And at $x = d_2$

$$\begin{bmatrix} p_{d_2} \\ u_{d_2} \end{bmatrix} = \begin{bmatrix} e^{-jk_2 d_2} & e^{jk_2 d_2} \\ e^{-jk_2 d_2}/Z_2 & -e^{jk_2 d_2}/Z_2 \end{bmatrix} \begin{bmatrix} A_2 e^{j\omega t} \\ B_2 e^{j\omega t} \end{bmatrix} \tag{2.29}$$

The term $A_2 e^{j\omega t}$ and $B_2 e^{j\omega t}$ is common to both equations (2.28) and (2.29), it can be eliminated to give

$$
\begin{bmatrix} p_0 \\ u_0 \end{bmatrix} = \begin{bmatrix} 1 & 1 \\ 1/Z_2 & -1/Z_2 \end{bmatrix} \begin{bmatrix} e^{-jk_2 d_2} & e^{jk_2 d_2} \\ e^{-jk_2 d_2}/Z_2 & -e^{jk_2 d_2}/Z_2 \end{bmatrix}^{-1} \begin{bmatrix} p_{d_2} \\ u_{d_2} \end{bmatrix}
\tag{2.30}
$$

Which simplifies to

$$
\begin{bmatrix} p_0 \\ u_0 \end{bmatrix} = \begin{bmatrix} \cos k_2 d_2 & j Z_2 \sin k_2 d_2 \\ j \sin(k_2 d_2)/Z_2 & \cos k_2 d_2 \end{bmatrix} \begin{bmatrix} p_{d_2} \\ u_{d_2} \end{bmatrix}
\tag{2.31}
$$

The matrix relating p_0 and u_0 to p_{d_2} and u_{d_2} is called the 'characteristic matrix' of the layer and relates to its physical properties.

If more than one layer is considered, then there is no reason to repeat the algebra because every bounded layer has a characteristic matrix of the same form. The general situation thus becomes

$$
\begin{bmatrix} p_0 \\ u_0 \end{bmatrix} = \begin{bmatrix} \cos k_2 d_2 & j Z_2 \sin k_2 d_2 \\ j(\sin k_2 d_2)/Z_2 & \cos k_2 d_2 \end{bmatrix} \cdots \begin{bmatrix} \cos k_n d_n & j Z_n \sin k_n d_n \\ j(\sin k_n d_n)/Z_n & \cos k_n d_n \end{bmatrix} \cdots \begin{bmatrix} p_{d_{n+1}} \\ u_{d_{n+1}} \end{bmatrix}
\tag{2.32}
$$

Where,

$$
\begin{aligned}
p_0 &= A_1 e^{j\omega t} + B_1 e^{j\omega t} \\
u_0 &= (A_1 e^{j\omega t} - B_1 e^{j\omega t}) \Big/ Z_1 \\
p_{d_{n+1}} &= A_{n+1} e^{j\omega t} \\
u_{d_{n+1}} &= A_{n+1} e^{j\omega t} / Z_{n+1}
\end{aligned}
$$

The form of these matrices is suitable for analysis by computer.

2.1.2.3 Ultrasound Transmission Across an Interface

The classical analysis considers the interaction of a normally incident plane wave with a plain boundary between two media. The normal incidence transmission coefficient is derived here following a similar approach to ref. [91].

Consider two material shown in Fig. 2.3 of cross sectional area A_o where materials of acoustic impedance Z_1 and Z_2 are connected perfectly at the interface $x=0$. The boundary conditions at the interface are that the pressure should be balanced and that the displacement be continuous giving

28
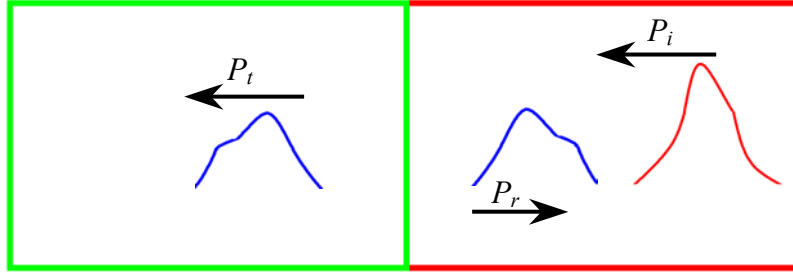
Fig. 2.3   Ultrasound transmission across a perfect interface.

$$P_i + P_r = P_t \tag{2.33}$$

and

$$y_i + y_r = y_t \tag{2.34}$$

The normal pressures of the incident, reflected and transmitted waves as a function of time t and distance propagated x can be given respectively as

$$P_i e^{j(\omega t - k_1 x)}$$
$$P_r e^{j(\omega t + k_1 x)} \tag{2.35}$$
$$P_t e^{j(\omega t - k_2 x)}$$

where the wave number k is the ratio of frequency ω over velocity c given as

$$k_n = \frac{\omega}{c_n} \tag{2.36}$$

the sound velocity c which is related to Young's modulus E and the material density ρ by

$$c_n = \sqrt{\frac{E_n}{\rho_n}} \tag{2.37}$$

from which the acoustic impedance is given as

$$Z_n = C_n \rho_n \tag{2.38}$$

For a linear system Hooke's law relates the pressure to the displacement by

$$P = -E \frac{\delta}{\delta x} y \tag{2.39}$$

which in terms of displacement is written as

$$y = -\frac{1}{E} \int P dx \tag{2.40}$$

Substituting Eq. (2.40) into the displacement boundary condition given in Eq. (2.34) and applying the pressure given in Eq. (2.35) gives

$$\frac{1}{E_1}\left[\int P_i e^{j(\omega t - k_1 x)} dx + \int P_r e^{j(\omega t + k_1 x)} dx\right] = \frac{P_t}{E_2}\int P_t e^{j(\omega t - k_2 x)} dx \qquad (2.41)$$

$$\frac{1}{E_1}\left[\frac{P_i e^{j(\omega t - k_1 x)}}{-jk_1} + \frac{P_r e^{j(\omega t + k_1 x)}}{jk_2}\right] = \frac{P_t}{E_2}\frac{e^{j(\omega t - k_1 x)}}{-jk_2} \qquad (2.42)$$

At the interface, by setting $x=0$, allows the factorisation of the exponential terms such that Eq. (2.42) reduces to

$$P_i - P_r = P_t \frac{E_1 k_1}{E_2 k_2} \qquad (2.43)$$

Substituting Eq. (2.33) and Eq. (2.38) into equation gives

$$2P_i = P_t\left(1 + \frac{Z_1}{Z_2}\right) \qquad (2.44)$$

The normal transmission coefficient T_p for the perfect interface is the ratio of transmitted over incident pressure, which form Eq. (2.44) gives the classical solution as

$$T_p = \frac{2Z_2}{Z_1 + Z_2} \qquad (2.45)$$

Now consider an imperfect interface at $x=0$ as shown in Fig. 2.4 where the rough faces of the two material of cross sectional area A_o are loaded against each other. The transmission across the interface is not only dependent on the acoustic impedances of the two materials but also on the degree of contact. From the friction studies, the true area of contact A_t can be considered as the sum of points where the atoms on one face are within atomic distance of the atoms of another. For dry coupled interfaces the areas not in contact are described as air gaps. For transmission across steel interfaces Kendal and Tabor, [91], have reported that where the surfaces are separated by more than 10 nm the transmission of a 200 kHz signal across the air gap is insignificant. It is for this reason that some form of liquid couplant, with much higher impedance to air, is often used to fill the air gaps to allow a significantly greater portion of signal energy to transmit across the interface. The true area of contact will be a function of the material properties, applied load, the geometry of the surfaces and the way the individual asperities deform.
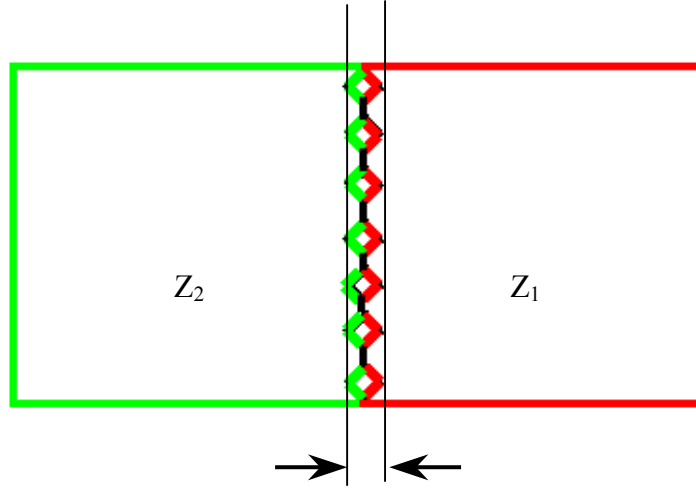
Fig. 2.4   Contact of an Imperfect surface.

To predict the transmission across an imperfect interface we will follow references [92, 93]. The derivation begins by firstly considering the static case where the application of the stress σ results in the closure of the interface, the relative displacement of two points in the far field on opposite sides of the interface can be given as

$$\frac{\Delta}{2} = \frac{1}{2}\left(\Delta_P + \Delta_I\right)$$
(2.46)

where Δ_P is the displacement for a perfect interface and Δ_I represents the deformation in the vicinity of the imperfect interface. It follows that we could approximate the interface by a spring of stiffness per unit area (N/m^3) given by

$$k = \frac{\sigma}{\Delta_I}$$
(2.47)

which when used to join the faces of the two bars together will reproduce the static displacement. For the dynamic case, if the signal wavelength is large compared to the individual contact areas then the dynamic response is said to be related to the static response.

The approach commonly known as the Quasi static model (QSM) where the spring stiffness for the QSM is again given by Eq. (2.47), and it may have a mass term in order to include the inertial effects [93].

The surface roughness can be approximated as a planer array of cracks. It is seen that for signal wavelengths which are large compared to such planer type defects the mass is negligible [93].

By considering that the contacts interact with one another, then following [91], the contacts can be lumped such that the interface can be approximated as a contriction between the two bars as shown in Fig. 2.5.
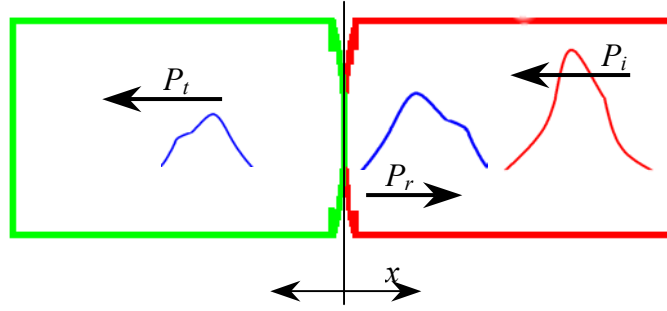
Fig. 2.5   Ultrasonic Transmission across an imperfect interface approximated as a
constriction.

If P_t is the pressure of the wave transmitted from left to right this exerts a force P_tA_0 on the interface and displacement in that direction of P_tA_0/S. The stiffness S in this case hase the more familiar units of force per unit displacement (*N/m*) and is related to Eq. (2.47) by

$$\frac{S}{A_0} = k \tag{2.48}$$

The boundary conditions for the imperfect interface are again that there should be equal pressures at the interface

$$P_i + P_r = P_t \tag{2.49}$$

Due to the deformation in the vicinity of the constriction the displacements are discontinuous at the interface such that the boundary condition is given as

$$y_i + y_r = y_t + P_t\frac{A_0}{S} \tag{2.50}$$

The solution for the normal incidence transmission coefficient for the imperfect interface is solved by the same procedure as for the perfect interface. Substituting Eq. (2.40) into Eq. (2.50) and arriving at a similar position to Eq. (2.43) we get

$$\frac{P_i}{Z_1} - \frac{P_r}{Z_1} = \frac{P_t}{Z_2} + P_t\frac{j\omega A_0}{S} \tag{2.51}$$

substituting the boundary condition Eq. (2.49) into Eq. (2.51) and rearranging as the ratio of transmitted pressure over incident gives

$$T_1 = \frac{2Z_2}{(Z_1 + Z_2) + \dfrac{j\omega Z_1 Z_2 A_0}{S}} \tag{2.52}$$

If the stiffness k is substituted for S/A_0 this gives the standard representation attributed to [92], but the form of Eq. (2.52) is preferred since it will useful later. A spring stiffness of zero would approximated a slack interface for which the magnitude of Eq. (2.52) would be zero. A perfect interface would be approximated by an infinitely stiff spring which would

result in a negligible imaginary term reducing Eq. (2.52) to Eq. (2.45). The efficiency of an interface can be given by the fractional transmission, which is the ratio of the transmission for an imperfect interface over that for a perfect one given by

$$T_f = \frac{T_1}{T_p} \qquad (2.53)$$

Substituting Eq. (2.52) and Eq. (2.45) in Eq. (2.53) gives

$$T_f = \frac{1}{1 + \dfrac{j\omega Z_1 Z_2 A_0}{S(Z_1 Z_2)}} \qquad (2.54)$$

For low values of transmission where $\left| jx \right| \gg \left(T_f^{-1} - 1 \right)$ the modulus can be approximated by

$$\left| T_f \right|_{<0.3} \approx \frac{S(Z_1 + Z_2)}{\omega Z_1 Z_2 A_0} \qquad (2.55)$$

Thus it follows that for low levels of contact the classical solutions predict that transmission across an imperfect interface will be proportional to the interfacial stiffness. It also follows from Eq. (2.55) that transmission is inversely proportional to frequency.

2.2 Damage Detection in Structures

The health-monitoring problem of an object consists of obtaining information about the existence, location, and extent of damage in the structure using non-destructive methods. One method is to monitor and interpret changes in structural dynamic measurements based on experimental modal analyses and signal-processing techniques. The extraction of the natural frequency and mode shape of a vibrating structure can be carried out using modern vibration testing equipment and instrumentation. The modal and structural dynamic data can then be utilized for health monitoring and operational life assessment without requiring the structure to be dismantled [94].

Damage detection technique has been studied by many researchers [95-99]. This technique is based on comparing the frequency changes obtained using experimental data collected from the structure with the sensitivity of the modal parameters obtained from an analytical model of the structure. The sensitivity of the natural frequencies of the structure to changes in the stiffness, mass, and damping are calculated using a finite element analysis.

Damage detection algorithms may be split into several categories based on whether they work in the frequency or modal domains and whether they adjust the mass and stiffness matrices directly (direct methods) or make parametric changes to the model (indirect or parametric methods) [97]. The presence of damage in a structure can be detected from the changes in the natural frequencies. It is difficult to determine the location of the damage. This is because damage at two different locations may produce the same amount of frequency change [100]. In this paper, the measured frequency response functions (FRFs) were used for detecting the structural damage using techniques based on the physical meaning of the stiffness matrices. The basis for that method is that damage produces a decrease in the

dynamic stiffness *EI*. A finite element method was used to simulate the measured FRFs, when a structure contains damage. The measured FRF differs from simulated FRF due to the stiffness reduction. Hence, the damage can be found by iterations through matching the measured FRF to the simulated FRF as shown in Fig. 2.6.
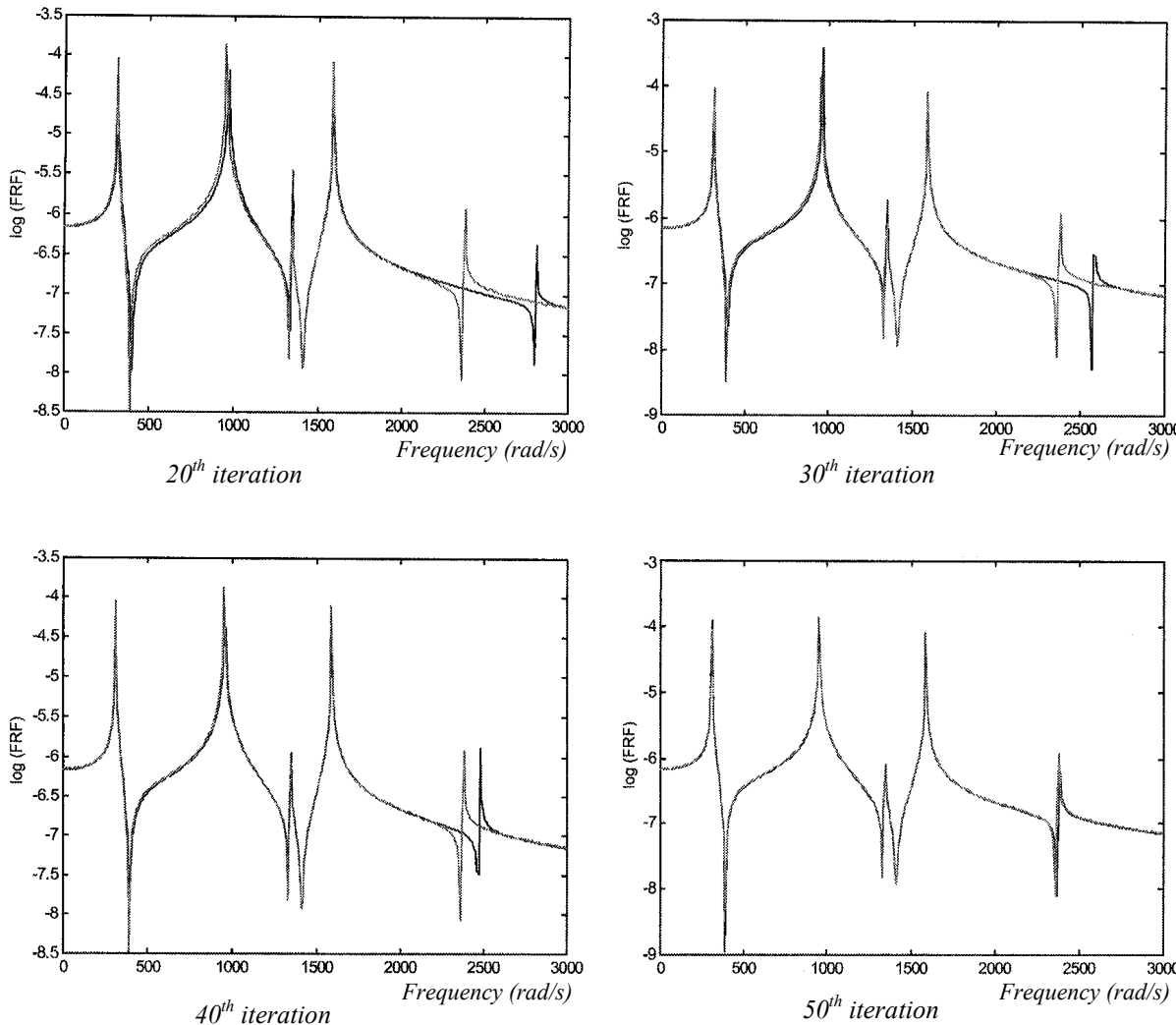
Fig. 2.6   FRFs at different iteration times, from [100].

Many research efforts have focused on the development and application of eigenvalue and eigenvector sensitivity analysis. For example, a complete formula for first order eigenvalue and eigenvector sensitivities was derived for standard eigenvalue problems and then applied them to improve an approximate set of eigenvalues and eigenvectors [101]. The theory was later extended to the case of generalized symmetric eigenvalue problems by considering changes of physical parameters in the mass and the stiffness matrices [102]. A general method for using limited amounts of data was developed to estimate both FRF sensitivities and eigenvalue/eigenvector sensitivities from vibration test data [103]. The work was based on earlier observations [104-106]. Design sensitivities were calculated directly from measured data and the relationship between the FRF sensitivities and eigenvalue and eigenvector sensitivities was established. A modal acceleration method for the frequency responses and a double-modal acceleration method for their sensitivities in undamped systems were also derived [107]. Similar methods for viscously damped systems were derived [108]. The two methods were based on a hybrid expansion, which involved a power series expansion and modal superposition, of the flexibility matrix. An empirical sensitivity technique has been

used for determine the system-level vibration [109]. In this work, embedded sensitivity functions ware derived in terms of FRFs because these ware commonly measured and computed analytically to diagnose noise and vibration problems in many applications. These sensitivity functions indicate the variation in FRF magnitude and phase with respect to perturbations in mass, damping, and stiffness parameters. The term 'embedded' was used to refer to the sensitivity functions because they are explicit functions of the FRFs; thus the individual mass, damping, and stiffness parameters are not needed to compute the sensitivity functions in contrast to the requirement for a full analytical or numerical model in typical parametric design studies. Note that the resulting sensitivity function can be expressed explicitly in terms of the FRF and does not require knowledge of any of the system parameters within the model. The only requirement in taking the partial derivatives was that the parametric form of the FRF in terms of the parameters be known.

2.2.1 Ultrasonic spectroscopic system

There are many possible design for an ultrasonic spectrum analysis system [110], each contains provisions for
(1) generating ultrasound,
(2) receiving a portion of the ultrasound which has interacted with the material under study, and
(3) analysing the received wave to determine the magnitude (and sometimes phase) of the ultrasound at a number of frequencies.

Figure 2.7 illustrates the major components of the generalized spectroscopic system. in this common system configuration (Fig. 2.7), an electrical waveform generated by the transmitter is applied to the transmitting transducer. Conversion of the electrical energy occurs within the transducer, producing an ultrasonic wave. As the wave propagates through the material being studied, interactions of the ultrasonic energy with the material alter the amplitude, phase, and direction of the wave. A receiving transducer intercepts a portion of the ultrasonic energy and conversion occurs from mechanical to electrical energy. Because the electrical signal is usually small, an amplifier is used to increase its amplitude. The purpose of the analysis system, which follows the amplifier is to sort out the magnitude and timing of the ultrasonic interactions (within the material) and present amplitude and phase spectra.
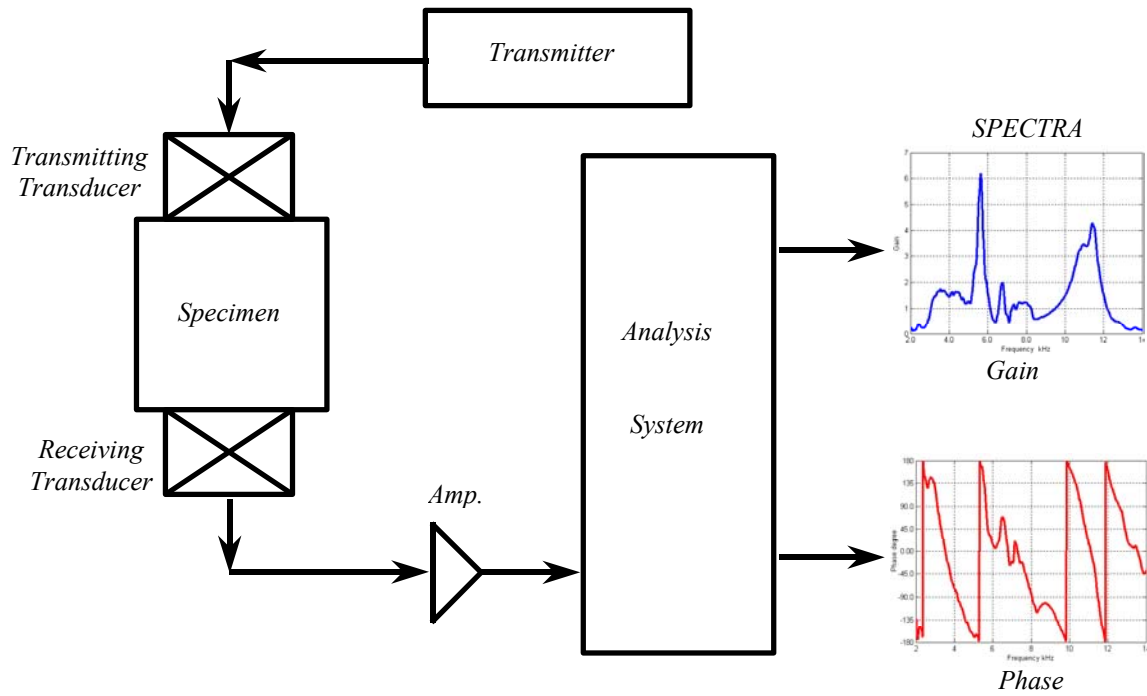
Fig. 2.7   Generalized ultrasonic spectroscopic System.

Each component of the system is considered a linear time –invariant (*LTI*)system. The behaviour of a linear time invariant (*LTI*) system is completely described by its impulse response (in the time domain) or its frequency response (in frequency domain). The two descriptions of system response are equivalent and are linked by the following relations:

$$H(f) = \int_{-\infty}^{\infty} h(t)e^{-j2\pi ft} \, dt \qquad (2.66)$$

$$h(t) = \frac{1}{2\pi} \int_{-\infty}^{\infty} H(f)e^{j2\pi ft} \, dt \qquad (2.67)$$

where *h(t)* is the impulse response and *H(f)* is the frequency response (transfer function). The responses *h(t)* and *H(f)* are said to form a Fourier transform pair.

The quantity *H(f)* is a complex number, that is ,

$$H(f) = \mathrm{Re}\{H(f)\} + j\,\mathrm{Im}\{H(f)\} \qquad (2.68)$$

and its magnitude spectrum is defined as

$$|H(f)| = \sqrt{\mathrm{Re}^2\{H(f)\} + j\,\mathrm{Im}^2\{H(f)\}} \qquad (2.69)$$

and the phase spectrum is

$$\angle H(f) = \tan^{-1} \frac{\mathrm{Im}\{H(f)\}}{\mathrm{Re}\{H(f)\}} \qquad (2.70)$$

For a linear time-invariant system the input and output are related as shown in Fig. 2.8.

Time Domain
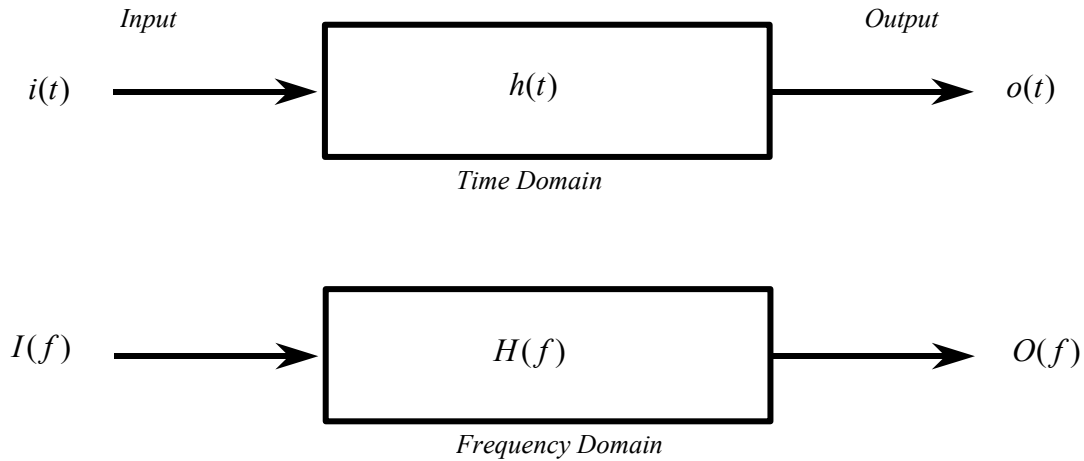
Frequency Domain

Fig. 2.8   Equivalent representation of a linear time invariant system.

The output *o(t)* is found by convolving the input *i(t)* with the impulse response of the system *h(t)*. That is,

$$o(t) = i(t) \otimes h(t) = \int_{-\infty}^{\infty} i(t')h(t-t')dt \tag{2.71}$$

convolution may also be carried out in the frequency domain, and the mathematics is reduced to a multiplication of two complex numbers. The output is

$$O(f) = \operatorname{Re}\{O(f)\} + j\operatorname{Im}\{O(f)\} = I(f)H(f) \tag{2.72}$$

$$\begin{aligned} O(f) = \ & \operatorname{Re}\{I(f)\}\operatorname{Re}\{H(f)\} - \operatorname{Im}\{I(f)\}\operatorname{Im}\{H(f)\} \\ & + j\{\operatorname{Re}\{I(f)\}\operatorname{Im}\{H(f)\} + \operatorname{Re}\{H(f)\}\operatorname{Im}\{I(f)\}\} \end{aligned} \tag{2.73}$$

At each frequency the output is just the product of the input and system frequency response at that frequency.

Figure 2.9 shows a block diagram of an ultrasonic spectroscope modelled as an *LTI* system. The signal of interest is an electrical waveform, which represents the propagation of the ultrasonic wave through the coupling medium and the material under study.

In general, the time-domain representation of the signal is that which is monitored; the analysis subsystem provides the transformation to the frequency domain. The natural selection of the independent variable through system components where an ultrasonic wave propagates is the distance *(x)*. Distance may be converted to time if the velocity of wave travel is known. System components in which ultrasonic wave propagate are seen with the impulse responses in terms of time-varying quantities and distance. Again recall that the transfer function (as well as the output, $V_2(f)$) are complex quantities.

$v_1(t)$	Transmitter (Pulser)	$V_1(f)$
$b_1(t)$	Electrical Network	$B_1(f)$
$x_1(t)$	Transmitting Transducer	$X_1(f)$
$c_1(t)$	Mechanical Coupling	$C_1(f)$
$h(t)$	Medium Under Test	$H_1(f)$
$c_2(t)$	Mechanical Coupling	$C_2(f)$
$x_2(t)$	Receiving Transducer	$X_2(f)$
$b_2(t)$	Electrical Network	$B_2(f)$
$a(t)$	Amplifier	$A(f)$
$g(t)$	Analog Gate	$G(f)$
$d(t)$	Digitizer	$D(f)$
$v_2(t)$	Output	$V_2(f)$
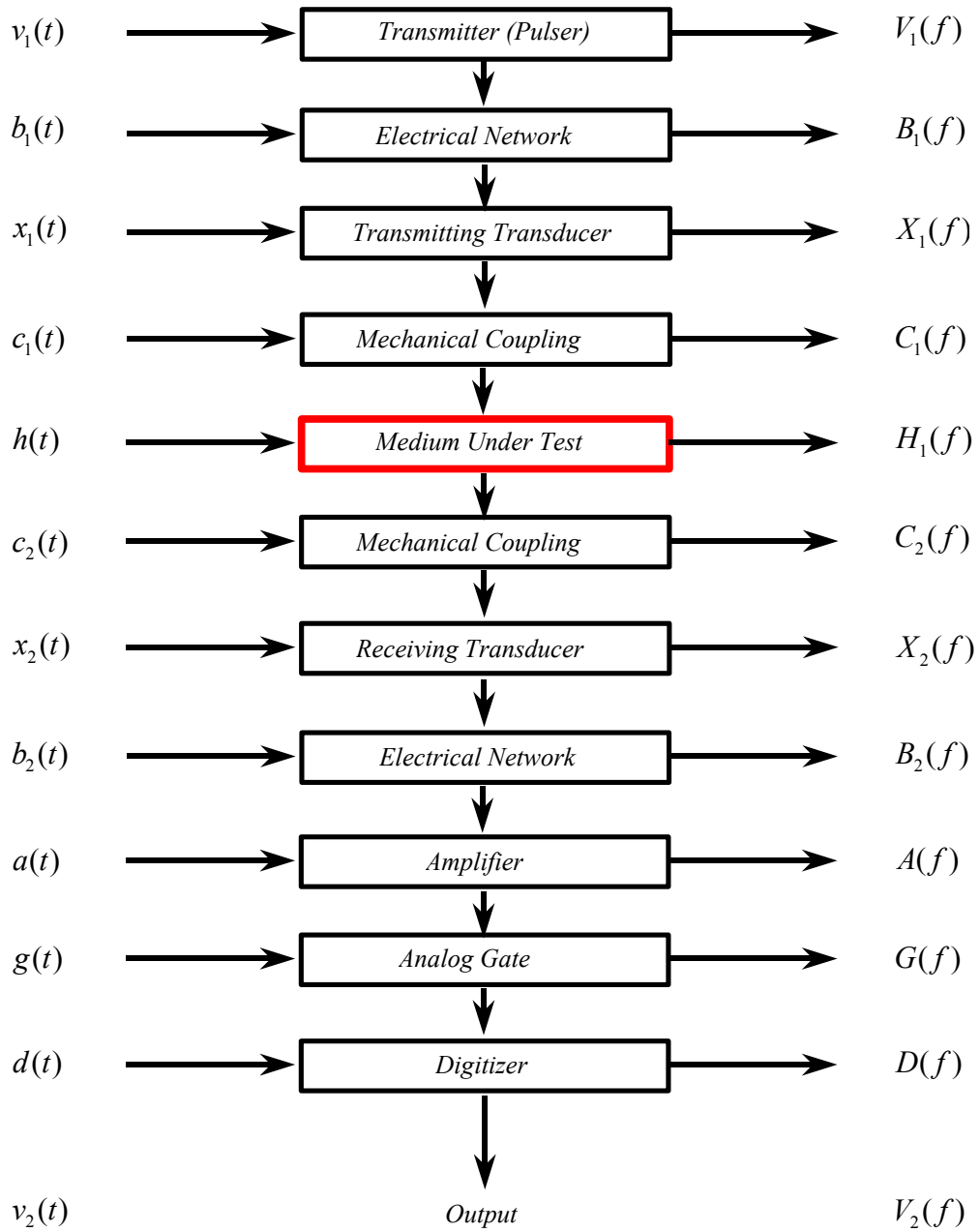
Fig. 2.9   Elements of an ultrasonic spectroscopic system modelled as a LTI system, from [110].

An ideal spectroscopic system would emit ultrasonic pulses whose spectrum is uniform over a large of frequencies (e.g., 20kHz to 500 MHz). For the model in Fig 3 this is implies

$$V_1(f)B_1(f)X_1(f)C_1(f) = T(f) = const. \tag{2.74}$$

for the frequency range. A receiving section whose is uniform over the same frequency range is also desirable. That is,

$$V_2(f)B_2(f)X_2(f)C_2(f) = R(f) = const. \tag{2.75}$$

If the ideal system just described were used to test a material, with impulse response *h(t)*, the output of the spectrum analysis ($V_2(f)$) would be *H(f)* multiplied by constant. However, such an ideal spectroscopic system is not strictly realizable over the wide frequency range mentioned earlier.

The *LTI* provides a method of correcting for the nonuniform frequency response in nonideal systems, if the transfer functions of the system components are known. Assume an ultrasonic detector is available whose response versus frequency is known. Then if the detector is placed such that it receives the ultrasonic wave produced by the transmitting transducer, the detector output will be *T(f)*. Coupling the transmission section of the spectroscope through a loos less, nondispersive medium (*H(f)=1*) to the receiver will produce output $V_2(f)$. The frequency response of these components are related by

$$T(f)H(f)R(f) = V_2(f) \tag{2.76}$$

or

$$R(f) = \frac{V_2(f)}{T(f)H(f)} \tag{2.77}$$

since *H(f)=1*

$$R(f) = \frac{V_2(f)}{T(f)} \tag{2.78}$$

The system transmitter and receiver, thus fully characterized by their frequency responses, can be used to analyze materials having an unknown transfer function (*H(f)*).

Suppose spectrum $T(f)$ was transmitted into the medium under test and $V_2(f)$ was the output of the spectroscopic system as shown in Fig. 2.10.

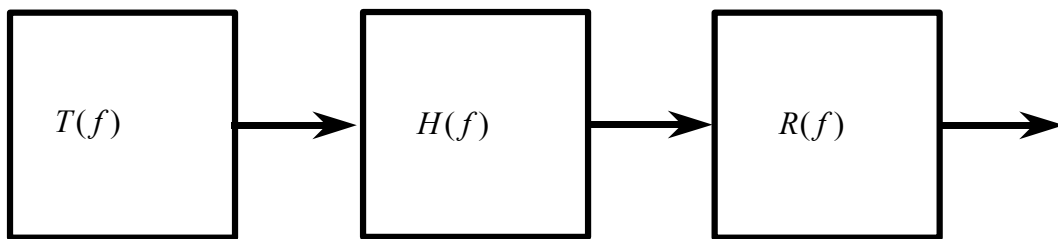$$T(f) \longrightarrow H(f) \longrightarrow R(f) \longrightarrow$$

Fig. 2.10   Spectroscopic system for the determination of a medium's transfer function.

The transfer function of the test medium is found by deconvolution. This process (although possible in the time domain) is most easily carried out in the frequency domain, where

$$H(f) = \frac{V_2(f)}{T(f)R(f)} \tag{2.79}$$

2.2.2 Formulation of the Equations of Motion

The dynamic characteristics of a structure will alter as a result of damage. This is characterized by changes in the modal parameters, i.e., the modal frequencies, damping values and mode shapes associated with each modal frequency. Changes also occur in some of the structural parameters, such as the mass, damping, stiffness and flexibility matrices of the structure.

The equations of motion of a structure with N degrees of freedom and viscous damping coefficients can be expressed as [111]

$$[M]\{\ddot{x}(t)\}+[D]\{\dot{x}(t)\}+[K]\{x(t)\}=\{f(t)\}, \tag{2.80}$$

where $[M]$, $[D]$, and $[K]$ represent the $n \times n$ mass, damping, and stiffness matrices. If we assume a harmonic input, the external force and displacement can be expressed as $\{f(t)\}=\{F(\omega)\}e^{i\omega t}$ and $\{x(t)\}=\{X(\omega)\}e^{i\omega t}$. Substituting into Eq. (2.80) yields

$$(-\omega^2[M]+j\omega[D]+[k])\{X(\omega)\}e^{i\omega t}=\{F(\omega)\}e^{i\omega t}. \tag{2.81}$$

From the above equation, the FRF matrix, $[H(\omega)]$, is defined as

$$[H(\omega)]=(-\omega^2[M]+j\omega[D]+[K])^{-1}. \tag{2.82}$$

Then Eq. (2.81) can be expressed as

$$\{X(\omega)\}=[H(\omega)]\{F(\omega)\}. \tag{2.83}$$

2.3 Dynamic Testing

A dynamic system is characterised or modelled by a differential equation or sets of such equations. The solution of differential equations both analytically and by numerical methods is a central topic in mathematics. The constraints due to the fact that the differential equations represent realisable systems enable linear time invariant systems to be modelled in the Laplace domain.

The dynamic response of the system under testing (*SUT*) is defined as the behaviour of the system when stimulated by a time varying input such as the unit step, unit-impulse or another signals. Consequently, a dynamic test is any test that yields information to the dynamic response of the SUT even if the data yielded do not completely describe the dynamic behaviour of the system. Dynamic testing offers advantages over static or steady state testing other than when considering fault location.

The relation ship between the input and output of a linear system can be represented by the knowing differential equation

$$\sum_{i=0}^{m} b_i \, d^i \, x(t) \Big/ dt^i = \sum_{i=0}^{n} a_i \, d^i \, y(t) \Big/ dt^i \tag{2.84}$$

By applying Laplace transformation on Eq. (2.84), the dynamic properties of the system can be determined by

$$H(s) = \frac{Y(s)}{X(s)} = \sum_{i=0}^{m} b_i \, s^i \bigg/ \sum_{i=0}^{n} a_i \, s^i \,,$$
(2.85)

which called the transfer function of the system [112]. If $s \to i\omega$ the relation will be called the frequency response function of the system, $H(i\omega)$, which can be measured by any measuring system. It enables the output of the system to be determined for any given input. If the input stimulus $x(t)$ has Laplace transform $X(s)$ then the output response $y(t)$ is given by

$$y(t) = L^{-1}\{H(s)X(s)\}$$
(2.86)

where L^{-1} represents the inverse Laplace transform.

The determination of the transfer function coefficients of a linear system from its frequency response measurements have been discussed in reference [113]. In which , the frequency response of the linear system

$$H(i\omega) = \frac{b_0 + i\omega b_1 + \ldots + (i\omega)^m b_m}{a_0 + i\omega a_1 + \ldots + (i\omega)^n a_n}$$
(2.87)

can be represented in the following form:

$$H(i\omega) = A_0 + \cfrac{1}{A_1 + \cfrac{B_0}{i\omega} + \cfrac{1}{A_2 + \cfrac{B_1}{i\omega} + \cfrac{1}{A_3 + \cfrac{B_2}{i\omega} + \bullet\bullet\bullet}}}$$

$$\bullet$$

$$\bullet\bullet\bullet + \cfrac{1}{A_n + \cfrac{B_{n-1}}{i\omega}}$$
(2.88)

to calculate the coefficients $A_0, A_1, B_0, A_2, \ldots, A_n, B_{n-1}$ from the measured frequency response by using an Algorithm.

A review for the methods of determination of transfer function coefficients from the measured frequency response of the system can be found in reference [112]. The certainty of approximation of the frequency response function depends on the ratio of the relative error [114].

2.3.1 Frequency Response Function Estimators and Coherence Function

Figure 2.11 shows the traditional measurement system model used to describe FRF measurement when noise is present on both measured force and response signals.
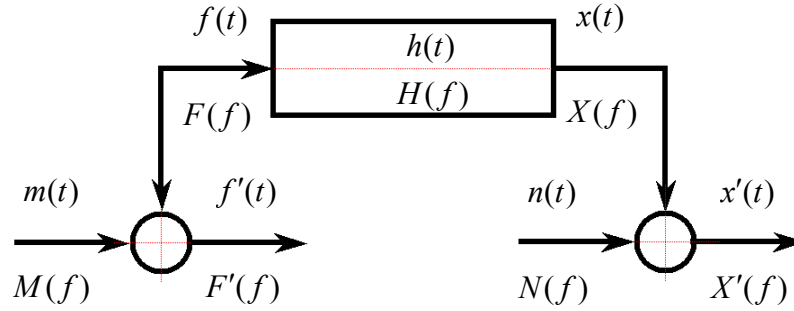

Fig. 2.11   Traditional measurement system model.

The estimation of the FRF can by averaging these quantities as follow

$$\hat{H}(f) = \frac{1}{N_a} \sum_{n=1}^{N_a} \left(\frac{X(f)}{F(f)} \right)_n , \tag{2.89}$$

the risk will be found if the value of $F(f) = 0$. Therefore, in practice, there are found to be advantages in using alternative ways of calculating $H(f)$, using auto- and crosspower spectrums:

$$H_1(f) = \frac{F'(f)X'(f)}{F'(f)F'(f)} \tag{2.90}$$

Another version of the frequency response function estimator, $H_2(f)$, is obtained by normalising the output auto-spectrum by the cross input-output spectrum:

$$H_2(f) = \frac{X'(f)X'(f)}{X'(f)F'(f)} \tag{2.91}$$

As $H_1(f)$ and $H_2(f)$ should give the same result, an indicator of the quality of the analysis can be defined as the ratio of these two estimator. Thus,

$$
\begin{aligned}
\frac{H_1(f)}{H_2(f)} &= \frac{F'(f)X'(f)}{F'(f)F'(f)} \frac{X'(f)F'(f)}{X'(f)X'(f)} \\
&= \frac{|F'(f)X'(f)|^2}{F'(f)F'(f)X'(f)X'(f)} \\
&= \gamma^2(f)
\end{aligned} \tag{2.92}
$$

where $\gamma^2(f)$ is called the ordinary coherence function. It is a normalised coefficient of correlation between the measured force and response signals evaluated at each frequency. The ordinary coherence function is always greater than zero but less than unity.

The main reason for calculating the frequency response function with equation (2.90) or (2.91) is the reduction of uncorrelated noise on the input or the output signals by averaging.

In practice the frequency response function will be estimated by averaged values of the auto- and crosspower spectrums as follows,

$$F'(f)F'(f) = \frac{1}{N_a}\sum_{n=1}^{N_a}\left(F'(f)F'(f)\right)_n$$

$$X'(f)X'(f) = \frac{1}{N_a}\sum_{n=1}^{N_a}\left(X'(f)X'(f)\right)_n$$

$$F'(f)X'(f) = \frac{1}{N_a}\sum_{n=1}^{N_a}\left(F'(f)X'(f)\right)_n$$

$$X'(f)F'(f) = \frac{1}{N_a}\sum_{n=1}^{N_a}\left(X'(f)F'(f)\right)_n$$

(2.93)

where N_a is the number of averages, yielding a least squares estimation for $H(f)$. Thus, the coherence function is a measure of the least squared error. The coherence is a correlation coefficient; hence, it varies between 0 and 1. A value of unity indicates that a perfect linear relationship exists between the two compared signals (e.g. input/output) over all averages [115].

When the ordinary coherence function is less than unity, one or more of the following four main conditions exist [116]:

1. Extraneous noise is present in the *FRF* measurements;
2. Resolution bias errors are present in the spectral estimates;
3. The system relating *f(t)* and *x(t)* is non-linear;
4. The measured response *x(t)* is due to other external inputs besides *f(t)*.

The coherence is able to measure the "goodness" of a transfer function test. It helps to answer the question "Who doing what". One of the important uses of the coherence function is to indicate the reliability of the measured transfer function [117].

2.3.2 Delta Function

Mathematicians use the term impulse to mean a signal that is short enough to be an impulse to any possible system. That is, a signal that is infinitesimally narrow. The continuous delta function is a normalized version of this type of impulse. It is mathematically defined by three idealized characteristics:

1. The signal must be infinitesimally brief,
2. The pulse must occur at time zero, and
3. The pulse must have an area of one.

Since the delta function is defined to be infinitesimally narrow and have a fixed area, the amplitude is implied to be infinite. The continuous delta function is given the mathematical

symbol: $\delta()$ Likewise, the output of a continuous system in response to a delta function is called the impulse response, and is often denoted by: $h()$ [118].

2.3.3 Convolution

The convolution of continuous signals can be viewed from the input signal as shown in Fig 2.12. An input signal, *x(t),* is passed through a system characterized by an impulse response, *h(t),* to produce an output signal, y(*t)*. This can be written in the familiar mathematical equation,
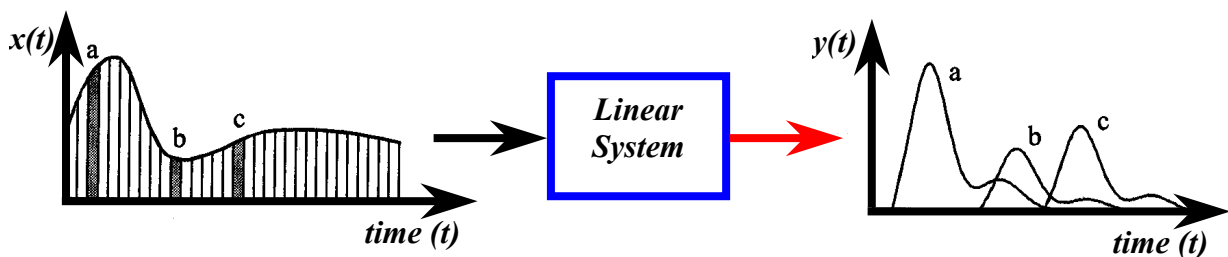
$$y(t) = x(t) * h(t) \tag{2.94}$$

Fig. 2.12   Convolution viewed the input side, from [118].

The input signal is divided into narrow columns, each short enough to act as an impulse to the system. In other words, the input signal is decomposed into a finite number of scaled and shifted delta functions. Each of these impulses produced a scaled and shifted version of the impulse response in the output signal. The final output signal is then equal to the combined effect, i.e., the sum of all of the individual responses.

Each instantaneous value in the output signal is affected by a section of the input signal, weighted by the impulse response flipped left-for-right. In the discrete case, the signals are multiplied and summed. In the continuous case, the signals are multiplied and integrated. In equation form:

$$y(t) = \int_{-\infty}^{+\infty} x(t) h(t - \tau) \, dt \tag{2.95}$$

This equation is called the convolution integral, which defines the meaning of Eq. (2.94). The goal is to find an expression for calculating the value of the output signal at an arbitrary time, t. The first step is to change the independent variable used to move through the input signal and the impulse response. That is, we replace t with τ. This makes $x(t)$ and $h(t)$ become $x(\tau)$ and $h(\tau)$, respectively. This change of variable names is needed because t is already being used to represent the point in the output signal calculated. The next step is to flip the impulse response to the location t, results in the expression becoming $h(t - \tau)$.

The input signal is then weighted by the flipped and shifted impulse response by multiplying the two, i.e., $x(t) \, h(t - \tau)$. The value of the output signal is then found by integrating this weighted input signal from negative to positive infinity, as described by Eq. (2.95). The discrete time convolution is defined as

$$y(n) = \sum_{k=-\infty}^{+\infty} x(k)\, h(n-k) = \sum_{k=-\infty}^{+\infty} h(k)\, x(n-k)\,. \qquad\qquad (2.96)$$

2.4   Finite Impulse Response (FIR) Filter

Digital finite impulse response (FIR) filters are discrete linear time-invariant systems in which an output number, representing a sample of the filtered signal, is obtained by weighted summation of infinite set of input numbers, representing samples of the signal to be filtered. The coefficients of the weighted summation constitute the impulse response of the filter and only a finite number of them take non-zero values. This filter is of the 'finite memory' type, that is, it determines its output as a function of input data of limited age. It is frequently called a non-recursive filter because, unlike the infinite impulse response filter, it dose not require a feedback loop in its implementation [119].

2.4.1   The Basic Structure of FIR-Filter

In the Finite Impulse Response (FIR) Filters, The output sequence is calculated by a linear combination of the current and M past input samples. Figure 2.13 shows a flowgraph and block diagram representing this filter type. The input data pass through an M- stage shirt register. After each shift operation, the outputs of the shift register are weighted with the coefficient b_r and summed. The sum is the output value of the filter associated with the respective clock cycle [120].
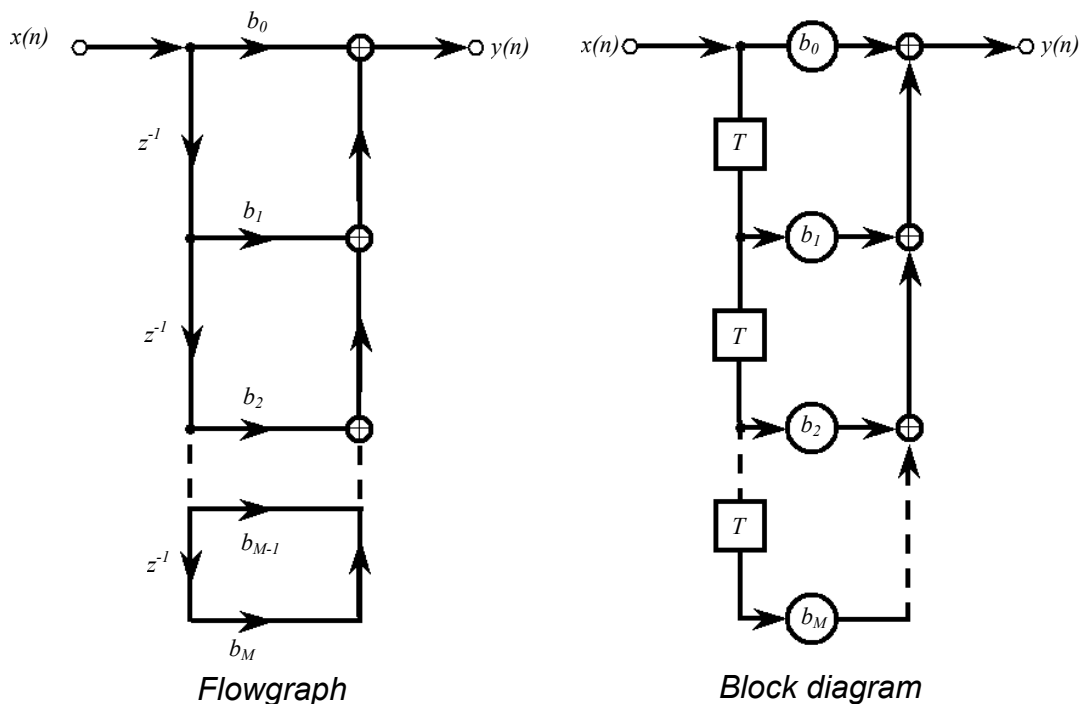

Flowgraph   Block diagram

Fig. 2.13   Flowgraph and block diagram of the FIR filter, from [120]

The weighting coefficients b_r, which determine the characteristics of the filter, have a clear meaning. Let us consider the unit-sample response of the filter, which we obtain by applying a unit sample sequence $\delta(n)$ to the input. This sequence has only one nonzero sample with the value 1. This unit sample propagates step-by-step through the shift register. It is evident that the coefficients b_r will appear at the output one after the other starting with b_o. This means that the coefficients are the samples of the unit-sample response $h(r)$ of the filter. From the flowgraph we can derive the following algorithm:

$$y(n) = b_0 x(n) + b_1 x(n-1) + \ldots + b_M x(n-M)$$ (2.97)

or expressed in compact form

$$y(n) = \sum_{r=0}^{M} x(n-r) b_r .$$ (2.98)

Relation (2.96) represent the convolution sum, because b_r can be replaced by $h(r)$.

$$y(n) = \sum_{r=0}^{M} x(n-r) h(r)$$ (2.99)

The FIR filter, therefore, has a structure that realises the convolution sum in direct form. The length of the shift register determines the length of the unit-sample response, which is finite and gives the filter its name. This is the reason why the summation in Eq. (2.98) extended over a finite number of elements, which is in contrast the general convolution sum Eq. (2.96). The transfer function of the FIR filter is obtained by z-transformation of the unit-sample response $h(n)$.

$$H(z) = \sum_{r=0}^{M} h(r)\, z^{-r}$$ (2.100)

Replacing $h(r)$ by b_r yields a relation between the transfer function and the filter coefficients.

$$H(z) = \sum_{r=0}^{M} b_r\, z^{-r}$$ (2.101)

The transition from z to $e^{i\omega T}$ yields the frequency response of the filter.

$$H(e^{i\omega T}) = \sum_{r=0}^{M} b_r\, e^{i\omega T} .$$ (2.102)

2.4.2 Poles and Zeros of the FIR-Filter

An alternative representation of Eq. (2.101) can be found by factoring out the term z^{-M}

$$H(z) = \frac{\sum\limits_{r=0}^{M} b_r \, z^{M-r}}{z^M} , \qquad (2.103)$$

All exponents in the sum then become positive. In the numerator we get a polynomial in z of degree M, resulting in M zeros of he transfer function. The denominator of Eq. (2.100) represents an Mth-order pole at $z = 0$.

$$H(z) = b_0 \frac{(z - z_{01})(z - z_{02})\ldots(z - z_{03})}{z^M} \qquad (2.104)$$

Figure 2.14 shows the possible locations of poles and zeros in the z-plan. The zeros may be located within, on or outside the unit circle. Since the coefficients b_r are real, the zeros must be real or occur in complex -conjugate pairs. Moreover, an even filter order leads to an odd number of coefficients [120].

The impulse response of the FIR filter depends on its number of stages. The impulse response may be symmetric or ant-symmetric as shown in Fig. 2.15 [121].
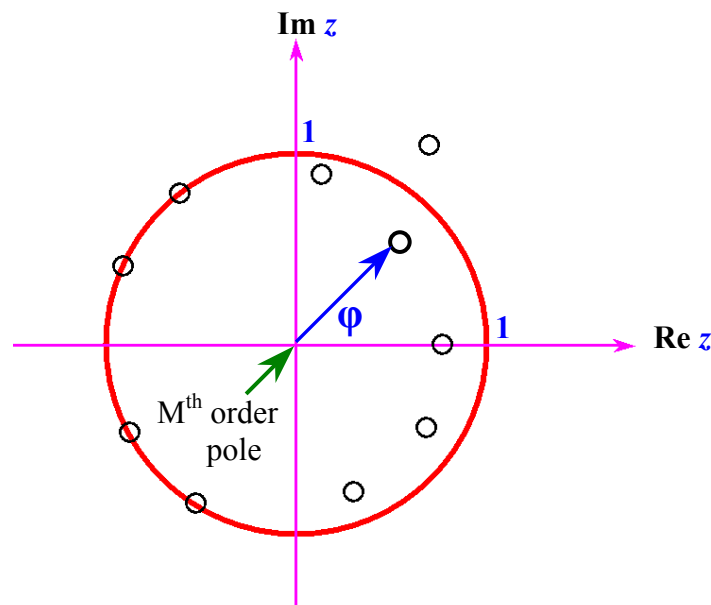

Fig. 2.14 Possible locations of poles and zeros in z-plan, from [120].
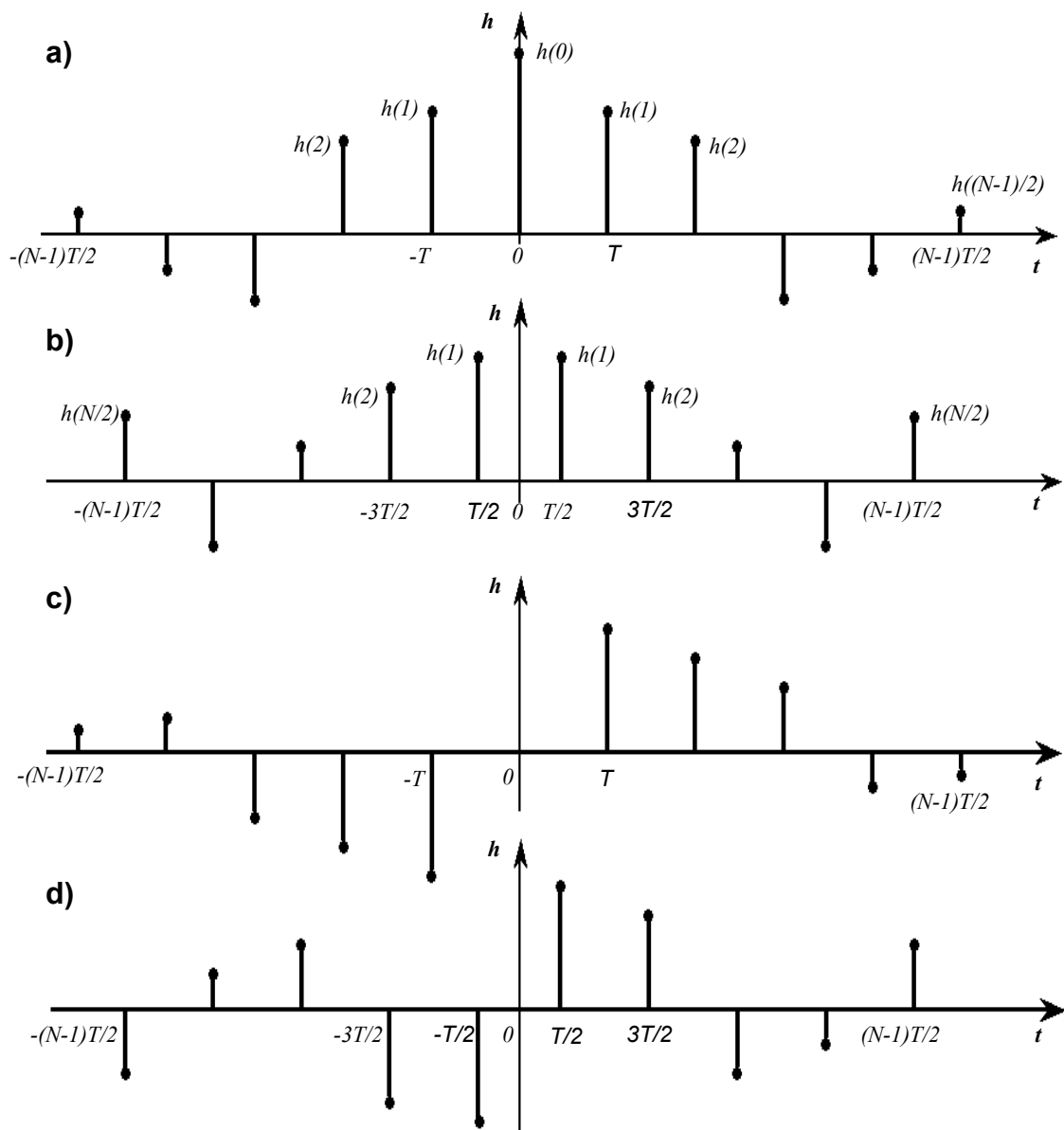
Fig. 2.15   The four possible impulse response of FIR-filter, from [121].
Case 1 the impulse response is symmetric about $t = 0$ and the number of samples is odd.
Case 2 the impulse response is symmetric about $t = 0$ and the number of samples is even.
Case 3 the impulse response is ant-symmetric about $t = 0$ and the number of samples is odd.
Case 4 the impulse response is ant-symmetric about $t = 0$ and the number of samples is even

CHPTER 3

EXPERIMENTAL PROCEDURES

3.1 Introduction

The damage and deterioration of hip prostheses caused by loosening of the shaft has become significant in the last decades. The development of non invasive methods for the inspection of hip prosthesis allowing loosening "damage" identification in an early stage is a very important for patients and surgeons.

3.2 Ultrasound Tests

3.2.1 Pulse-Echo method

A pulse-echo technique is used in institute of material science to examine our model. A Krautkrämer ultrasonic equipment is used for sounding the system. The resulted echo-signal is disappeared into the noise. The dissipation of echo-signal may be due to the high damping capacity of the composite system.

3.2.2 Sine Sweep Method

Ultrasound excitation can be done by using a sine sweep signal as shown in Fig. 3.1. A signal generator OR-X 402A is used to generate the sine sweep signal of rate 18 ms. The sweep voltage will be feed into a piezoelectric shaker "Jodon Piezoelectric Shaker®", which works as an actuator. The resulted mechanical vibration "acoustic energy" will be coupled to the thigh model by an ultrasonic gel "Auxynhariol Ultrasonic Gel®". The transmitted signal will be recorded by an accelerometer "Brüel&Kjær 8312". The accelerometer couples with the model by an ultrasonic gel too. An amplifier "Brüel&Kjær 2638" is used to amplify the accelerometer's output. Both of excitation and response signals will be feed into the signal analyzer "AS24000 Signal Analyzer" for triggering, averaging, digitization and displaying. The data acquisition system will be connected with a Pentium® III PC to display and record the measured data which will be processed off-line with MATLAB® program as shown in Fig. 3.2.
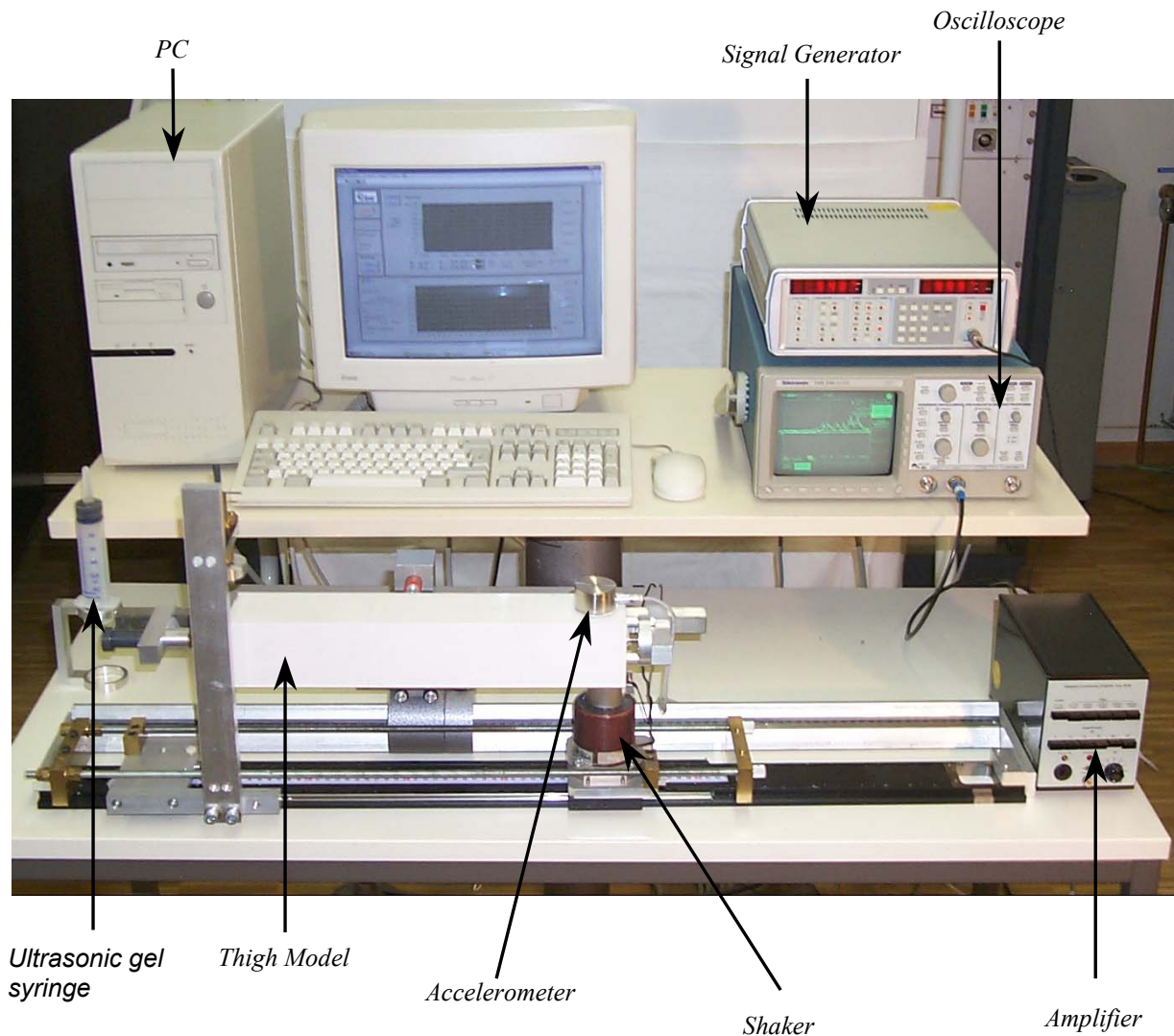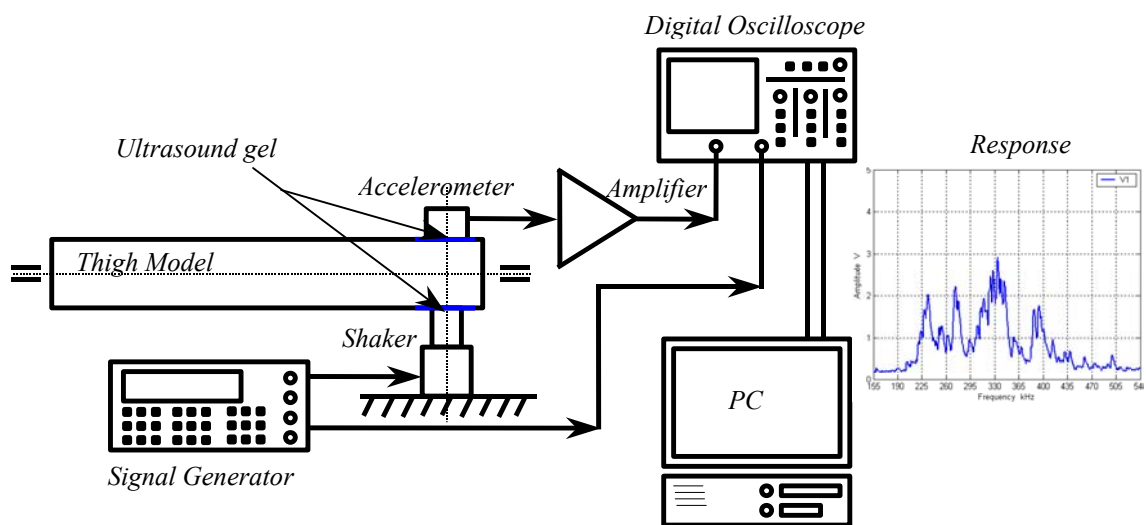
Fig. 3.1   A sine sweep testing set-up.

Fig. 3.2   Schematic of sweep experiment

50

Figure 3.3 illustrates the frequency response of the system to a sine sweep. It is obvious that the resonance frequencies of the system lie in the ultrasound range. These resonance represent the system resonance for secured case. The system displays many resonance. The maximum resonance frequency is found at frequency of 334.35 kHz. It has an amplitude of 2.9 volt. In the loosening case, these frequencies could be damped or disappeared in the noise. Thus we have to look for another satisfy method to detect the loosening of the shaft.
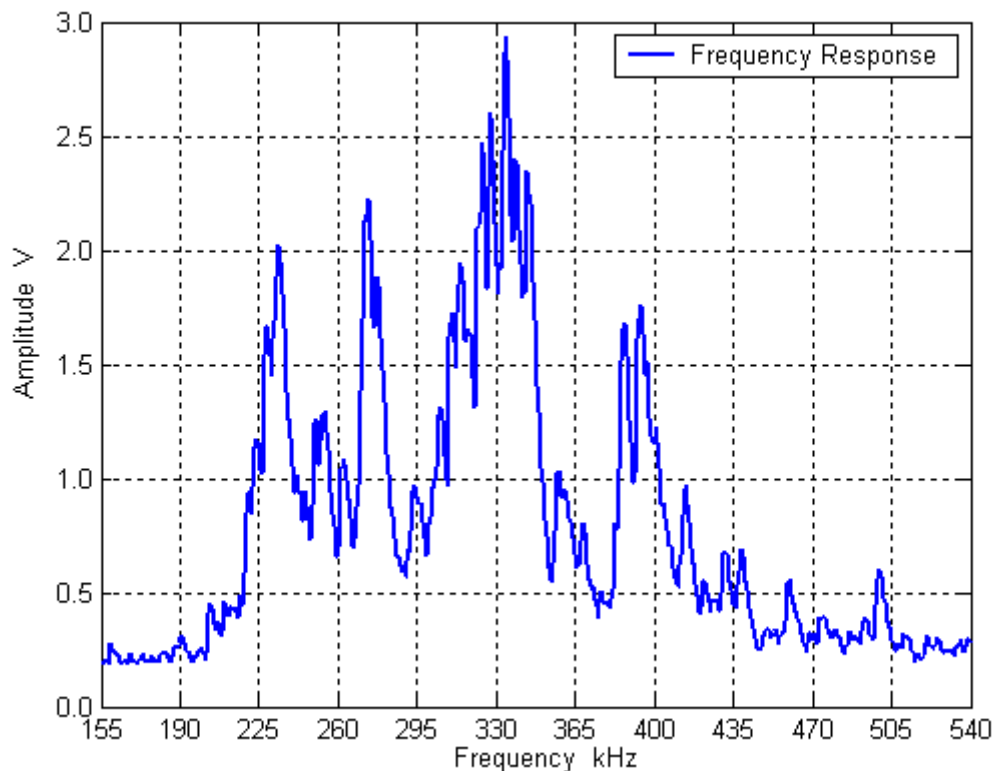

Fig. 3.3   System frequency response to a sine sweep.

3.3 Vibroacoustical Method (Pulse-Transmission)

Another type of test signals is the impact "impulsive" load. The impact excitation is characterized by an almost instantaneous rise in magnitude followed by a rapid decrease, the duration of the impact load being of order of a few millisecond or microseconds.

Vibration measurements offer an efficient way of non invasive testing of prostheses. They can be used to detect those damages which alter their dynamic characteristics. This alteration is characterized by changes in vibration parameters.

The application of vibration measurements will be used to identify the damage of the thigh model. Its parameters demonstrate the sensitivity to any physical changes within the system. The analysis of the experimental data will be used to detect the loosening (damage). The frequency response function of the system could be used as a tool for assessing the state of health of a prosthesis, also refered to as "Health Monitoring".

3.3.1 Experimental Set-up

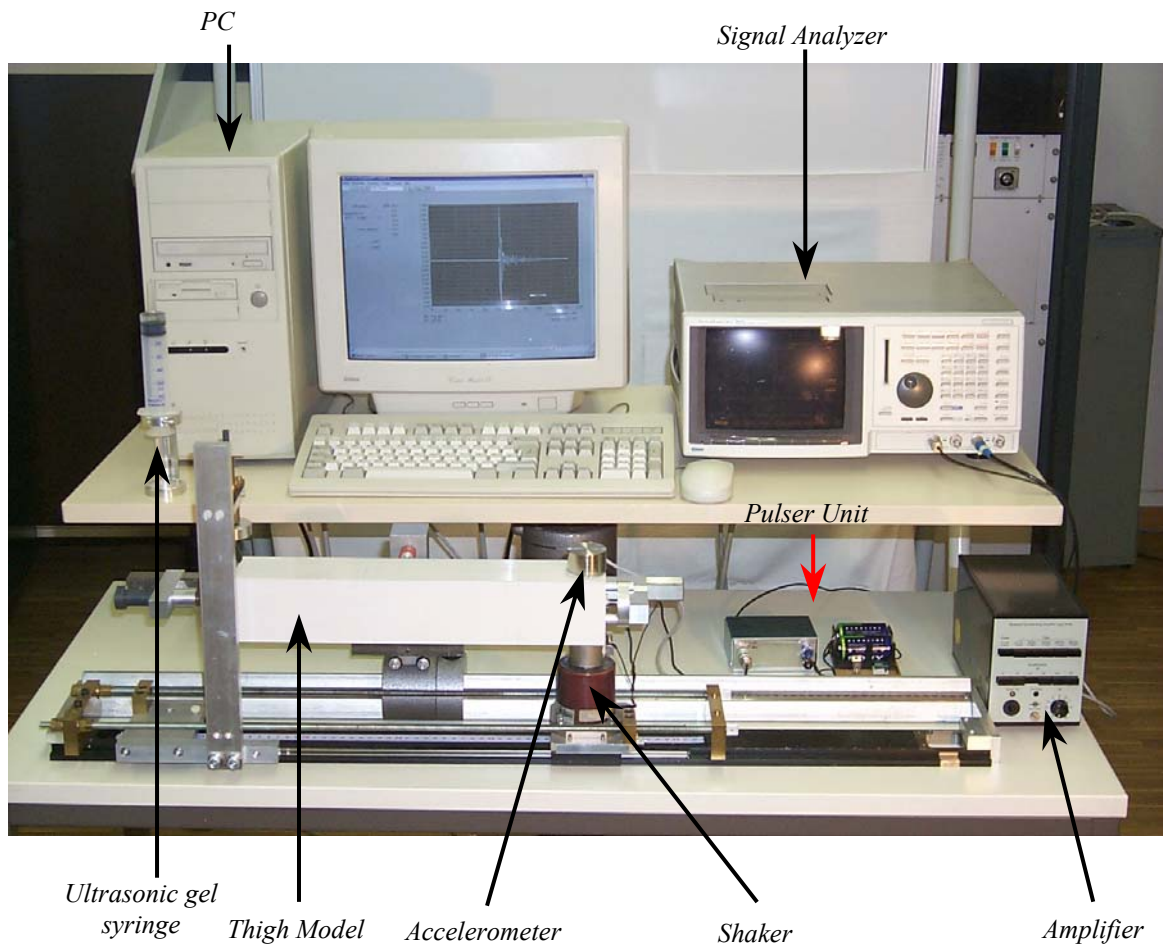The experimental work will be carried out on a thigh model as shown in Fig. 3.4.

Fig. 3.4   Pulse-Transmission set-up.

An electrical pulse will be generated from an electrical pulser to excite the test model. The excitation voltage will be released by pressing the knob of the pulser. This voltage will be feed into a piezoelectric shaker "Jodon Piezoelectric Shaker®", which works as an actuator. The resulted mechanical vibration "acoustic energy" will be coupled to the thigh model by an ultrasonic gel "Auxynhariol Ultrasonic Gel®". The transmitted signal will be recorded by an accelerometer " Type 8312 Brüel&Kjær". The accelerometer couples with the model by an ultrasonic gel too. The output signal of the accelerometer will be passed through an amplifier "Type 2638 Brüel&Kjær". Both of excitation and response signals will be feed into the signal analyzer "AS24000 Signal Analyzer" for triggering, averaging, digitization and displaying. The data acquisition system will be connected with a Pentium® III PC to display and record the measured data which will be processed off-line with MATLAB® program as shown in Fig. 3.5.
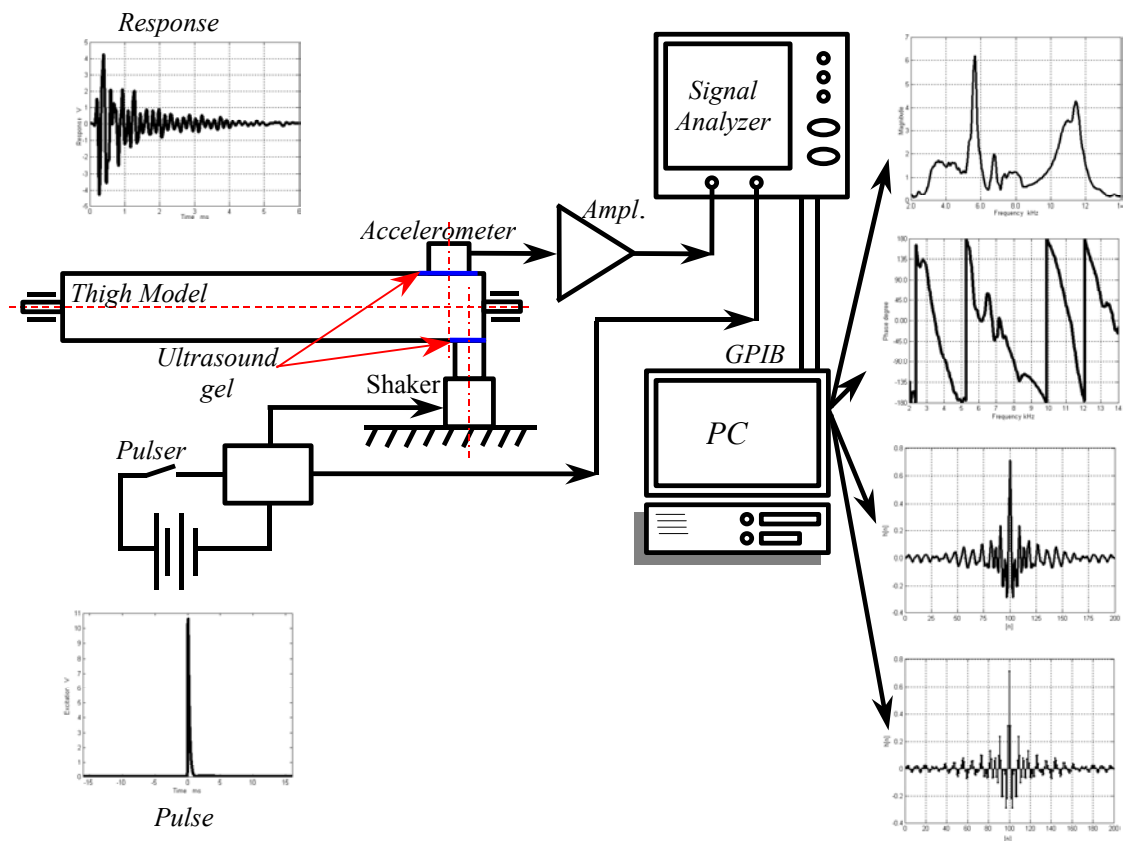
Fig. 3.5 Schematic of the pulse-transmission experiments.

3.3.2 Analysis of VA Excitation

3.3.2.1 Effect of Sensor Position

Figure 3.6 illustrates the gain of the FRF10 and the FRF20 with respect to the frequency for secure case. The changing of accelerometer position affect on the value of gain for FRF_{10} and FRF_{20} as seen in Fig. 3.6. The maximum effect appears on the 2nd resonance. A great reduction of 47.6 % of the gain is appeared. The 1st resonance displays only a reduction of 10.1 % for the changing in accelerometer's position from P#1 to P#2 on the model. The 2nd resonance indicates the largest sensitivity to the change in sensor's position. This result will help the surgeons during the non-invasive examination of THA to know the effect of the uncertainty of determination of the reference point on the dynamic characteristics of the femur, since they can not exactly put the sensor on the early reference point.
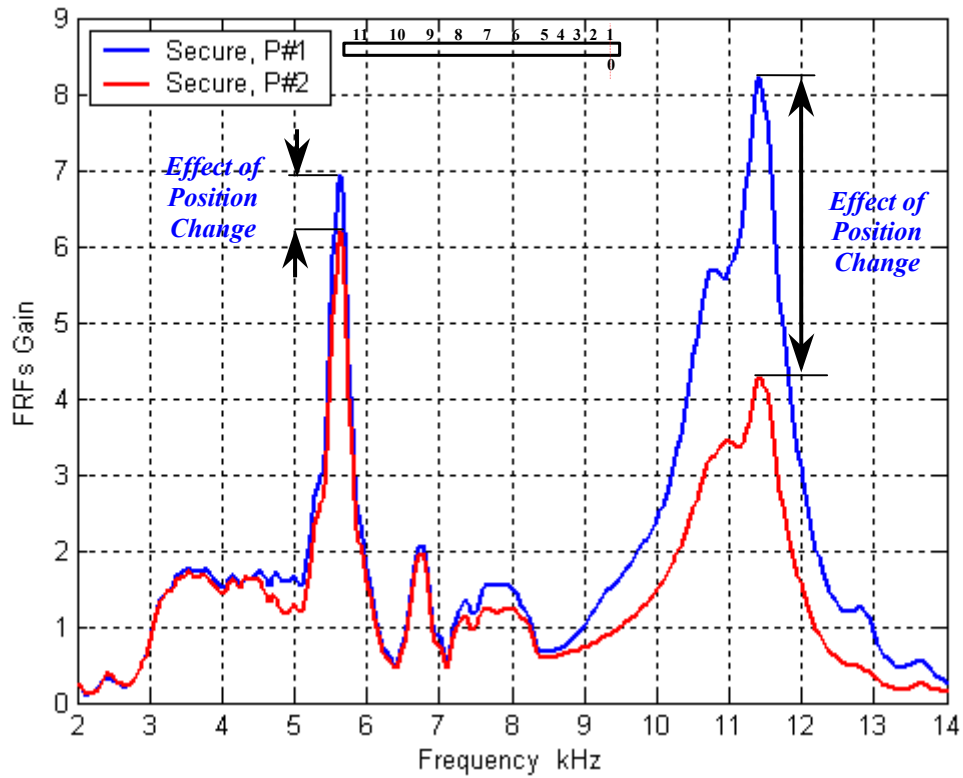
Fig. 3.6   Sensitivity of the 1st and 2nd resonance to the change of position.

3.3.2.2 Loosening Effect

The FRF_{10} and FRF_{20} will be again measured after the loosening of the shaft. The loosening will be made by hammering the shaft from the rear end. This process will be done with a great carefully to avoid the destruction of the bone-cement replacement mantel. A gain the hammer will be used to return the shaft to its original place. For this case we consider the loosening is 0 mm. This process is used to release the shaft from stresses which resulted during the solidification process of the bone-cement replacement material. In another word we can say that the junction between bone-cement replacement and the shaft is destroyed.

Figure 3.7 shows the effect of loosening "L=0 mm" on the 1st and 2nd resonance of the FRF_{10}. The 1st resonance shows the largest sensitivity to the loosening where the gain is reduced from 6.9 to 3.1, i.e., 56.4 %. The 2nd resonance is reduced by 26.6 %.
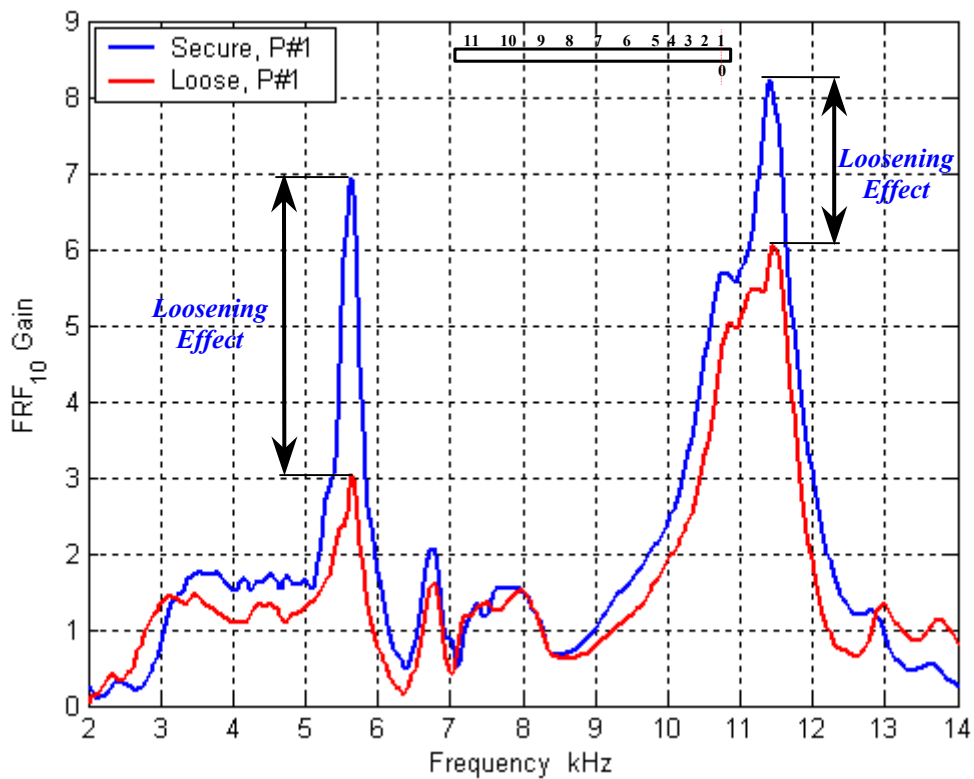
Fig. 3.7   Sensitivity of the 1st and 2nd resonance of FRF$_{10}$ to the loosening.

Figure 3.8 illustrates the effect of loosening on the gain of the FRF$_{20}$. The dynamic characteristics of the system is changed and the 1st and the 2nd resonance are reduced. The greatest reduction appears at the frequency of 5.6 kHz (1st resonance). The 1st resonance is reduced by 45.7 % where the 2nd one is reduced by 25 %. Again, the 1st resonance shows the largest sensitivity to the loosening of the shaft. It is conclude that the pulse-transmission technique could give us more information about the system under testing. The frequency band of the 1st resonance is found to be the more sensitive to the loosening of the prosthesis's shaft. So, we will use it to demonstrate the loosening of the shaft in the experimental analysis. The useful frequency band is illustrated in Fig. 3.9. So, we will use this Vibro-Acoustic technique to monitor the health of the shaft.
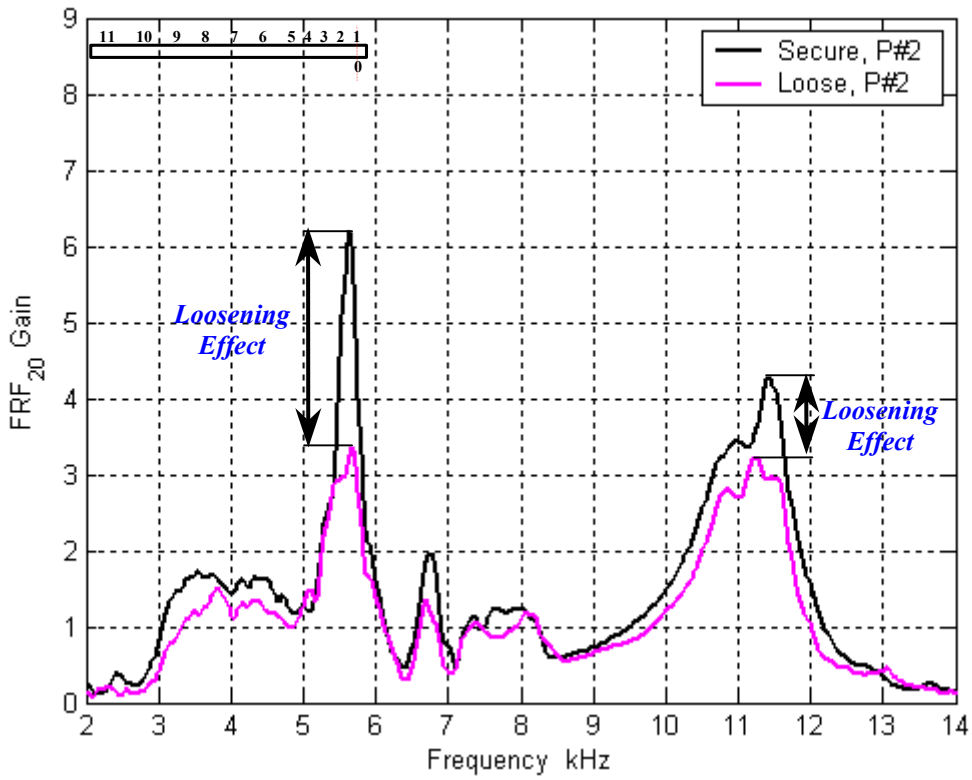
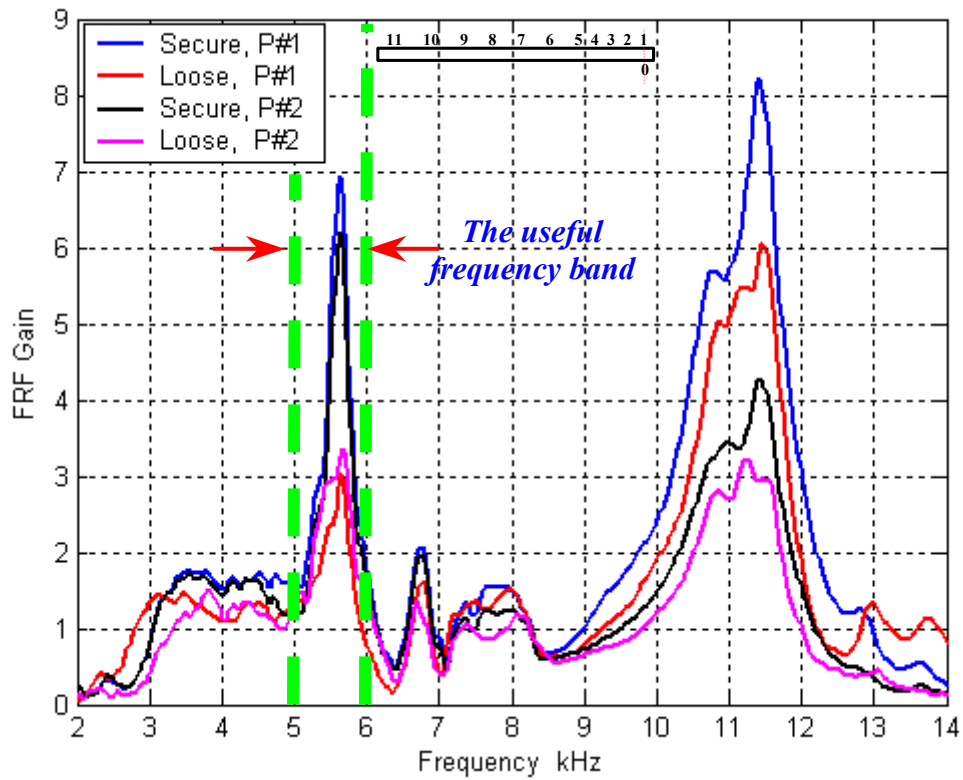Fig. 3.8 Sensitivity of the 1st and 2nd resonance of FRF$_{20}$ to the loosening.

Fig. 3.9 The useful Frequency band for detection the shaft loosening.

3.4 Thigh model

3.4.1 Geometry of Thigh Model

A model of composite material of 40 cm length, 7 cm width and 7 cm hight will be used for the laboratory in vitro tests as shown in Fig.3.10.
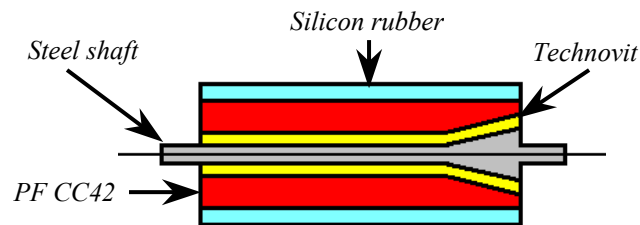

Fig. 3.10   Thigh model.

3.4.2 Materials of Thigh Model

The thigh model, shown in Fig.3.10 consists of Silicon rubber "Sicovoss-RF Art.-Nr.3445 Vosschiemie$^{®}$" as a replacement material for human tissue, round laminated moulded rod (PF CC42) as a bone replacement material [122], bone cement replacement material "Technovit$^{®}$ 4004 Kulzer" and a Steel shaft as a prosthesis shaft. The model "beam" is clamped from its ends. The Shaker support the beam from its right end. The centre of the shaker lies two cm from the right end of the model on the centre of model. This point will be the excitation pint. It takes the number zero (0) in the FRF to indicate the position of excitation.

3.4.3 X-Ray Test

A plain radiography test is carried out in institute of non-destructive testing to determine the interface between model's layers as seen in Fig. 3.11. With some care we could determine the interfaces between layers. The density of the Technovite$^{®}$ material is nearly close to the density of PF CC42 "laminated moulded rod". For the THA "real system", the surgeon look for the radiolucent region between interfaces i.e. between shaft and bone-cement or between bone and bone-cement to determine the loosening of the prosthesis.
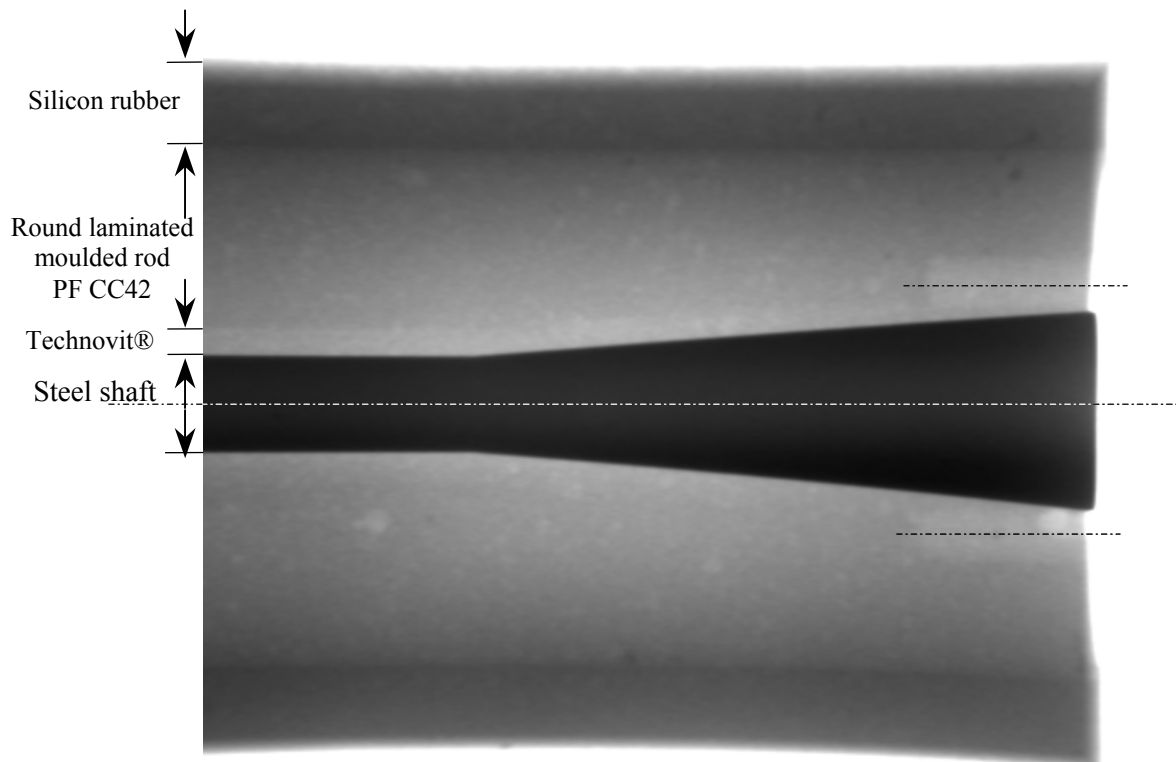
Silicon rubber

Round laminated moulded rod PF CC42

Technovit®

Steel shaft

Fig. 3.11   Plain radiograph of the model.

3.5 Test Procedures

3.5.1 Excitation Techniques

An electrical pulse generated from an electrical pulser will be used to produce the stress wave in the model by the shaker as shown in Fig.3.2. This impulsive excitation will help us to induce the natural vibrations of the model. The knob of the pulser unit will be pressed to have the excitation voltage of the shaker. The resulted mechanical vibration from the shaker "acoustic energy" will be coupled to the model by an ultrasonic gel. Eight strokes will be applied for each measurement and the average will be taken to calculate the required response, frequency response function (FRF) and the power spectral density function (PSD). The driving force will always introduced from the blow on the bottom side of the beam in the model centre line. The energy of impulsive force concentrate in frequency band f =1.85 to 18 kHz.

58

3.5.2 Response Measurement

The vertical dynamic response of the beam will be measured with a single accelerometer B&K 8312 acoustic emission-wide band recorder. The accelerometer is perpendicular to the upper face of the beam on its centre line too as shown in Fig.3.12.
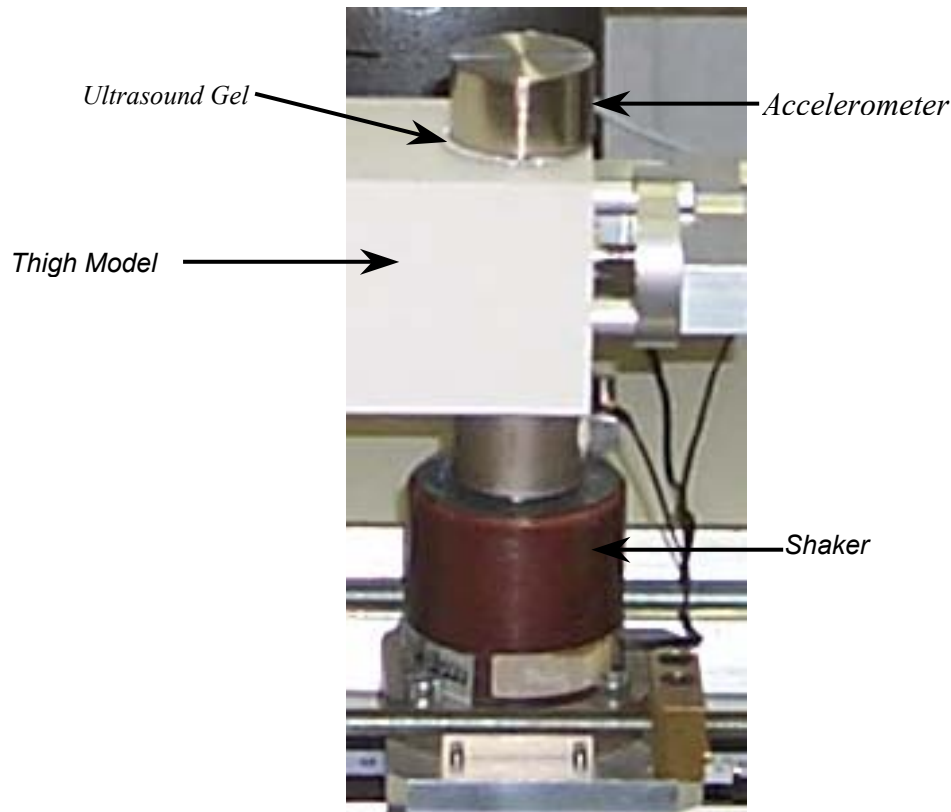

Fig. 3.12 Shaker-accelerometer arrangement.

The accelerometer works as a receiver for the transmitted acoustic wave. The ultrasonic gel is the coupling medium between the beam and the receiver. The transmitted signal will be feed into an amplifier with the gain 10-60 dB "wide band amplifier type 2638 Brüel&Kjær". Both of excitation signal and the response signal will be feed into the signal analyzer for triggering, averaging, digitization and displaying. The data acquisition system will be connected with a Pentium® III PC to display and record the data which will be processed to have the frequency analysis. The Signal Analyzer has the ability to display the signals in frequency domain.

3.5.3 Data Acquisition and Processing

The measured signals, one excitation signal and one acceleration signal will be acquired by the signal analyzer 24000. The signals will be transferred into the memory of the analyzer and immediately transformed into the frequency domain. The frequency response function (FRF) calculated from the spectra will be then stored on the hard disk of an PC through GPIB for further off-line processing.

A sampling rate of 64 kHz is used in digitizing the measured signal during a 32 ms time window. The subsequent frequency analysis cover the band from 0 Hz to 25 KHz, with a frequency resolution $\Delta f = 31.25$ Hz between 0…25 KHz.

3.5.4 Frequency Analysis

The signal analyzer will be used for acquisition and transformation of the input force signal and the beam response signal up to determination of the FRF. For determination of the FRF the following measurement function set-up was used in all cases of excitation with the shaker.

Reference channel window type	Haning
Response channel window type	Haning
Average Type	Stable
Number required	8

3.6 Measurement Strategy

The non invasive evaluation of the loosening of the hip prosthesis in-vitro will be done as follow:

1. The accelerometer and the Shaker will be centred two cm from the right edge of the of the beam to perform the secure condition (undamaged) experiments.
2. Excitation the system by an electrical pulses (8 pulses).
3. Acquiring the response by an accelerometer.
4. Storing the measured response (average of 8 pulses) on PC. This vector represents the base line (reference signal) for this measuring position.
5. Loosening the prosthesis without destruction of its mantel.
6. Shaft reinstallation into its original position.
7. Repeating of (2).
8. Repeating of (3).
9. Repeating of (4).
10. Processing of signals (4) and (9) (off-line processing).
11. Obtaining the system transfer function from (10) for secure and loose cases.
12. Approximation the system transfer function by FIR-Filter.
13. Comparing the transfer functions for secured and loosed cases.
14. Comparing the Nyquist plot for secured and loosed cases.
15. Determination of the more sensitive resonance frequency.
16. Comparing the FIR-Filter coefficients for secured and loosed cases.
17. The error in (13) or (14) or (16) represents the loosening signature.

Hence, each series of experiments will be carried out on the same position with the level of loosening equal 0 mm. A flow chart of the of the impulse test analysis procedure is illustrated in Fig. 3.13.
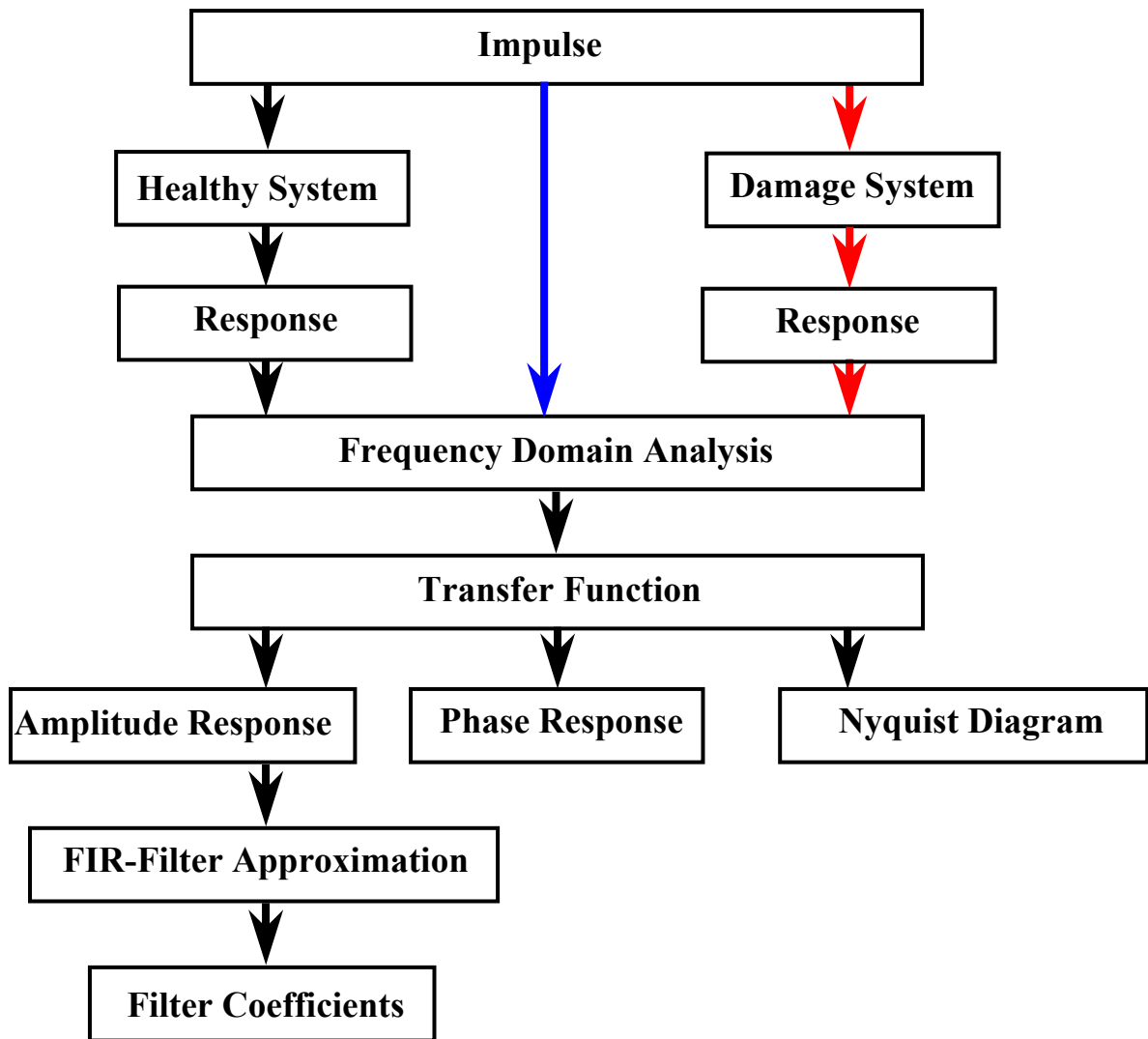
Fig. 3.13   Application of a VA technique for detection the loosening of the shaft in THA.

CHAPTER 4

RESULTS AND DISCUSSIONS

Prediction of the hip prosthesis loosening by a non invasive method is a dream for the patient and surgeon. This thesis is dedicated to vibroacoustical (VA) diagnostic of prosthesis, that is, to the estimation or monitoring of its internal state within the thigh through an appropriate processing of measured vibration signal. The diagnostic algorithm is based on measurement of natural frequencies of the thigh model. The results are compared with the reference, or baseline, ones, obtained initially for secure (undamaged) prosthesis. The analysis of measured data will be processed to get the indication about the loosening of the prosthesis. The time domain data is transformed to a frequency domain data by Fourier transform. These frequency domain measurements are processed by MATLAB algorithm to construct the FIR-Filter. A comparison between FIR-Filter coefficients is done to investigate the influence of the loosening on the filter coefficients.

4.1 Excitation and Response

The dynamic system may be described completely by its responses to a certain set of baseline, or reference input signals, provided that any given input signal may be consider to be composed of these baseline signals. This can be done either in the time domain or in the frequency domain. In our study an impulse response function $h(t,t')$ is used, which yields the system response at a time instant t to a Dirac delta-function external input $\delta(t - t`)$ applied at the time instant $t` < t$. The input pulse is characterized by an instantaneous rise in magnitude followed by a rapid decrease as seen in Fig. 4.1. The pulse has a duration time of 1 ms.
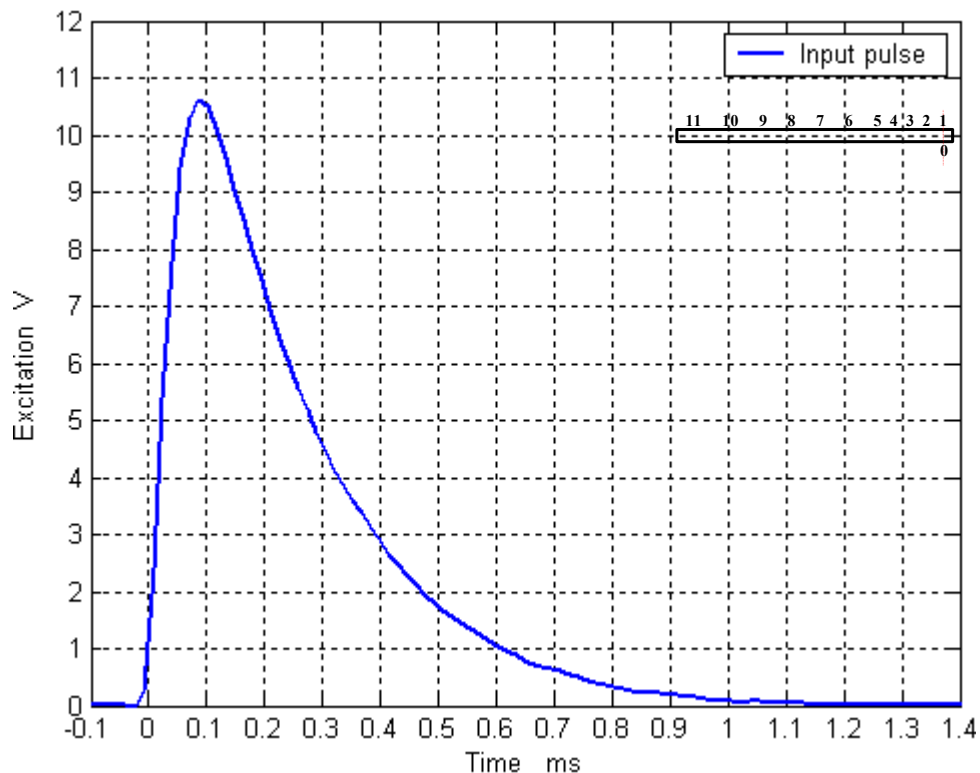

Fig. 4.1   Excitation pulse (System input).

The system response is recorded separately as an acceleration signal over the whole frequency range at different locations. Eleven experiments are carried out in our study. Excitation point is fixed at 20 mm from the right end of the model. It takes a number 0 in Fig. 4.2. The measuring positions take the number from 1 to 11 as shown in Fig. 4.2. The distance apart between points 1-2, 2-3, 3-4 and 4-5 is 10 mm.
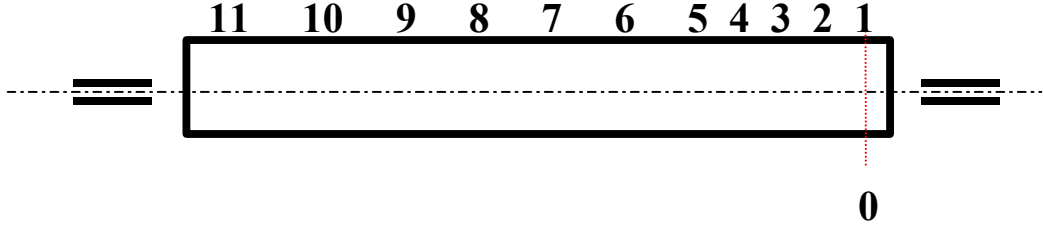

Fig. 4.2   System excitation and measuring points.

The response of the system to the direct transmission of the vibroacoustical energy is illustrated in Fig. 4.3. This response is a harmonic function having amplitude, which decays exponentially with time. Figure 4.3 shows the effect of shaft loosening on the transmitted energy. There are two measurements: one is measured at the secure case (the blue line in Fig. 4.3) and the other is at the loose case of prosthesis's shaft (the red dash-line). The acceleration in the loosed case is quickly decayed as in the secure case.
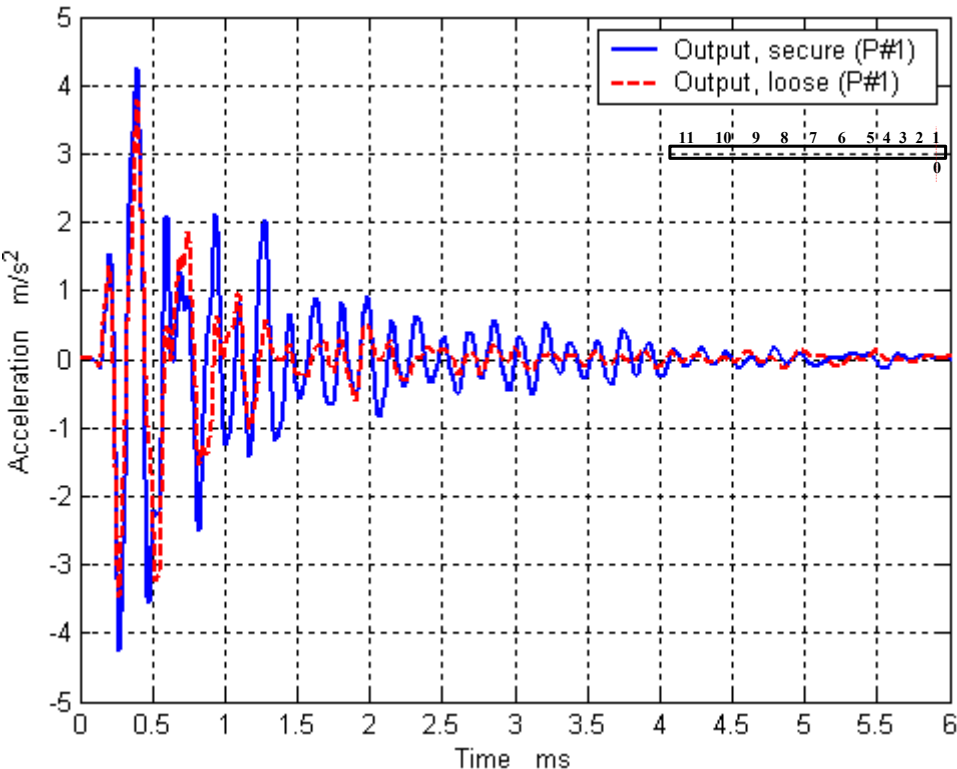

Fig. 4.3   System response (acceleration) at P#1 for secure and loose cases.

The direct transmission in this case means that both of accelerometer and the shaker have the same centerline as shown in Fig. 4.4.
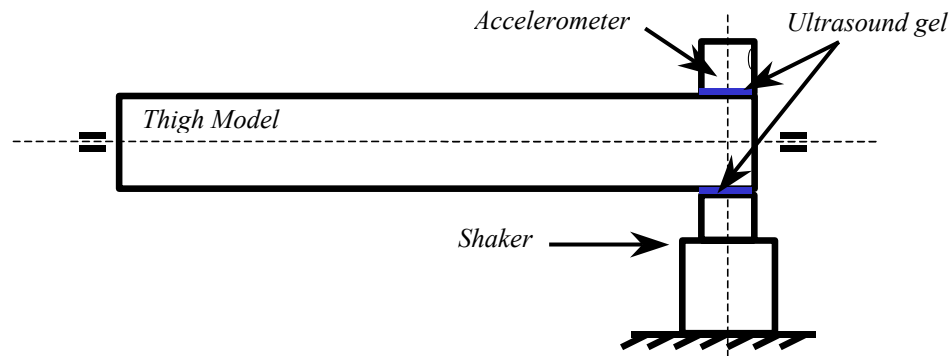
Fig. 4.4   Direct transmission of the vibroacoustical energy at P#1.

The next figure (Fig. 4.5) compares the system responses measured in secure and loose conditions at the measuring point 2. These responses ware captured through indirect transmission as shown in Fig. 4.6.
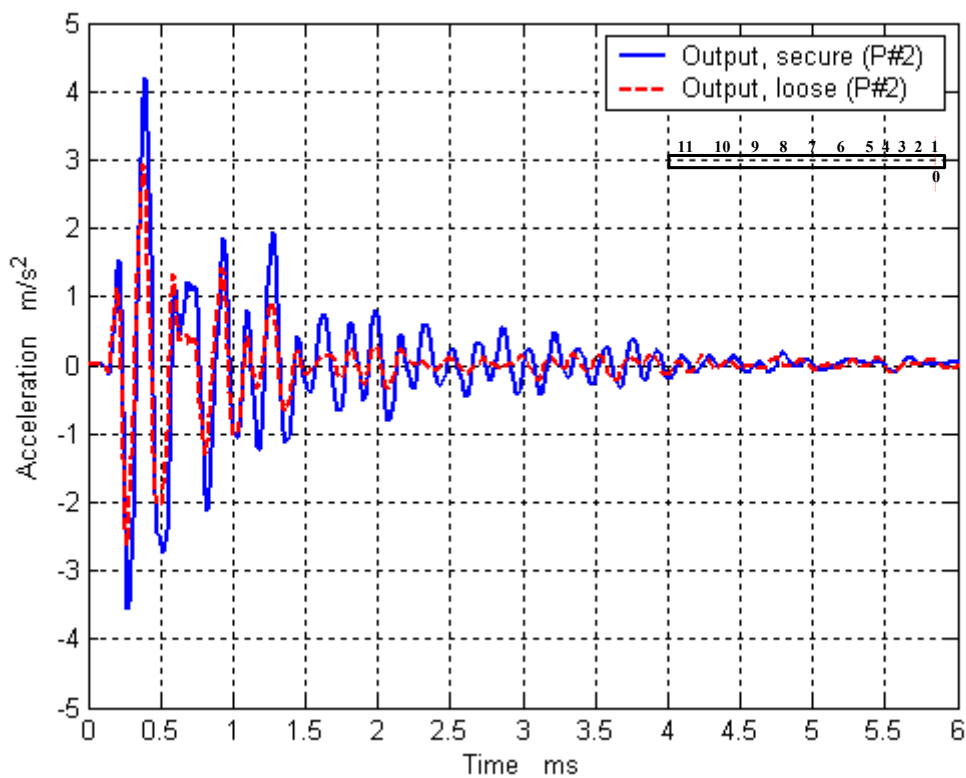

Fig. 4.5   System responses at P#2 for secure and loose cases.

The effect of the traveling path on the system response can be detected by comparing Figs. 4.5 and 4.3. It is obvious that the damping in the measured signal at P#2 is greater than that at P#1. Therefore, the indirect transmission has a different propagation mechanism with respect to the direct transmission. Figure 4.5 displays clearly the effect of the loosening on the acceleration. Here, the reduction of the vibration energy is as expected. Note that the loosed measurement is smaller than that of the secure one.
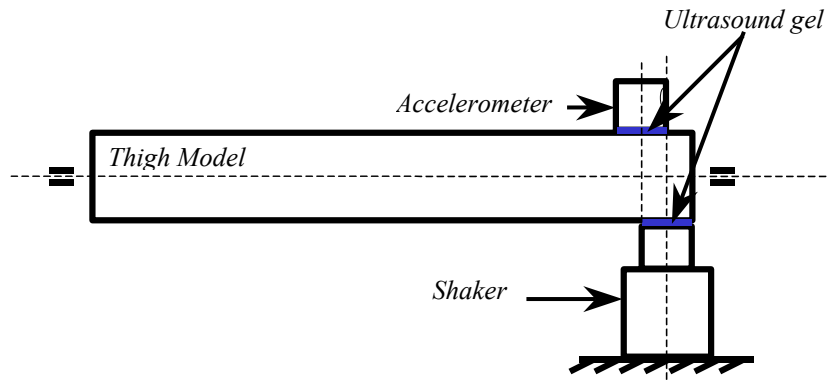
Fig. 4.6   Indirect transmission of the vibroacoustical energy at P#2.

In Figure 4.7 the corresponding responses are shown for the measuring point P#3. In this case, significant energy absorbing occurs, as evidenced by the accelerations plot.
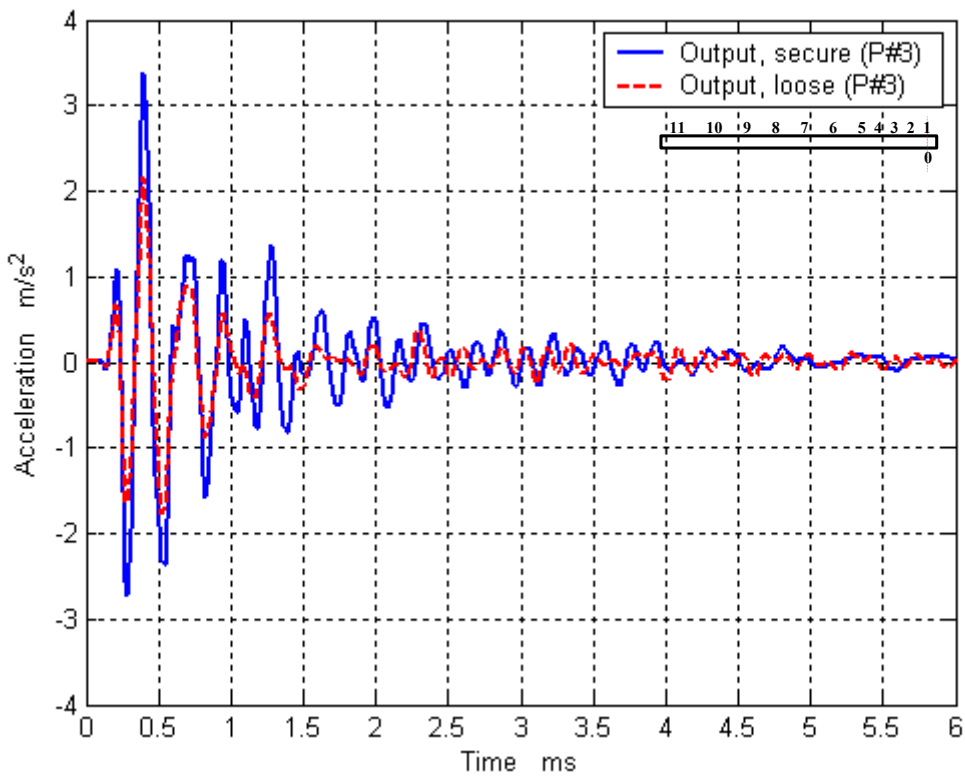

Fig. 4.7   System responses at P#3 for secure and loose cases.

The propagation path of the acoustic energy is increased, which resulted in a lower amplitude signal and a lower time of duration. A schematic of shaker-accelerometer arrangement for experiment 3 is illustrated in Fig. 4.8.
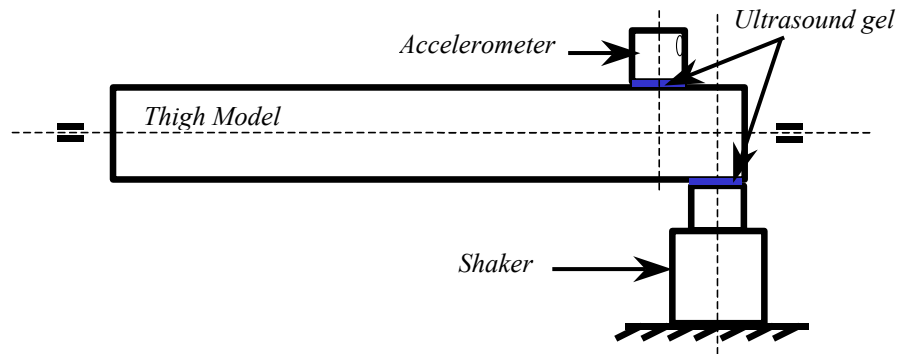
66

Fig. 4.8   Indirect transmission of the vibroacoustical energy at P#3.

Figure 4.9 depicts the responses at point P#4 on the model for the secure and loose cases. The distance apart the centerlines is 30 mm. The responses are highly decayed as that measured at P#3.
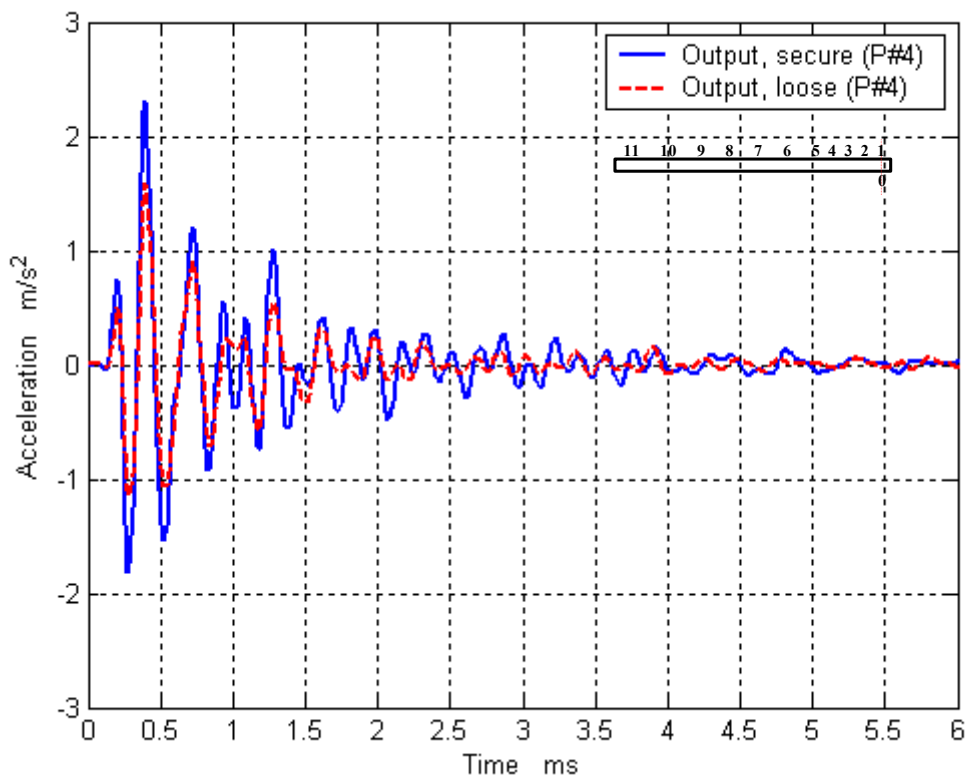

Fig. 4.9   System responses at P#4 for secure and loose cases.

The damping increases with the increase of the propagation path (the blue line) as seen in Fig. 4.9. Note that the first amplitude is 2.3 m/s^2. In addition to the path of travel, the loosening produces an additional damping (the red dash line) as seen in Fig. 4.9. Again, the first amplitude is reduced to 1.6 m/s^2. Based on these results, a reasonable speculation is that the loosed response has a different form of oscillation with respect to the secured response at the same measuring point. Figure 4.10 shows the position of the accelerometer with respect to the shaker.
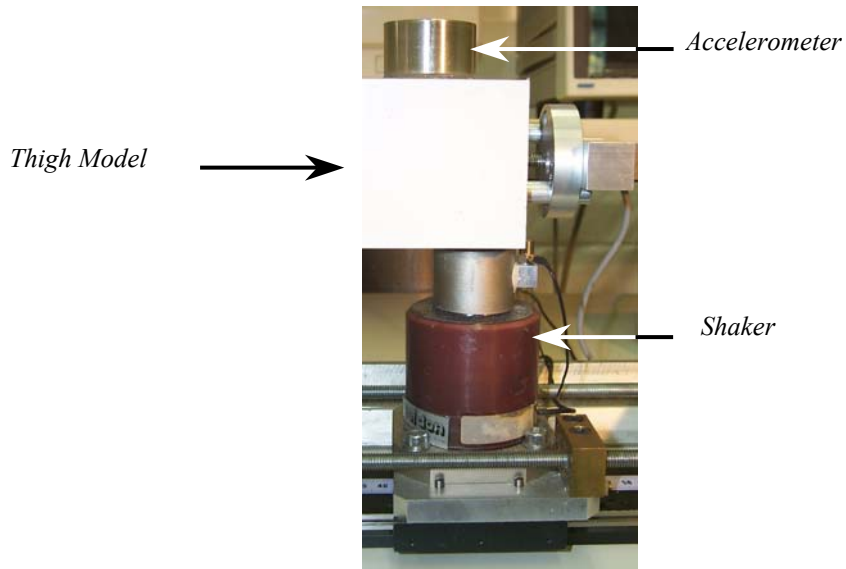
Fig. 4.10   Shaker- Accelerometer Arrangement at P#4.

Figure 4.11 shows the system responses when the centrelines distance is 40 mm. It is obvious that the amplitude of the first oscillation is reduced to 1,8 m/s^2 and 1.4 m/s^2 for the secure and loose cases respectively. The reduction in the oscillation of the secured response resulted from the influence of the loosening of the hip prosthesis on the propagation of the vibroacoustical signal. Where, the air gap between hip prosthesis and cement mantel works as a perfect reflect surface for the acoustic wave.
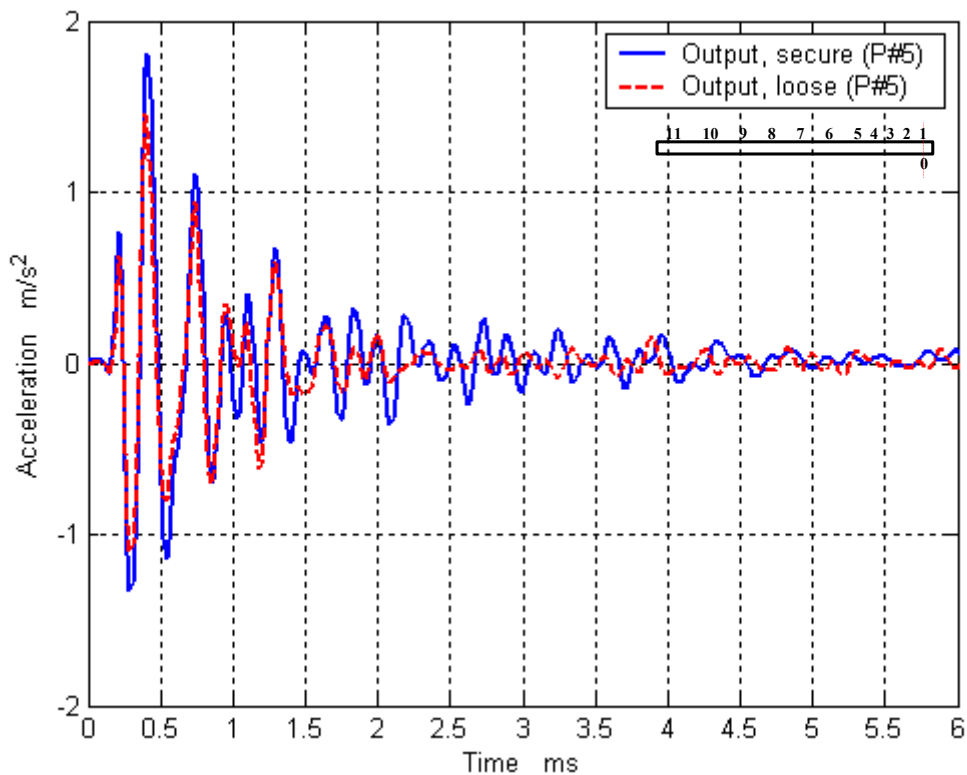

Fig. 4.11   System output at P#5 for secure and loose cases.

It is clearly that, the rate of damping is differ from point to point on the system and depends on the distance between the shaker (sender) and the accelerometer (receiver). If the travelling path increases, the damping rate increases as shown in Fig. 4.12.

Figure 4.12 depicts the responses at points 1 and 5 on the model for the secure case. The distance apart between P#1 and P#5 is 40 mm. It is obvious that the response at P#5 (red line) is highly decayed as at P#1 (blue line). It is clear that the energy of the secured response is greater than the energy of the loosed one and the measured vibration signatures contain a wealth of information, which can be used to monitor "health". That is, the changes in the characteristics of vibration signature can be used for detection the loosening of the hip prosthesis.
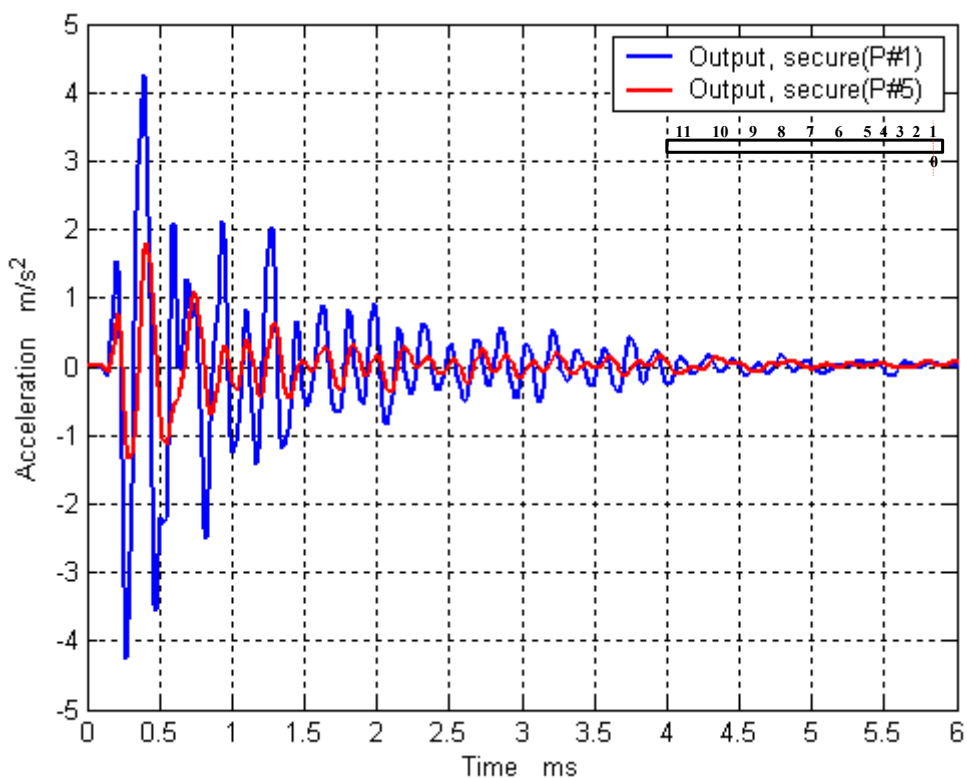

Fig. 4.12 Comparison between output at P#1 & 5 for secure and loose cases.

4.2 FFT Analysis

The goal of this research is to find out weather the changes in the frequency response of the damage prosthesis can be used as a diagnostic tool for detection the loosening of the shaft in the femur component of the THA. To perform this detection we have to know the frequency content of the system's input and output. An FFT algorithm is used to decompose the system's signals into its frequency components using the signal analyzer.

From a signal processing point of view, FFT produces the spectrum of the system's response (output signal). From an acoustic point of view, the amplitude of each spectral line is proportional to the density of the transmitted acoustic energy.

Figure 4.13 shows the frequency components of the input signal (Fig.4.1). It is used with the spectrum of the output signal to construct the transfer function of the system.
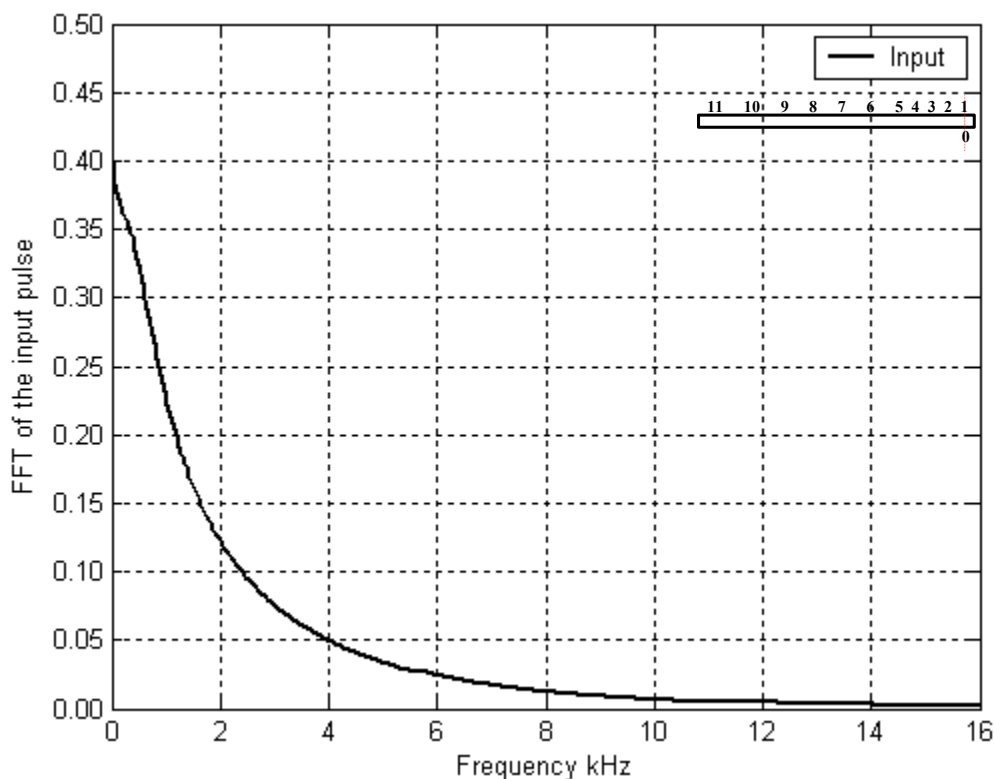

Fig. 4.13   FFT of the input pulse.

Figure 4.14 depicts the spectral analysis of the responses at P#2. It indicates the changes in the transmitted energy from point 0 to point 2. In another word, the presence of loosening might have modified the structure of propagating waves.

Comparing the reference signal for the transmission mode 0-2 in secure case (blue line) with the fault one (red line) indicates the reduction of the transmitted energy from 0.18 to 0.085 at frequency of 5.6 kHz. At frequency of 3.3 kHz, the transmitted energy is reduced from 0.11 to 0.08 as shown in Fig. 4.14. Also, a new modes of vibration are appeared after loosening, e.g., the splitting of the modes **a**, **b** and **c**. These splitting of the peaks of resonance are resulted because of loosening. The largest reduction in the transmitted energy, which resulted from loosening, is found to be 50% at frequency 5,6 kHz.
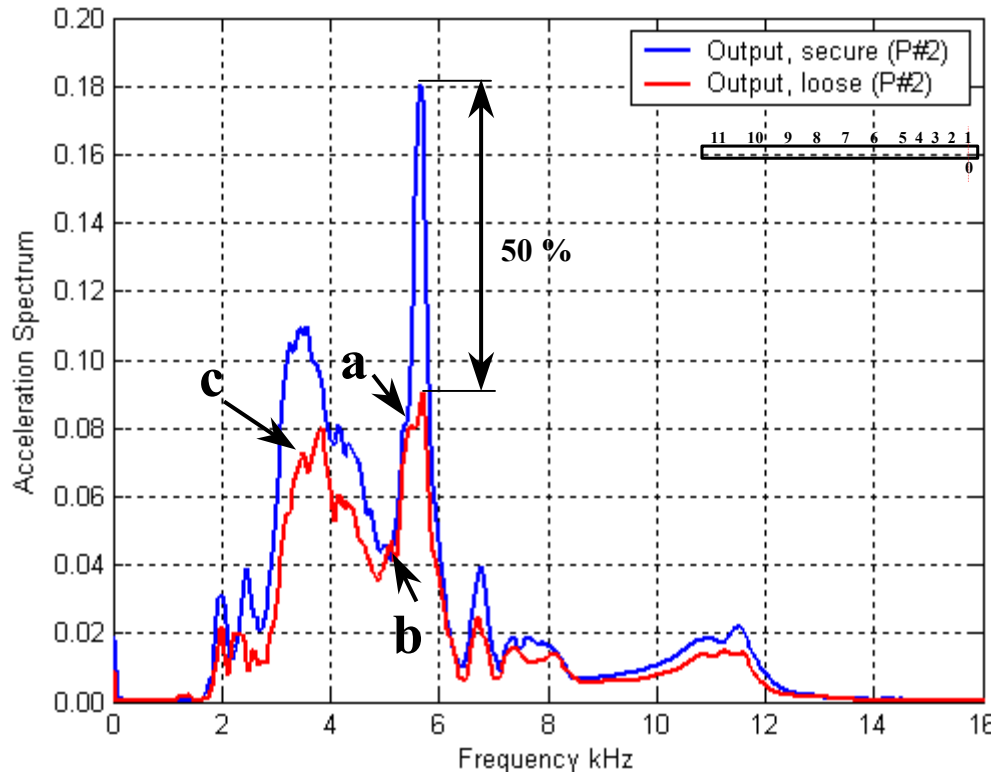
Fig. 4.14   FFT of the system response at measuring point P#2.

Figure 4.15 compares the 0-3 transmission mode of the system's responses in secure and loose conditions. The largest resonance frequency of the response appears at 5.6 kHz. Again, the frequency of 5.6 is affected by the loosening. The acceleration spectrum at 5.6 kHz is reduced from 0.12 to 0.042. The maximum resonance peak is splitted to form new vibration modes at frequency of 5.3 kHz (peak **a** in Fig. 4.15) and 5.7 kHz. A new vibration mode is separated from the resonance at 3.3 kHz (peaks **b** in Fig. 4.15). Between 7.3-7.5 kHz a new resonance peaks is appeared. The total reduction of the spectral energy at 5.6 is 65 %.

It is clearly that the damping increases with the increasing the shaker-accelerometer transmission path. The comparison between Figs 4.14 and 4.15 indicates the reduction of the transmitted energy at 5.6 kHz from 0.18 (mode 0-2) to 0.12 (mode 0-3). This reduction is approximately 33.3 %. Also, the main reduction of spectral energy appears particularly at the resonance frequency 5.6 kHz.
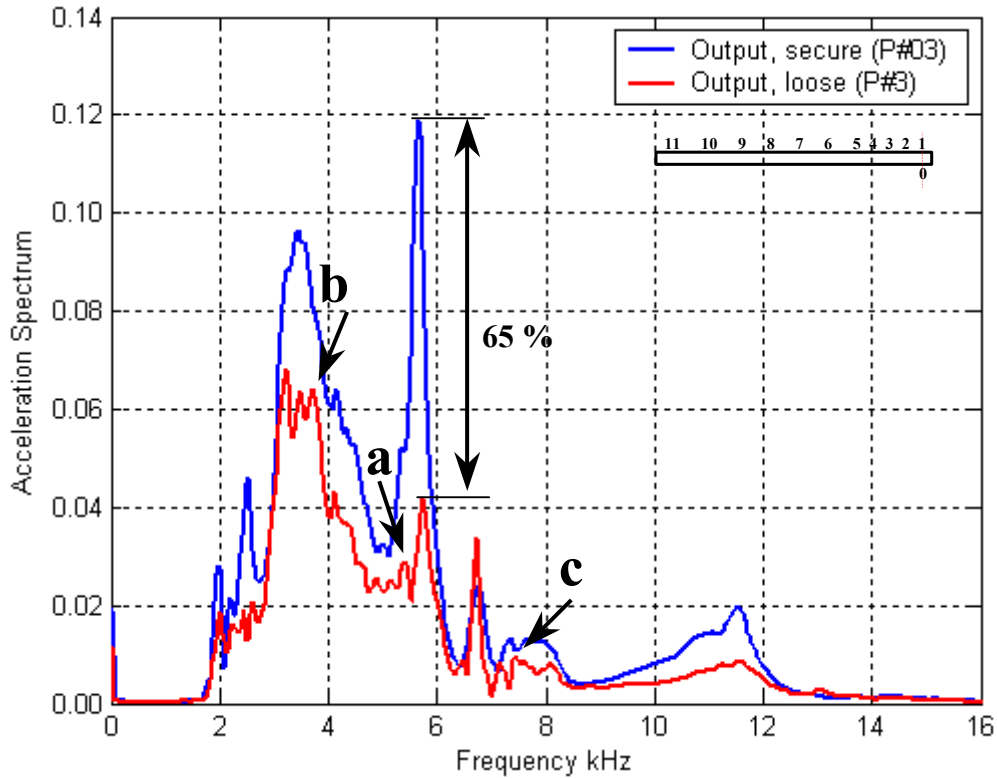
Fig. 4.15   FFT of the system response at measuring point P#3.

4.3 Frequency Response Analysis

4.3.1 Amplitude Response Analysis

The linear time-invariant dynamic system can be described adequately by its impulse response or transfer function. The plotting of amplitude frequency response (AFR) and phase frequency response (PFR) from the input excitation and the output response requires a special data processing. The resonates are determined by the maximum of the frequency response function. Which can be obtained by writing down the differential equation relating model output to model input in terms of operator s. For a linear system the transfer function is a ratio of two polynomial in s. If we substitute $j\omega$ for s the transfer function will then available as a vector quantity with a specific magnitude and phase angel for a particular value of frequency (Eq. (2.87)). The point of increased amplitude occurs at the natural frequency of the system. Where the natural frequency of any structure depends on the mass and stiffness distributions in that structure. The variation in the gain at selected frequency indicates that the loosening is produced. A fault (loosening) in the hip prosthesis is diagnosed by comparing the pattern vector (measured vector after loosening) with the stored one (measured vector before loosening). The loosening information (the change of the vector) resulted from the physical changing in the system under testing (SUT).

The gain of the FRF can be evaluated graphically as shown in Fig. 4.16. It depends on the ratio between the input and output. In another word, on the zeros of the system. The increasing of the zero's values increases the amplitude response. This means that, the residuum adopts the gain scale of the FRF. Consequently, the increase of residue leads to increase in the FRFs gain and vice versa. So, the reduction in the 1st resonant results from the decreasing of the value of residuum.
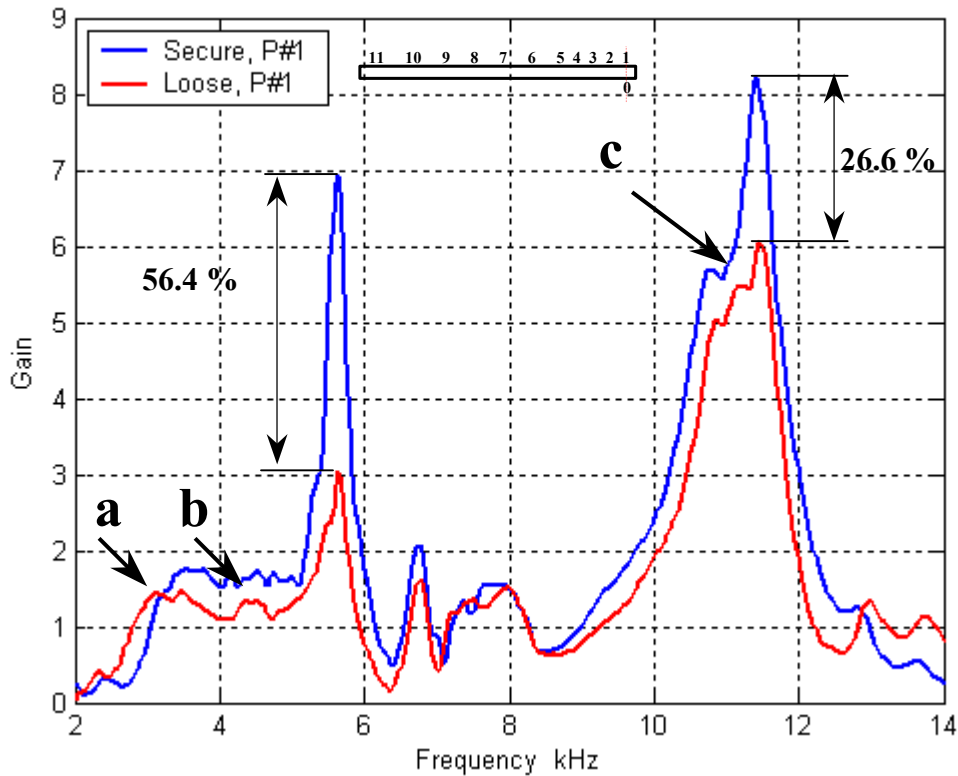
72

Fig. 4.16   FRFs$_{10}$ measurements error.

The dynamic characteristics of the system are investigated experimentally. Figure 4.16 shows the gain of the FRFs$_{10}$ (the subscript 10 corresponds to the transmission mode 01 as shown in Fig. 4.4, where 0 refers to the excitation point and 1 refers to the measuring point).

The gain of FRFs$_{10}$ displays many peaks of resonance. The main peaks are found at the frequencies of 5.6 kHz and 11.4 kHz. The first and the second resonance are shortened to the 1st and the 2nd in reminder of thesis. Also, our concentration will be paid to the 1st and the 2nd resonance frequency, according to section 3.3.2.

It is clear that the prosthesis loosening would yield low gain in the FRF$_{10}$. Considering the transmitted energy, the effect of the loosening is to sharply absorb vibrational energy at the 1st resonance frequency. This result proves the effectiveness of the loosening in absorbing impulsive energy. Also, the loosening produces a new resonance peaks (a, b & c) in the FRF$_{10}$.

Comparing the transmitted energy (responses) of the system with and without loosening, we conclude that the loosening results in a reduction of 26.6 % of the maximum level of transmitted vibration (2nd resonance) and 56.4 % of the 1st resonance. We conclude that, at this level of the loosening (L=0 mm), the energy transferred is absorbed, enhancing the shock isolation properties of the system.

Figure 4.17 illustrates the gain of FRFs$_{20}$ for experiment two as shown in Fig. 4.6. The gain of FRFs$_{20}$ for both case documents the changes in the model zeros specially for the 1st and the 2nd resonance frequencies. Consequently, a lost of 45.7 % and 25 % in the transmitted vibration energy for the 1st and the 2nd resonance frequencies respectively, and
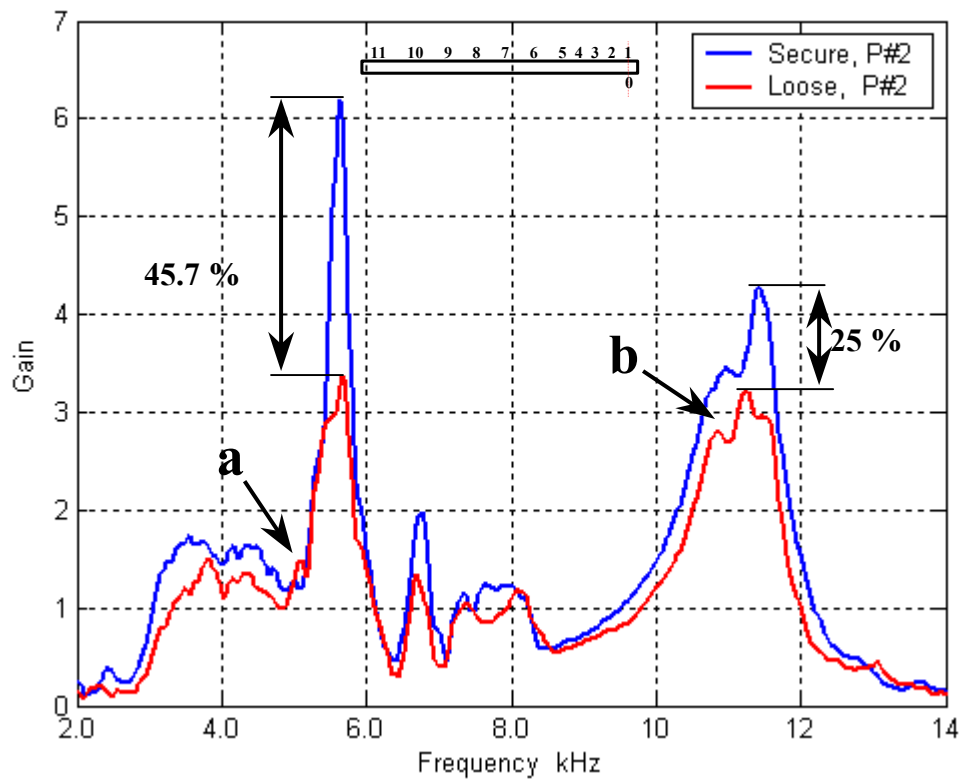
Fig. 4.17   FRFs$_{20}$ measurements error.

this is the cause of the changing of the mode shape at this frequency, as we will see in the Nyquist diagrams later. It is seen that the loosening sharply absorbs the transmitted energy at the 1st resonance frequency. A new resonance peaks (**a & b**) are appeared in the FRF$_{20}$ for the loose case as shown in Fig.4.17.

Figure 4.18 compares the gain of the FRFs$_{30}$. This experiment represents an indirect transmission of the excitation signal too as seen in Fig. 4.8.

Again, the maximum absorption of the transmitted energy occurs at the 1st resonance frequency. The absorbed energy is found to be 61.4 %. Also a new resonance peaks (**a**, **b** and **c**) are found in the FRF$_{30}$ for the loose case

Figure 4.19 reports the FRFs$_{40}$ measurements error for the shaker-accelerometer arrangement showed in Fig. 4.10. Also, a reduction of 46.9 % of the transmitted energy occurred at the 1st resonance after loosening. New peaks (**a**, **b & c**) are showed in the FRF$_{40}$ diagram too.

It is clear that the maximum resonance is occurred in the direct transmission case at frequency of 11.4 kHz (mode 0-1 as seen in Fig. 4.4) as shown in Fig. 4.16. On the contrary of the other experiments (indirect transmission, the maximum resonance was found at 5.6 kHz. For all FRF measurements, the 1st resonance frequency was found to be very sensitive to the loosening.

Based on the experimental observation, the 1st resonance frequency is found to be an important factor in the detection of the loosening of the hip prosthesis.
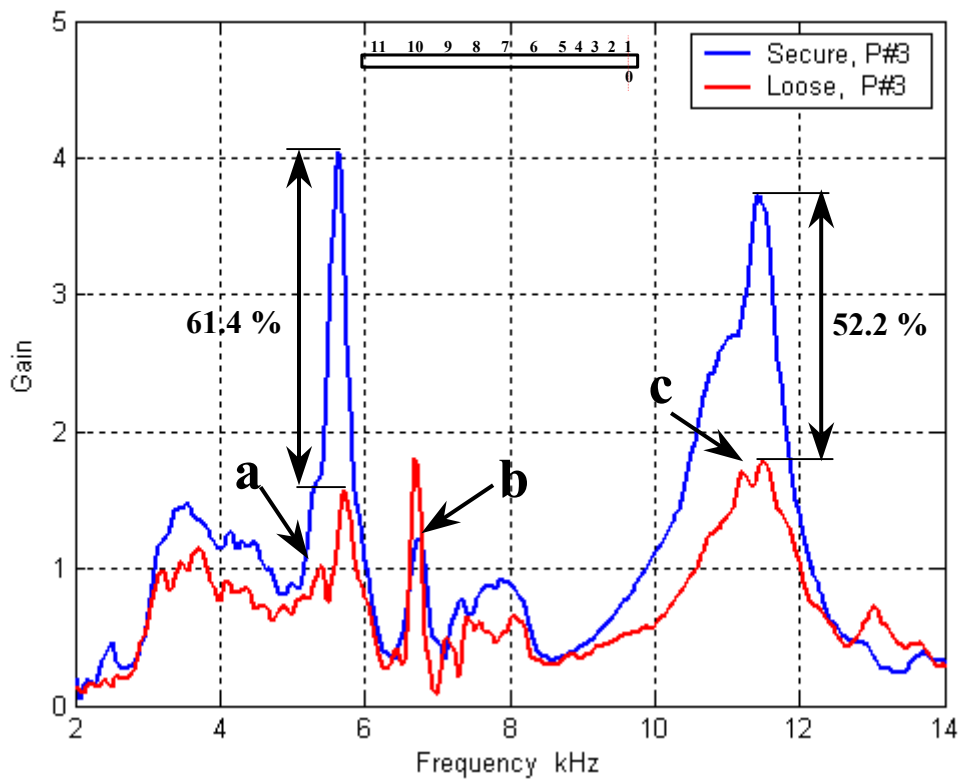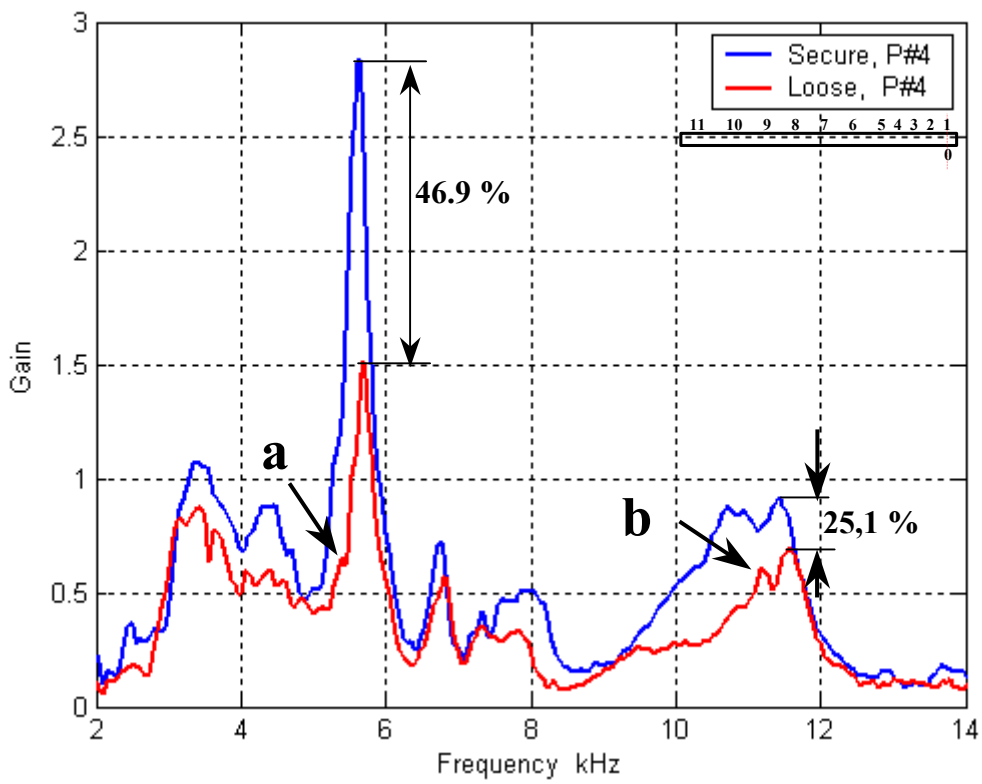
Fig. 4.18 FRFs$_{30}$ measurements error.

Fig. 4.19 FRF$_{40}$ measurements error.

4.3.2 Measurements and Results Quality Analysis

According to Eq. (4.44), the coherence function can test the quality of the measurements and the results. Where, the coherence is a correlation coefficient, which informing us about the degree of consistency of all averages of the frequency response function. Coherence equal to 1 indicates that each average is exactly the same. Lower coherence indicates a (significant) variance exists on the average.

Figures 4.20 illustrate the coherence function of the $FRFs_{10}$. The correlation coefficient is equal to unity for the required range of measurements. There is a good coherence every where. Also, a perfect linear relationship exists between the pulse and the response over all averages for the $FRFs_{10}$.
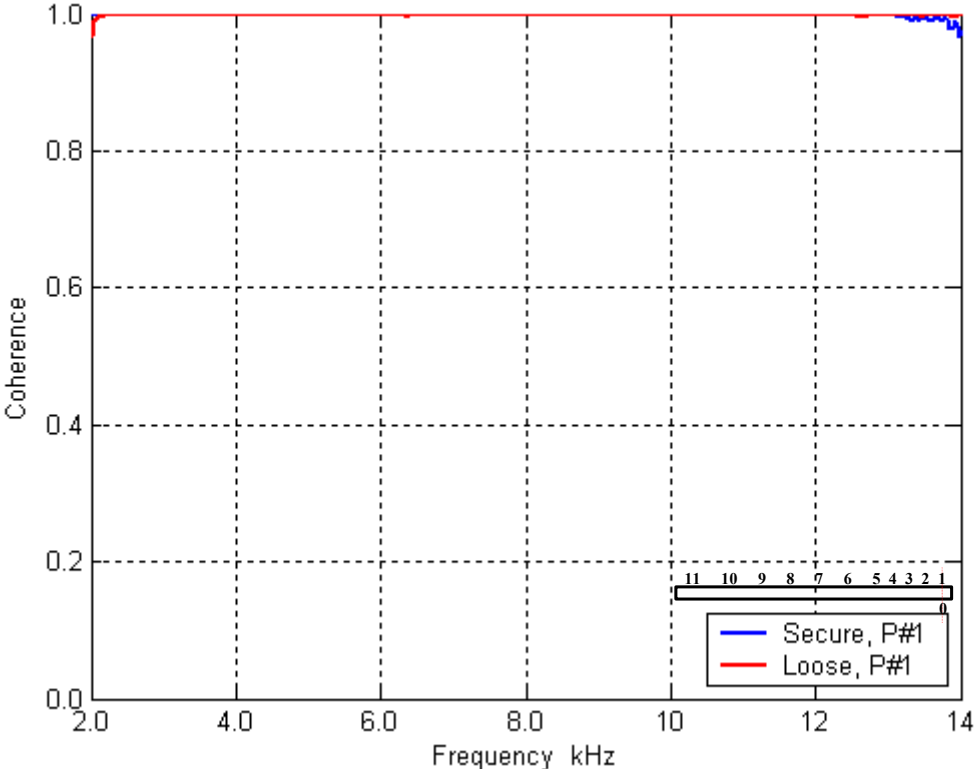

Fig. 4.20   Coherence function of FRF_{10}.

Figure 4.21 illustrates the coherence function of the $FRFs_{20}$. It documents that the correlation coefficient equal to unity for the required range of measurements except after the 2nd resonance. Also, a perfect linear relationship exists between the pulse and the response over all averages for the $FRFs_{10}$ except after the 2nd resonance, where the correlation coefficient is decreased as shown in Fig. 4.21. This reduction in correlation coefficient is occurred at frequency of 12.3 kHz, i.e., after the 2nd resonance of the $FRFs_{20}$ as shown in Fig. 4.17. These reductions may be due to the influence of noise on the measured spectra of pulse, according to Ewins [111].
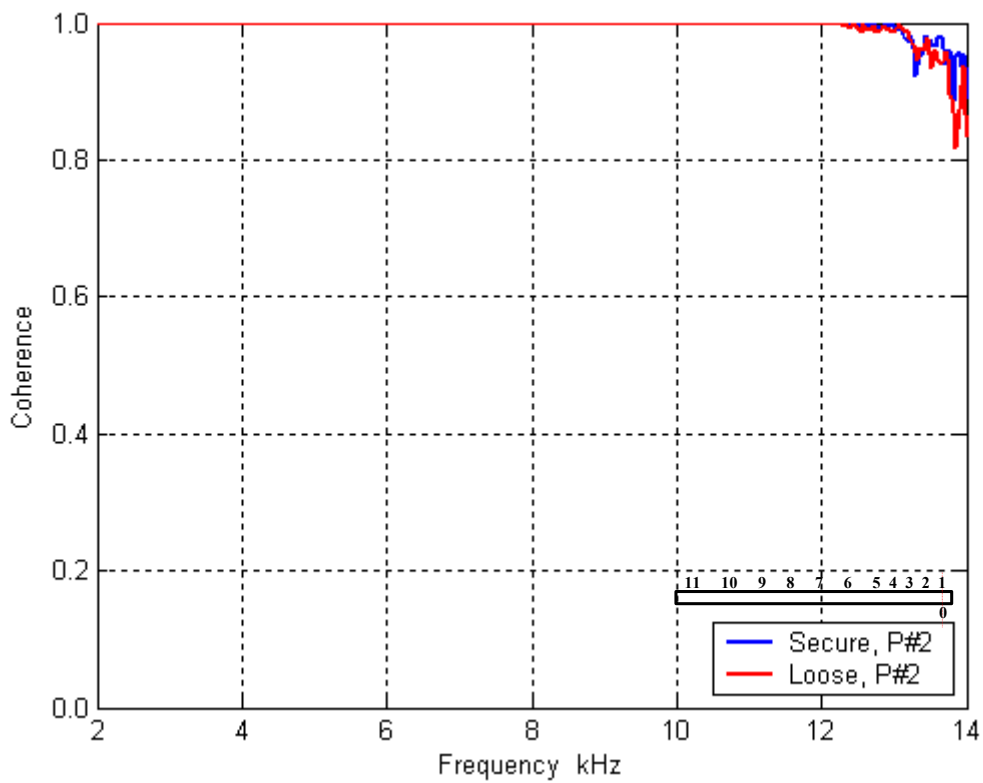
Fig. 4.21   Coherence function of FRF$_{20}$.

Figure 4.22 shows the coherence function of FRFs$_{30}$. Again, there is a good coherence every where except insignificant reduction at some frequencies.
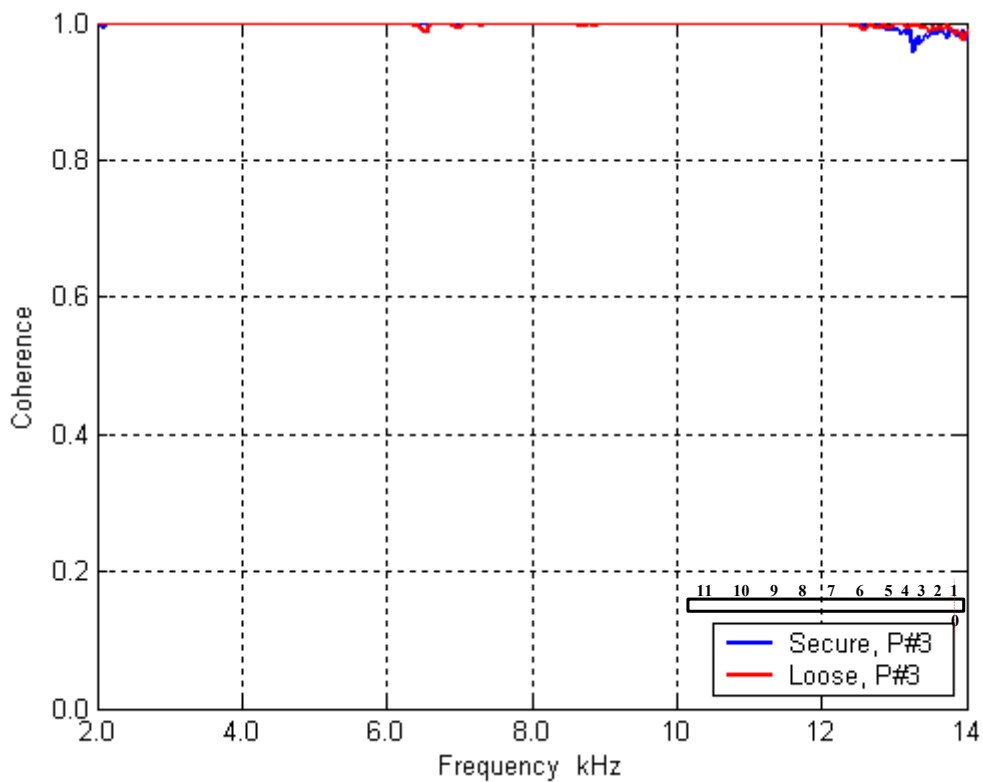

Fig. 4.22   Coherence function of FRF$_{30}$.

4.3.3 Phase Response Analysis

Equation (2.70) represents the phase spectrum of the frequency response function of the system. It shows that, the phase angel is the argument of the ratio between the imaginary and the real parts of the FRF, in our case FRF_{10}. It is obvious that the phase angel changes with the changing in *Im(f)* and *Re(f)*.

Figure 4.23 shows two measurements of the phase frequency response (PFR_{10}) measured at point #1 in degree. The blue line represents the PFR_{10} for the secured case of prosthesis's shaft and the red line represents the PFR_{10} for the loosed one. Comparing the reference phase frequency response (blue line) with the fault (red line) one indicates the changes in the phase angel as seen at pint *a*, *b*, *c* and *d* in Fig. 4.23.

The changes of the phase angel may be demonstrated by the radian plot of the phase response as shown in Fig. 4.24. Again, the red line dose not coincides with the blue one. Any one can interpret this plot by shifting of 2π of the phase angle for the loosed case, but the true is the changing of the of the phase angel in the loosed case with respect to the secured one as we will see in the next section.

Also, the difference between two phase angels can be seen clearly in the Nyquist diagram as we will seen later in this chapter.

Figure 4.5 displays clearly the effect of loosening on the phase frequency response (PFR_{20}) measured at point #2 in degree. Again, The red line (base vector) dose not coincides on the blue one (fault vector), which exhibits the occurrence of loosening i.e. the physical changes in the system as shown in Fig. 4.25 (e.g. *a*, *b* and *c*).

Based on the experimental observation of the FRF_{30}, the occurrence of loosening is determined by comparing the phase spectrums for both secured and loosed prosthesis as seen in Fig. 4.26. The differences between the two measurements are clearly appears (for example *a*, *b*, *c* and *d*) in Fig. 4.26.
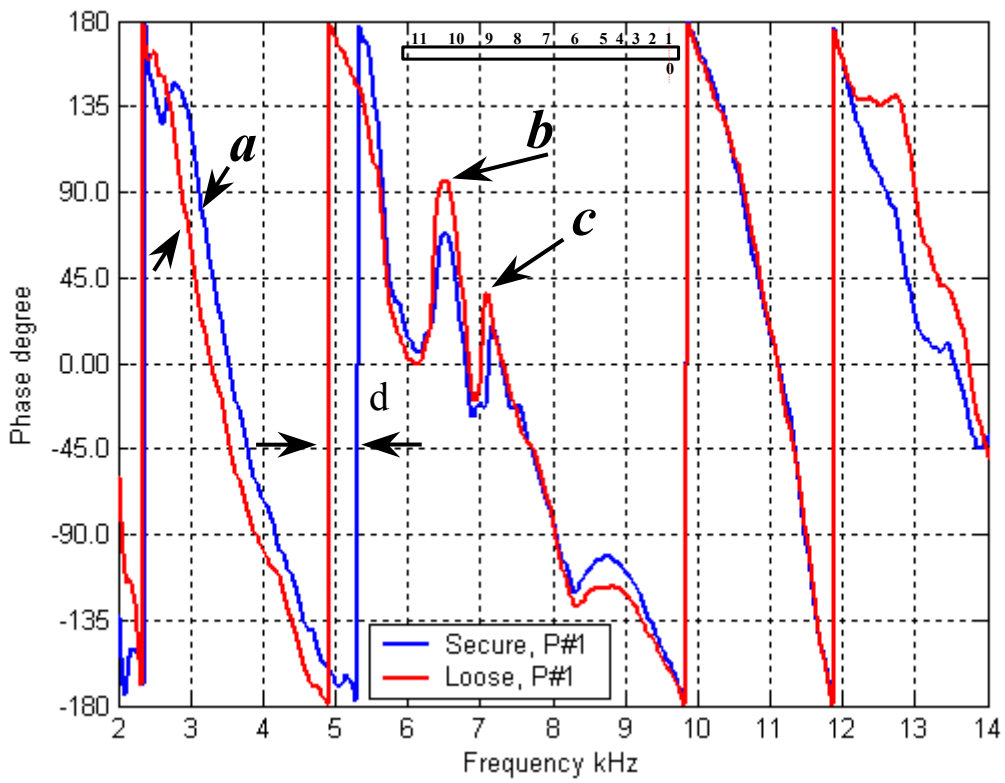
Fig. 4.23   Phase error of FRF_{10} for secure and loose cases in degree.

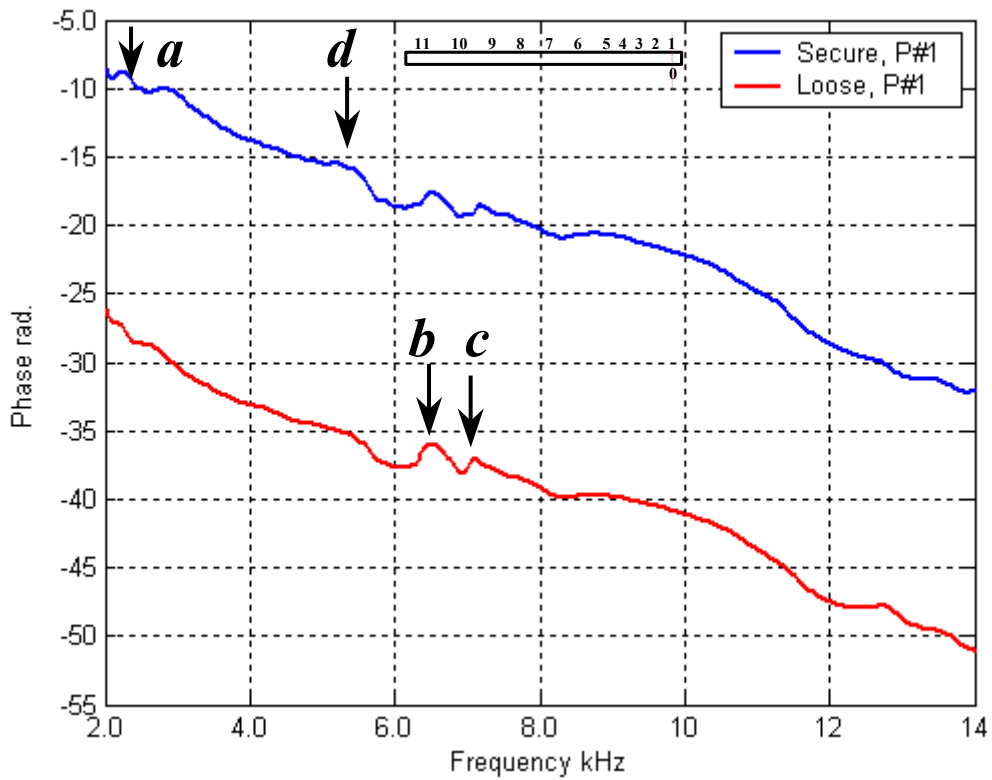

Fig. 4.24   Phase error of FRF_{10} for secure and loose cases in radian.
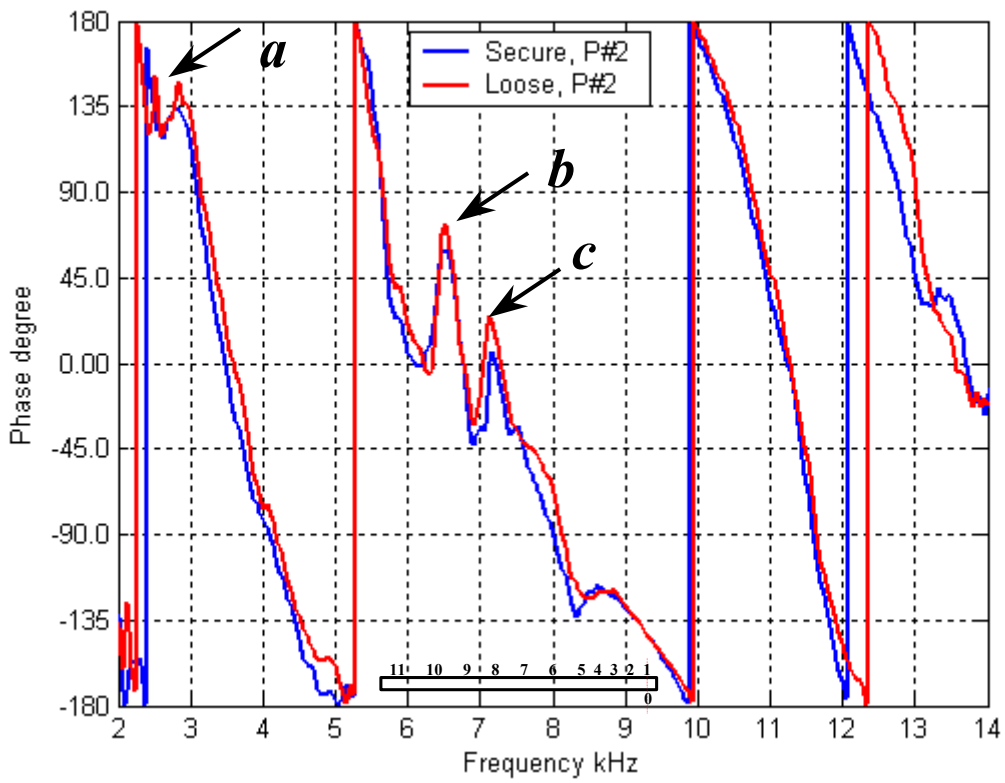
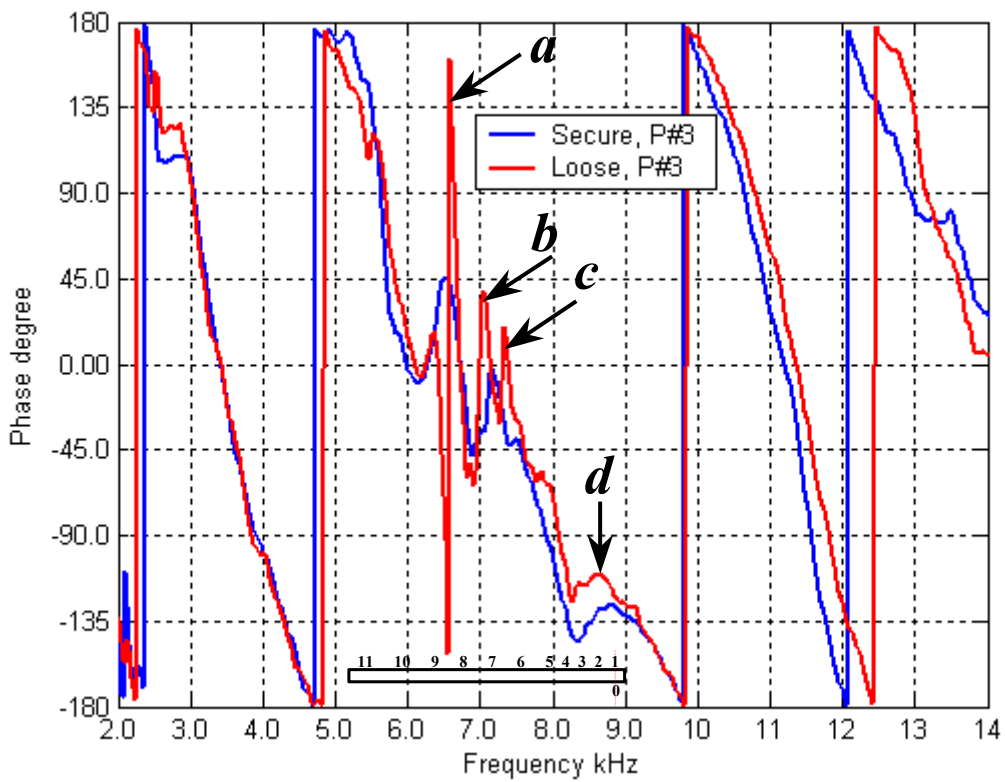Fig. 4.25   Phase error of FRF$_{20}$ for secure and loose cases in degree.

Fig. 4.26   Phase error of FRF$_{30}$ for secure and loose cases in degree.

4.3.4 Imaginary-Real Part and Nyquist Analysis

The transfer function of the system or FRF is a complex quantity. It consists of two parts, one called the Real part *Re(f)* and the other called the imaginary part *Im(f)*. From these two parts the amplitude and phase frequency response can be constructed. Equation (2.68) displays these two parts.

The loosening detection strategy depends on the comparison between transfer functions before (base vector) and after (fault vector) loosening as given in Fig. 3.13. From that measuring strategy each component of equation (2.68) is compared with its corresponding component for both secure and loose state of the prosthesis.

Figure 4.27 illustrates the imaginary part of the FRF_{10}. There are two measurements, one for the secure case (blue line) of prosthesis and the other of the loosed one (red line).
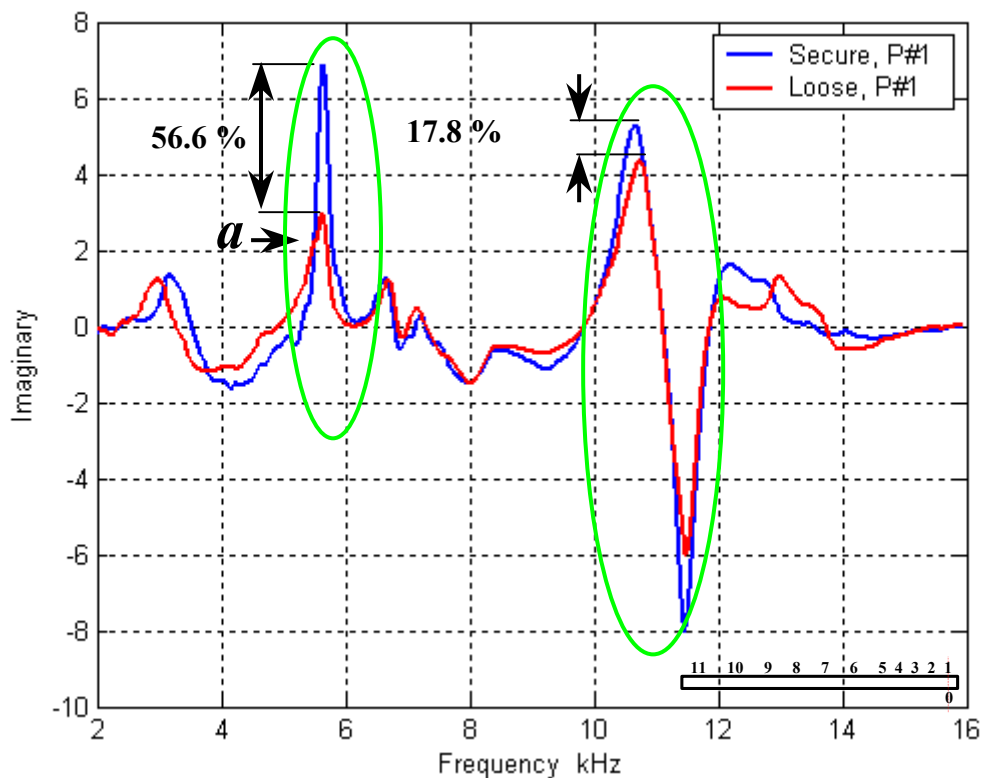
Fig. 4.27   Imaginary part error of FRF_{10}.

The greatest difference (error) between the base vector and the fault one appears at the first natural frequency. The percentage of reduction for the 1st resonance frequency at 5.6 kHz was found to be 56.6 %. The reduction in the imaginary part of FRF_{10} resulted from the physical changes in the system (loosening).

Analysis of Figure 4.27 illustrates a decoupling of a new mode from the 1st resonance frequency (point a). This new mode appears at 5.5 kHz.

It is obvious that the damping resulted from loosening at the 1st resonance frequency is the greatest one at any where on the curve. From that we can conclude that the 1st resonance frequency is the most sensitive frequency to loosening.

The comparison between Fig. 4.27 and 4.16 at the 1st resonance frequency indicates that the FRF_{10} becomes imaginary at this frequency.

Figure 4.28 shows the error due to loosening for the real part of frequency response function for mode 0-1. It is clearly that the greatest distortion appears in the frequency band 5-6.5 kHz i.e. the 1st resonance frequency band (green ellipse).
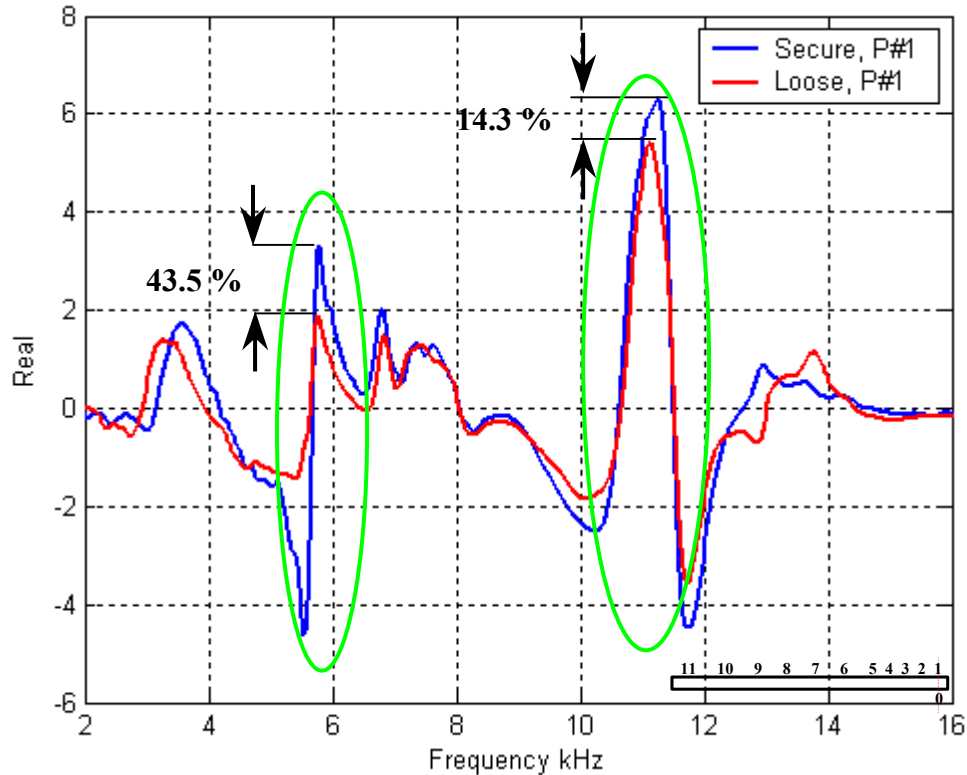

Fig. 4.28   Real part error of FRF_{10}.

If we call equation (2.70) which represent the relation between phase angel spectrum and the both of the imaginary and the real part specially for the frequency band 5-6.5 kHz, we can concluded that a changing in phase must be appeared at these frequencies (5-6.5 kHz) as given in Fig. 4.23. These changes will be clearly appeared in the Nyquist analysis.

The deviation between both FRF measurements (secure and loose) becomes even more obvious if the Nyquist plots are used. However, each resonance region is expected to trace out at least part of a circular arc, the extent of which depends largely on the interaction between adjacent modes. It is to be expected that each resonance will generate the major part of the circle. The Nyquist plot should ideally exhibit a smooth curve. The required information for detecting the loosening of hip prosthesis will be discussed as follow.

Figure 4.29 shows the magnitude and phase deviations between the FRF_{10} measurements. It depicts the great reduction of the gain of the FRF_{10} in the loosening state (shape **B**) in comparison with the secure state (shape **A**). So, the loosening becomes more obvious.

It is clear that the first natural frequency (1st resonance) generate the major part of the circle. The difference in size between shape **A** (base vector) and shape **B** (fault vector)

82

informs us about the existence of the physical changes in the system (prosthesis loosening) as shown in Fig. 4.29.
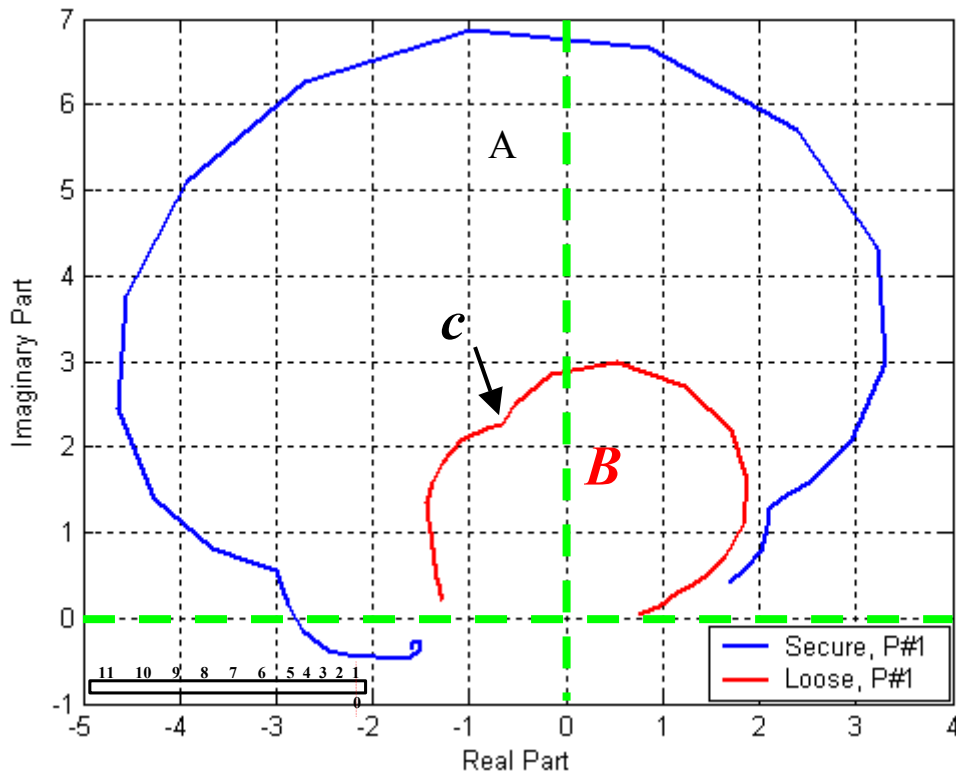

Fig. 4.29   1st resonance distortions due to loosening for FRF$_{10}$ (top view of Fig.4.46).

The distortions in both real (*Re(f)*) and imaginary (*Im(f)*) of the FRF$_{10}$ becomes very clearly due to loosening, where the size of B is strongly reduced. The linking between Fig. 4.29 and Figure 4.16 gives us very clear information about the existence of loosening.

By investigating the parallelism between both contour or profile of shape *A* and shape *B* the shifting in phase angel can be assessed. In other words, the centeroied of shape *A* lays on the left side of the Imaginary axis (Im.) and shape *B* has its centroied in the right side of the same axis as shown in Fig. 4.29. Also, shape *B* loos its curvature at some circumference points (*c*). These changes (non-parallelism) indicate the phase shift, which resulted from loosening.

The important of using the Nyquist diagram for monitoring the loosening of the hip prosthesis is clearly now illustrated.

Figure 4.30 documents the relationship between the imaginary (*Im(f)*) and Real (*Re(f)*) parts of the FRF$_{10}$ and frequency (3D Nyquist diagram).
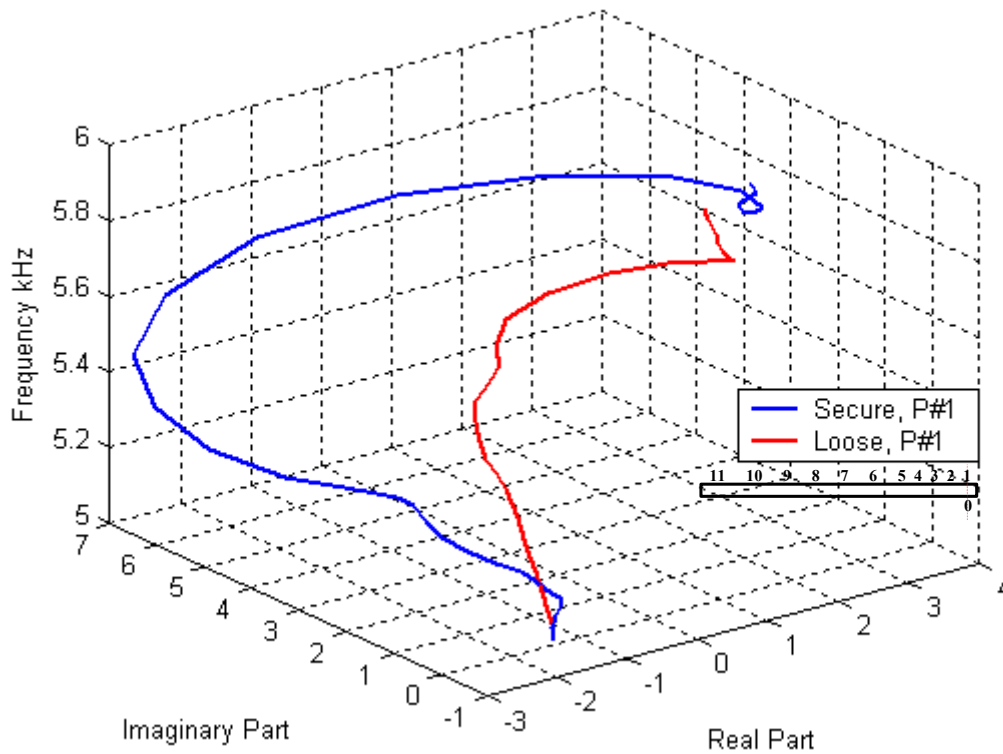
Fig. 4.30   3D plot of the 1st resonance distortions due to loosening for FRF_{10}.

Figure 4.31 depicts in 3D the relationship between the real (*Re(f)*) and imaginary (*Im(f)*) part of the FRF_{10} and frequency (*f*) for the 2nd natural frequency band (10-12 kHz).

Figure 4.32 shows the top view of Fig. 4.30. It has tow FRF_{10} measurements for the same frequency band (10-12 kHz) one for secure case (blue heart **A**) and the other for the loosed one (red heart **B**). The distortion due to loosening can be assessed by comparing both of them (heart **A** & **B**).

Heart **B** is smaller than heart **A**, which can be related to the reduction in gain as previously shown in Fig. 4.16.

If we imagine an axis (RR) divided the two hearts as shown in Fig. 4.32, the symmetry of the two hearts can be investigated. They are approximately symmetrical about the imaginary axis RR.

Many points on the circumference of heart **B** are lost its curvature to have a straight line shape (L in Fig. 4.32). This non-parallelism (L) indicates the change in the phase as a result of loosening.
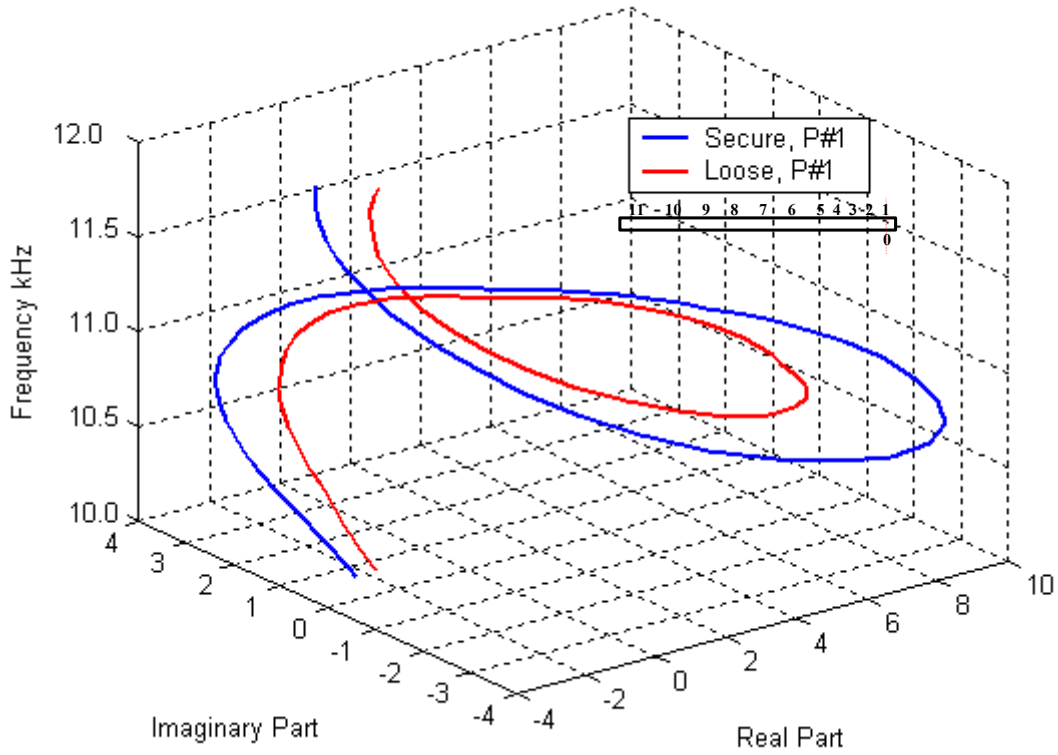
84

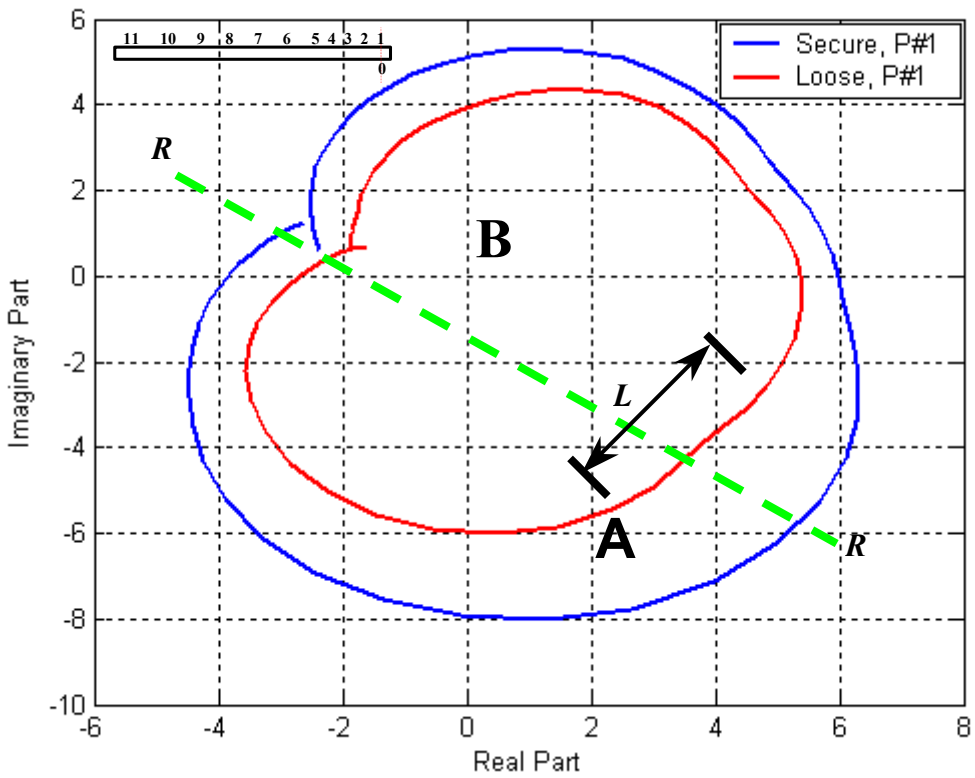Fig. 4.31   3D plot of the 2nd resonance distortions due to loosening for FRF_{10}.

Fig. 4.32 2nd resonance distortions due to loosening for FRF_{10} (top view of Fig.4.31).

The relationship between the imaginary part of FRF_{20} for the indirect transmission mode 0-2 (Fig. 4.6) and frequency is shown in Fig. 4.33.
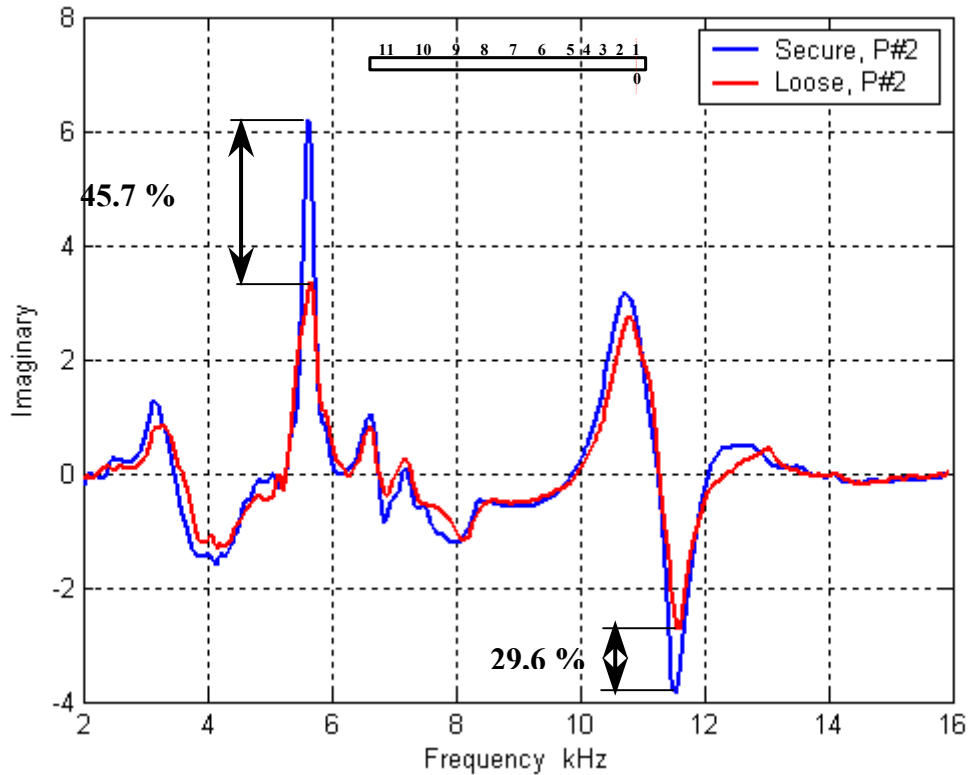

Fig. 4.33   Imaginary part error of FRF_{20}.

It is obvious that, the loosening reduces the values of the imaginary part of the FRF_{20} by 45.7 % at frequency of 4.6 kHz and 29.6 % at frequency of 11.5 kHz. This indicates that the damping at the 1st natural frequency is greater than the damping at the 2nd one.

The other part of the FRF_{20} is the real part. Figure 4.34 shows the reduction of the real part's values at 5.7 kHz and 11.3 kHz.

These reductions in both real and imaginary parts of the FRF20 are reflected on the construction of the amplitude response (Fig. 4.17) and phase response (Fig. 4.25). From this point of view the, the loosening of hip prosthesis produces a significant changes in the FRF of the system.

Again, the Nyquist diagram will be used to demonstrate the influence of loosening on the main parts of the FRF_{20}. Figure 4.35 illustrates in 3D the distortions in Nyquist diagram, which resulted from loosening. It indicates that, the first and the second natural frequency construct the main circular shape (arcs) in the plot. The top view of Fig. 4.35 is given in Fig. 4.36. It is clearly that the 1st and the second natural frequencies construct the main arcs. Every resonance will be discussed separately as follow.

Figure 4.37 documents the effect of loosening on the Nyquist plot of FRF_{20} for frequency band 5-6.5 kHz. To simplify the analysis, the secure shape will take the Letter **A** and the loosed one will take the letter **B** as given in Fig. 4.37.
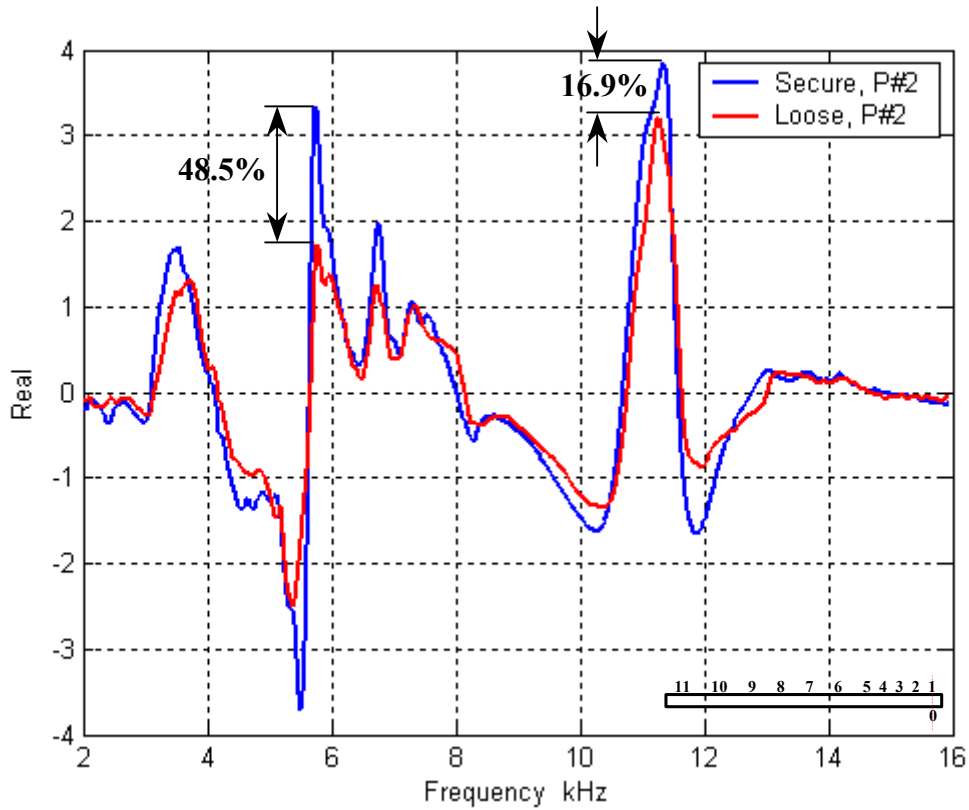
Fig. 4.34   Real part error of FRF_{20}.

It is clearly that, shape **A** is symmetrical about the imaginary axis. Shape **B** rotates itself in the left direction. A great sector of shape **B** profile lost its curvature to have the straight line shape (sector L) as shown in Fig. 4.37. Also shape **B** is smaller than shape **A**, i.e. the damping resulted from loosening affect on the size of shape **B**, in another word, on the gain of the FRF_{20}.

Non-parallelism property appears at some frequencies (e.g. L sector), which indicates the changes in phase angel between the input and output of the system as a result of loosening as given in Fig. 4.37.

Figure 4.38 illustrates the Nyquist plot of FRF20 for frequency ranges 10-12 kHz for both cases (secure and loose) of prosthesis's shaft. It is obvious that, shape **B** (loose case) is smaller than shape **A** (secure case) for the 2nd natural frequency band. This reduction in size is a sign for the reduction in gain as given in Fig. 4.17 too.

Fig. 4.35   Nyquist diagram distortions in 3D plot for FRF_{20}.

Fig. 4.36 FRF_{20} distortions due to loosening (top view of Fig.4.35).

88

Fig. 4.37   1st resonance distortions of FRF$_{20}$ due to loosening.
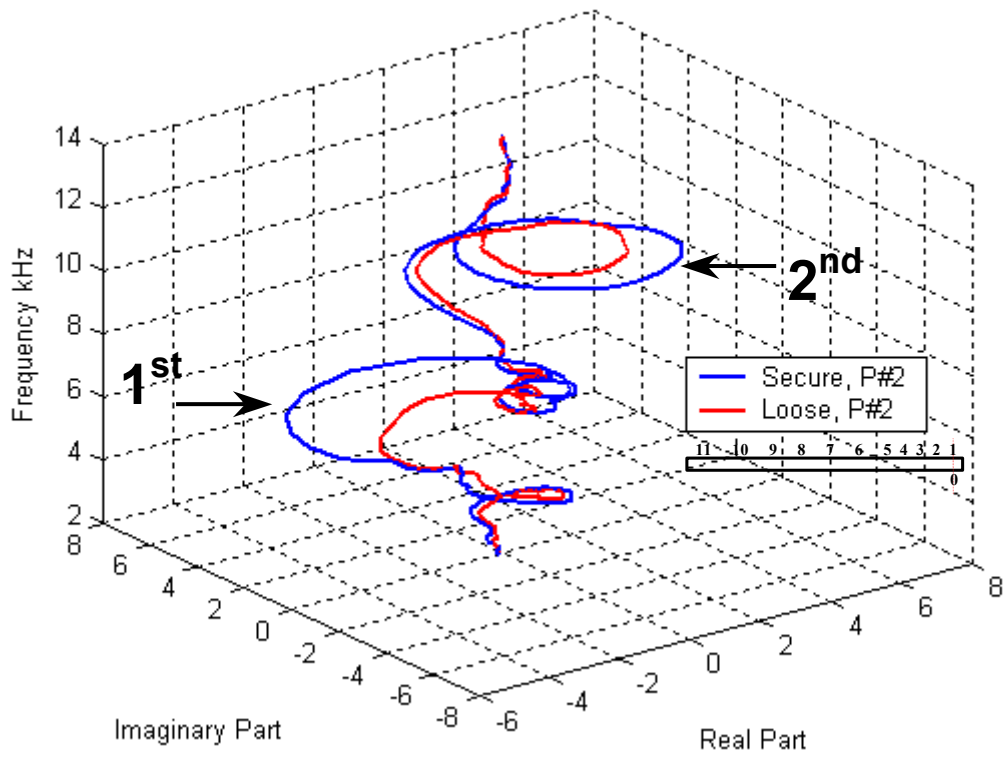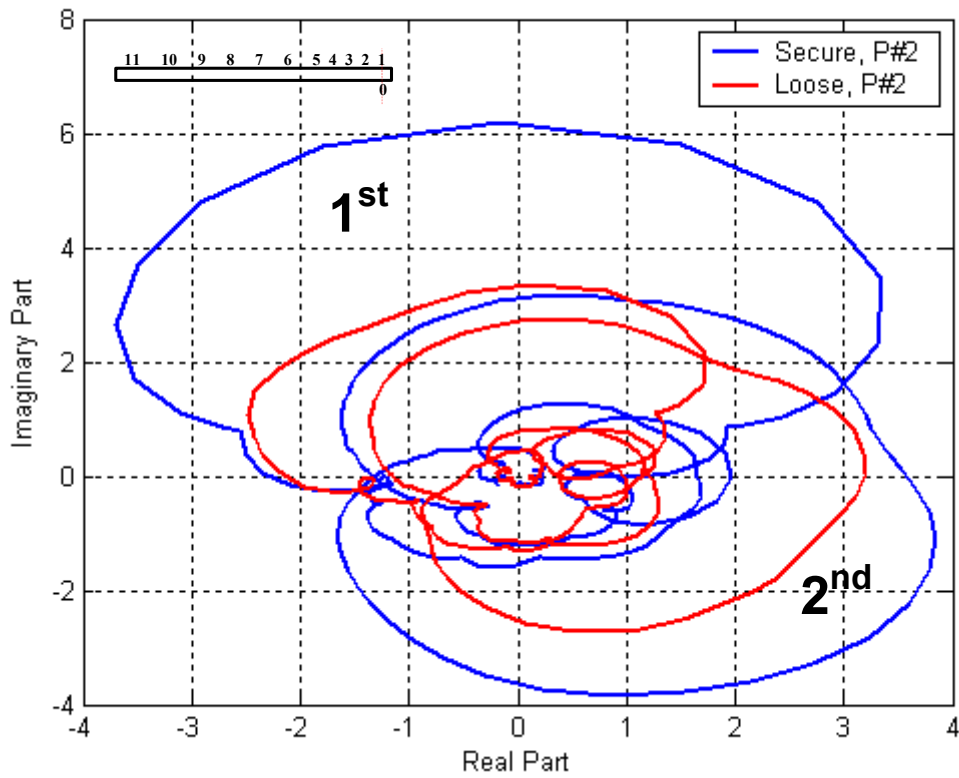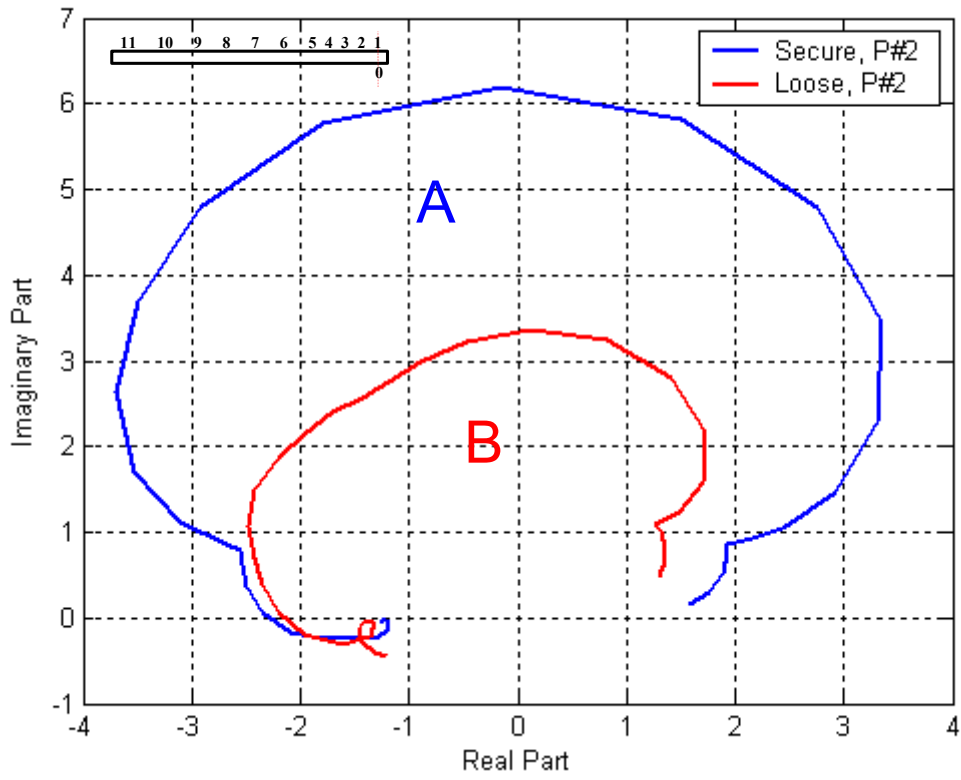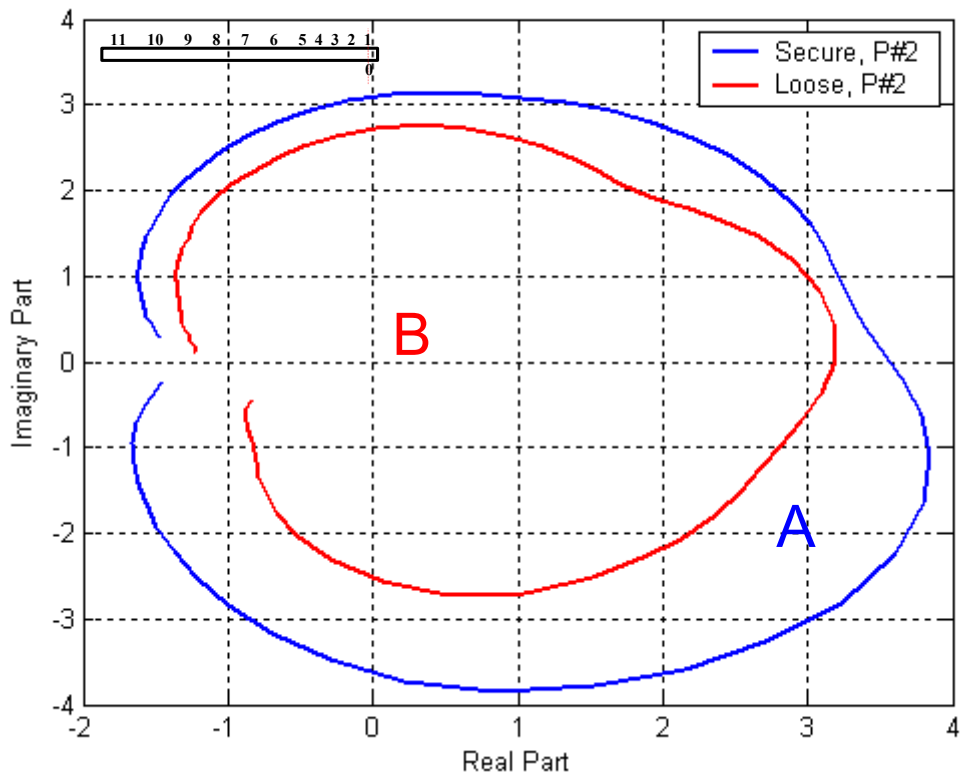

Fig. 4.41   2nd resonance distortions of FRF$_{20}$ due to loosening.

The effect of loosening on the FRF_{30} components can be seen in Figs. 4.39 and 4.40. The greatest reduction in the imaginary and real parts of FRF_{30} appeared on these Figures.

Figure 4.39 shows a reduction of 61.7 % at the 1st resonance frequency. Also new peaks appear at frequency of 5.4 kHz and the natural frequency is shifted to 5.7 kHz. The reduction at the 2nd natural frequency was found to be 61 % and the 2nd natural frequency is shifted to 11.7 kHz.

The gain of the FRF_{30} at 5.6 kHz becomes imaginary (compare Figs. 4.18 and 4.39).

Figure 4.40 displays the changes of the real part of the FRF_{30}. The greatest reduction of 63.4 % appears at frequency of 5.7 kHz.

The greatest reduction in the gain of the FRF30 will be clearly appeared in the Nyquist plot as given in Figs. 4.41 and 4.42.

Figure 4.41 documents the effect of loosening on the size of the Nyquist diagram. Shape **B** represents the relationship between the imaginary and real parts of the FRF_{30} (loose case) for frequency range of 5-6.5 kHz. Shape A represents the same relationship but for the secure case.

It is obvious that the loosening reduces the size of shape **A** to be small as shape **B**. This reduction in size for the base vector at the given frequency range indicates the existence of loosening in the system.

Also, Figure 4.42 represents the same relationship for the FRF_{30} for both secure and loose cases but for frequency range 10-12 kHz. It is clearly that the loosening reduces the size of the base vector (shape **A**) to be smaller as **B** as given in Fig. 4.42.
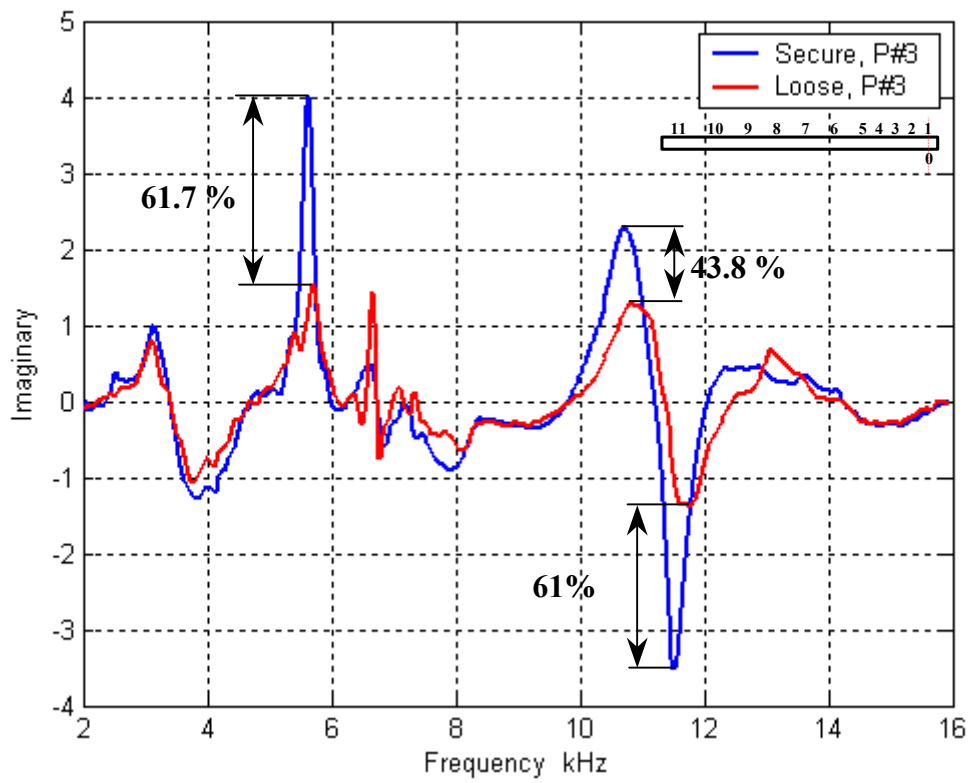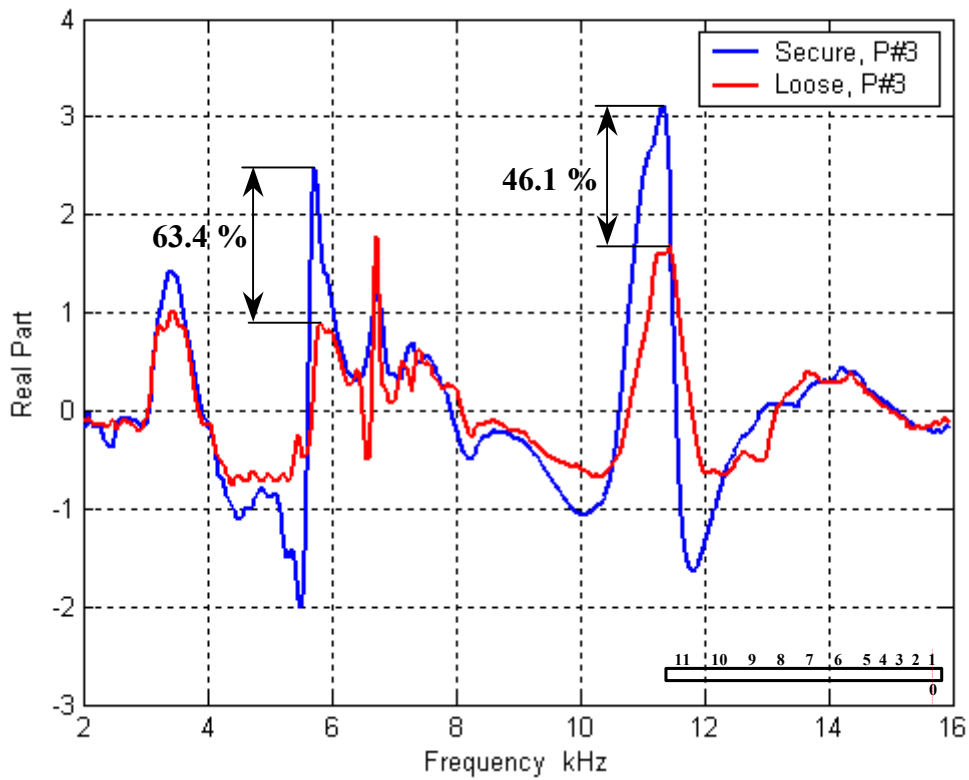
Fig. 4.39   Imaginary part error of FRF$_{30}$.
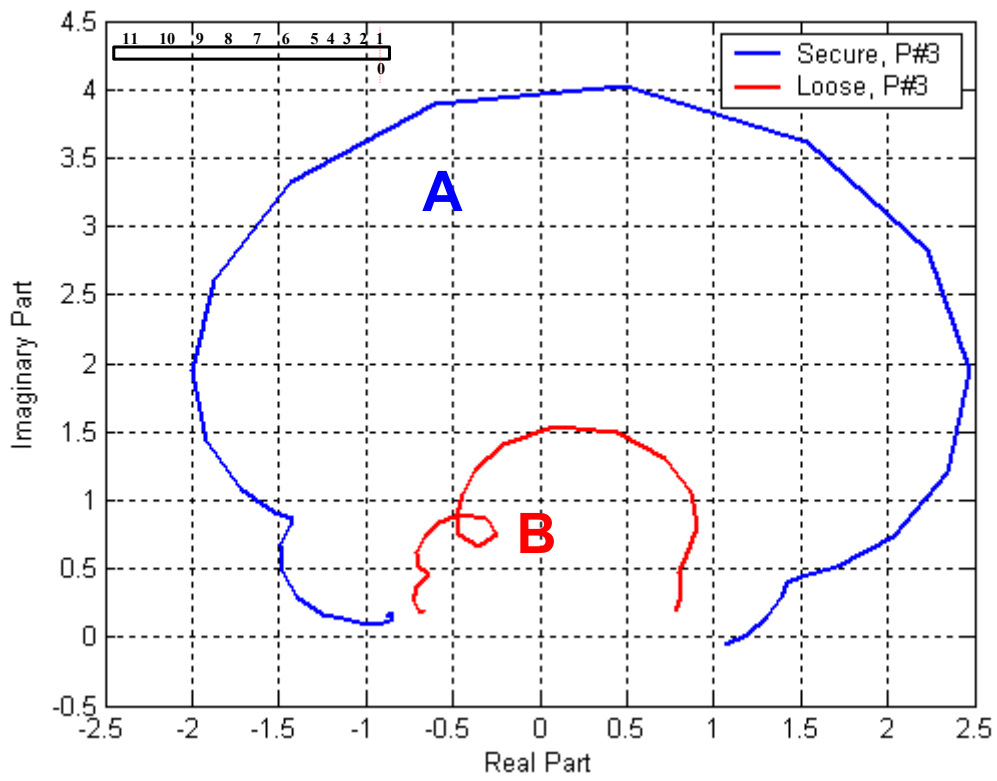

Fig. 4.40   Real part error of FRF$_{30}$.

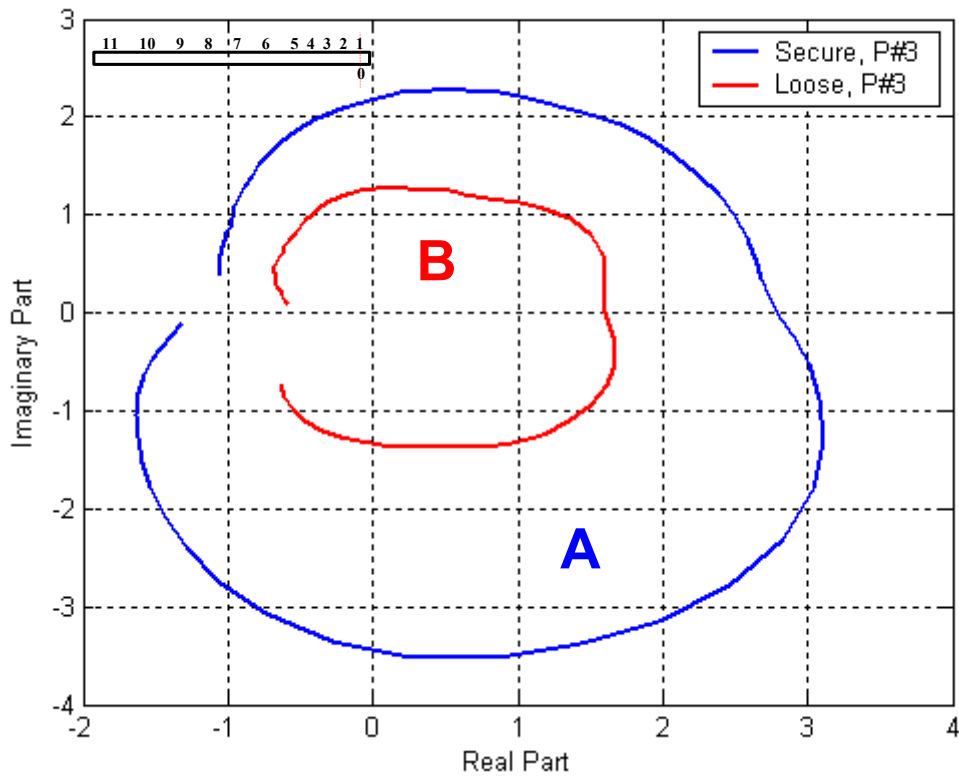Fig. 4.41   1st resonance distortions of FRF_{30} due to loosening.

Fig. 4.42   2nd resonance distortions of FRF_{30} due to loosening.

4.4 FIR-Filter Approximation

The effect of loosening on the system frequency response function was investigated in the previous sections. We have been found that the system's natural frequency of 5.6 kHz is very sensitive to loosening. The system's natural frequencies represent the roots of system's characteristics equation. This equation depends on the physical system itself not on the excitation force. The changes in the system parameters such as mass and stiffness resulted in changing of the natural frequencies.

According to Ref. [100], The damage produces a decrease in dynamic stiffness of the system, which can be determined by a finite element analysis. The matching between the measured FRF and the simulated one was used to extract the damage information (*IE*). In this thesis we will use the matching technique to extract the loosening information from the signal processing view point. The system is considered as a finite impulse response filter (FIR-Filter.) A MATLAB algorithm will do the matching between the FIR-filter and the measured FRF. The comparison between filter's impulse responses and consequently the filter's coefficients will give us the loosening information.

In this case the FIR-filter is considered as a replacement system for the real one. The experimental results in secure and loose cases are used to design the filter transfer function. Figure 4.43 shows the frequency response functions of the FIR-filter (replacement system) in comparison with the real system's frequency response functions for the $FRFs_{10}$. The FIR-filter approximation is found to be very closely to the measured $FRFs_{10}$ for both cases (secure and loose). To extract the loosening information from the FIR-filter, we need to know the filter's impulse response and the filter's coefficients. Figure 4.44 shows the comparison between FIR-filter's impulse response for secure and loose cases. The impulse response of the filter for secure case is greater than the FIR-filter impulse response in the loosening case. This is because of the filter's coefficient in the loosening case is lower than the filter's coefficients for the secure case, compare Figs. 4.45 and 4.46. The filter impulse response is symmetry about the time $t = 0$, which means that the resulted frequency response is exactly linear-phase as given in Fig. 4.44.

The reduction of the system stiffness may be contributed to the decreasing in the FIR-filter's coefficients as shown in Figs. 4.46.

Figure 4.47 reports the matching between the measured $FRFs_{20}$ and the Filter's $FRFs_{20}$ for both cases, secure and loosening. The filter approximation is fond to be very closely to the real system. The difference between the filter's impulse response (base vector) in secure case and the impulse response in the loosening case for the same filter (fault vector) is shown in Fig. 4.48. Figures 4.49 and 4.50 illustrate the changes of the filter's coefficients as a result of the decreasing of the systems stiffness (loosening).

The comparison between FIR-filter's coefficients for direct and indirect transmission mode (0-1 & 0-2) indicates that the indirect transmission mode 0-2 has the lowest filter coefficients. This means that the transmitted vibroacoustical energy in the 0-1 mode is greater than the transmitted energy for 0-2 mode.

Figure 4.51 shows the matching between the measured $FRFs_{30}$ and the filter's $FRFs_{30}$ for both case (secure and loose). The filters impulse response for mode 0-3 is given in Fig. 4.52. It is obvious that the loosed impulse response is lower than the secured impulse response. In order

to determine the effect of loosening on the system, the FIR-filter's coefficients must be compared to find the error between the base and the fault vectors. It is clearly that the filter's coefficient affected by the loosening (damage), compare Figs. 4.53 and 4.53.

Figure 4.55 documents the matching between the measured $FRFs_{40}$ and the Filter's $FRFs_{40}$ for secure and loose states. The filter's impulse response for both cases is given in Fig. 4.56. The loosening reduces the filter's coefficients as a result of the reduction in the transmitted vibroacoustical energy, compare Figs. 4.57 and 4.58.

Fig. 4.43 Matching between the measured $FRFs_{10}$ and FIR-Filter $FRFs_{10}$.

Fig. 4.44 FIR-Filter impulse responses for FRF_{10}.
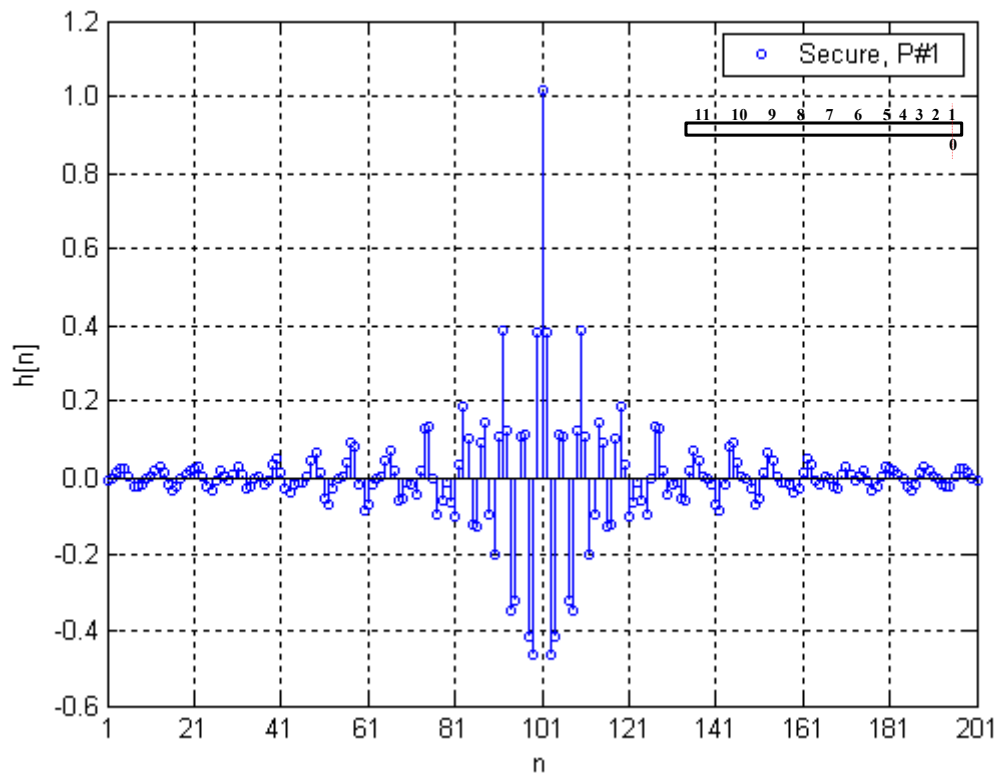
Fig.4.45   FIR-Filter coefficients before loosening for transmission mode 0-1.
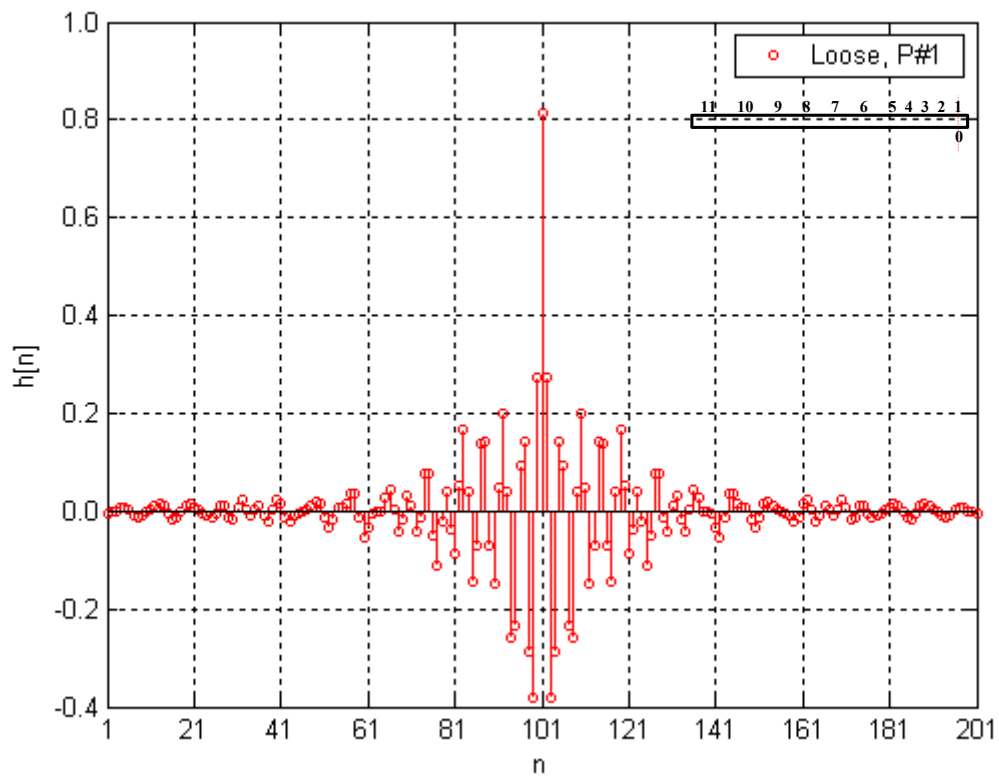
Fig.4.46   FIR-Filter coefficients after loosening transmission mode 0-1.
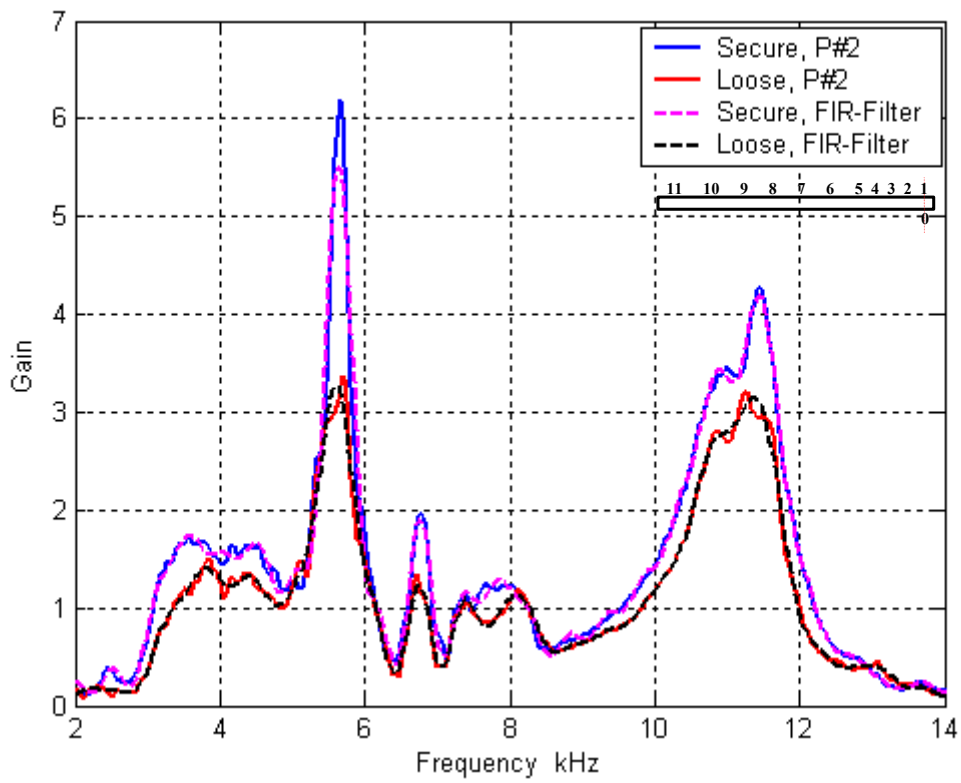
Fig. 4.47   Matching between the measured FRFs$_{20}$ and FIR-Filter FRFs$_{20}$.
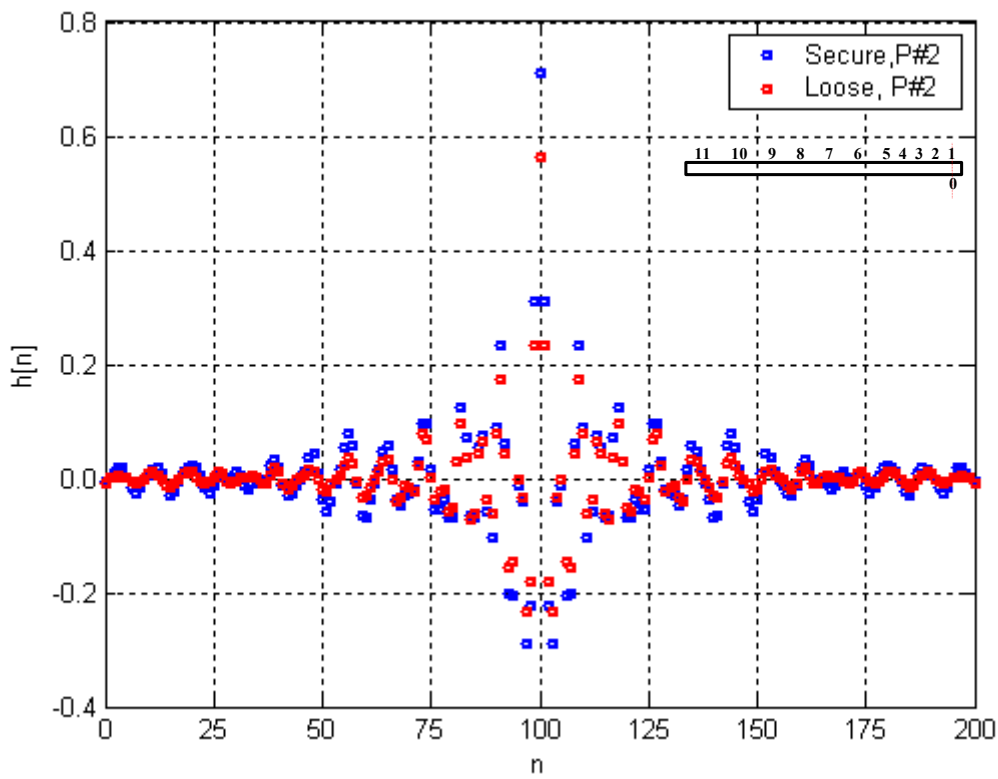
Fig. 4.48   FIR-Filter impulse response for FRF$_{20}$.
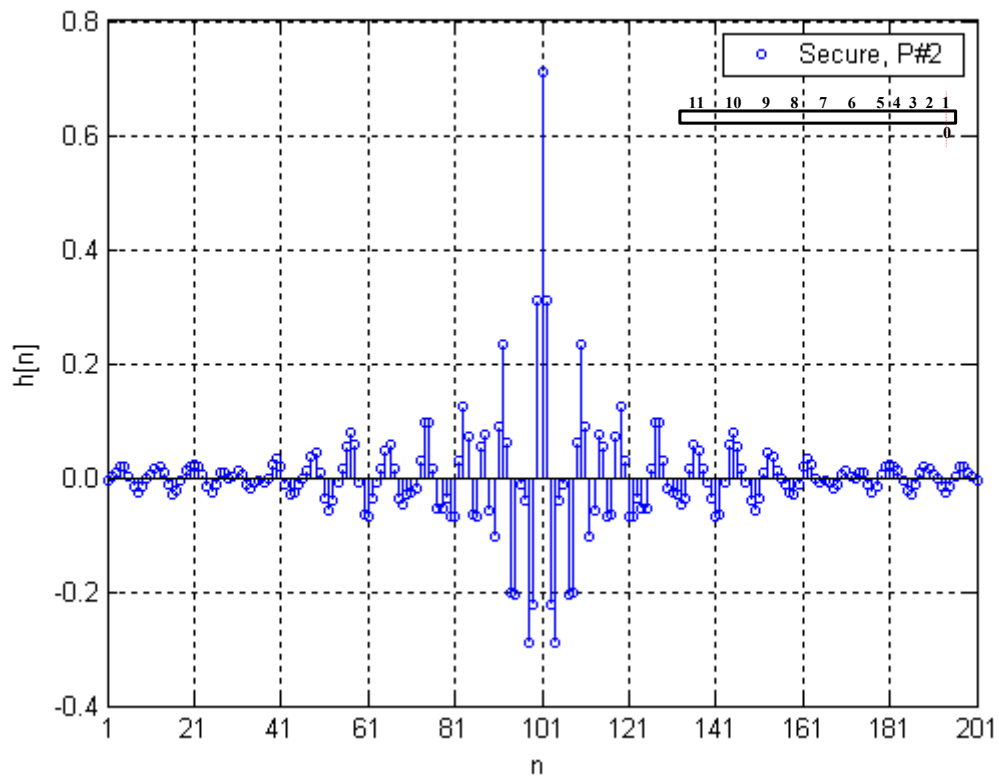
Fig.4.49   FIR-Filter coefficients before loosening for FRF_{20}.
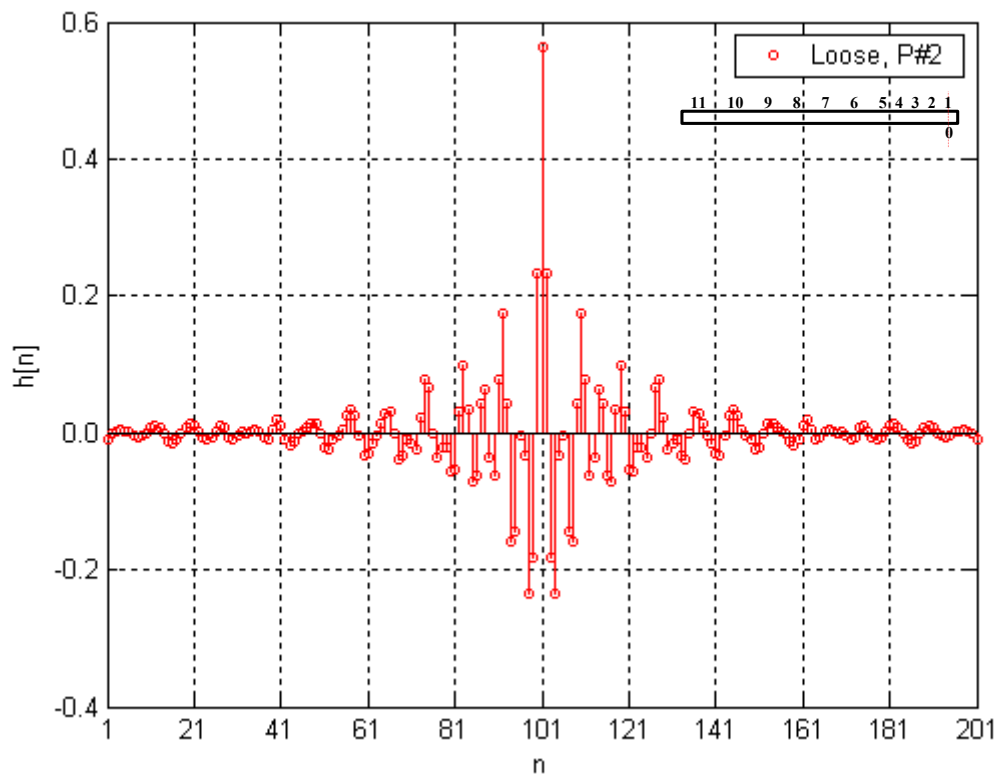
Fig.4.50   FIR-Filter coefficients after loosening for FRF_{20}.

98
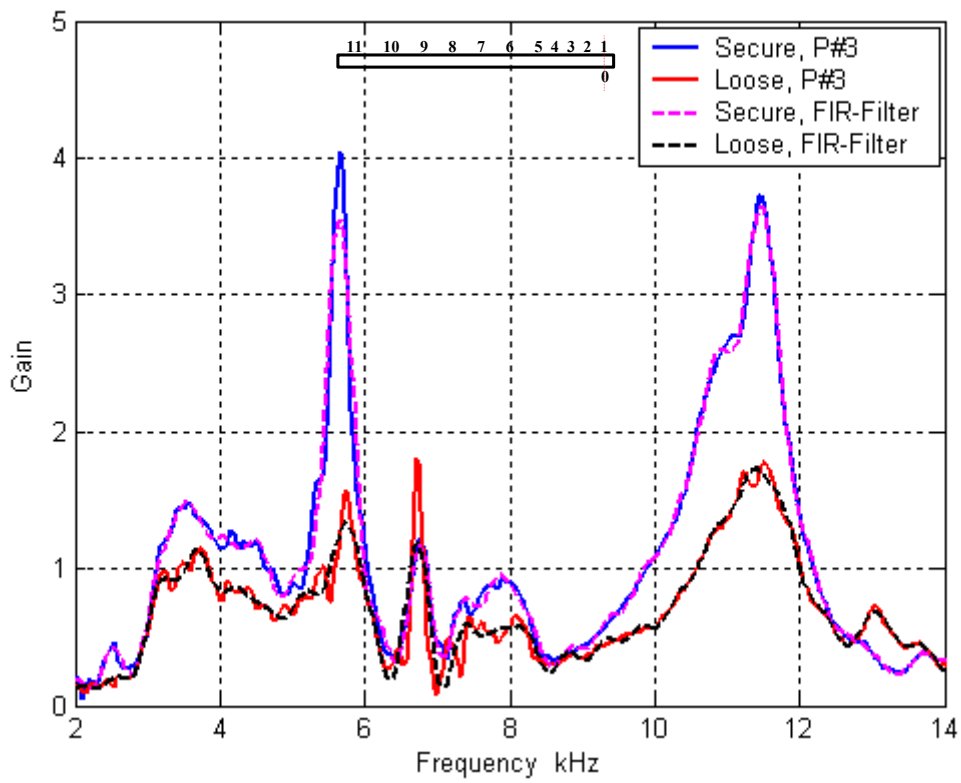
Fig. 4.51   Matching between the measured FRFs$_{30}$ and FIR-Filter FRFs$_{30}$.
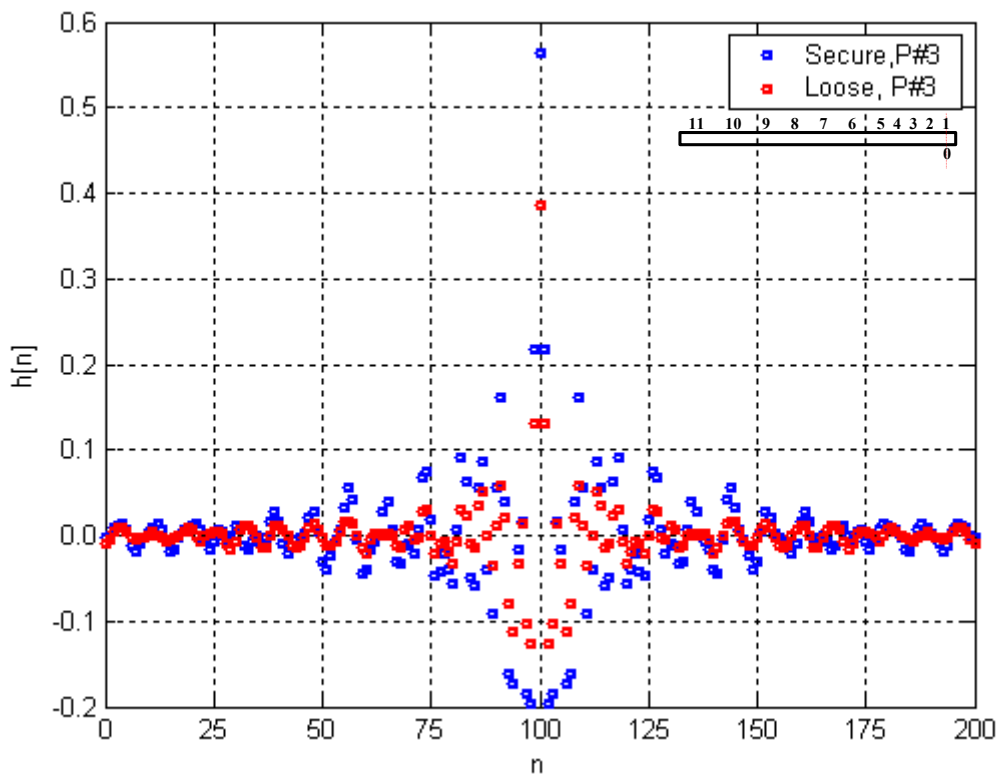
Fig. 4.52   FIR-Filter impulse response for FRF$_{30}$.
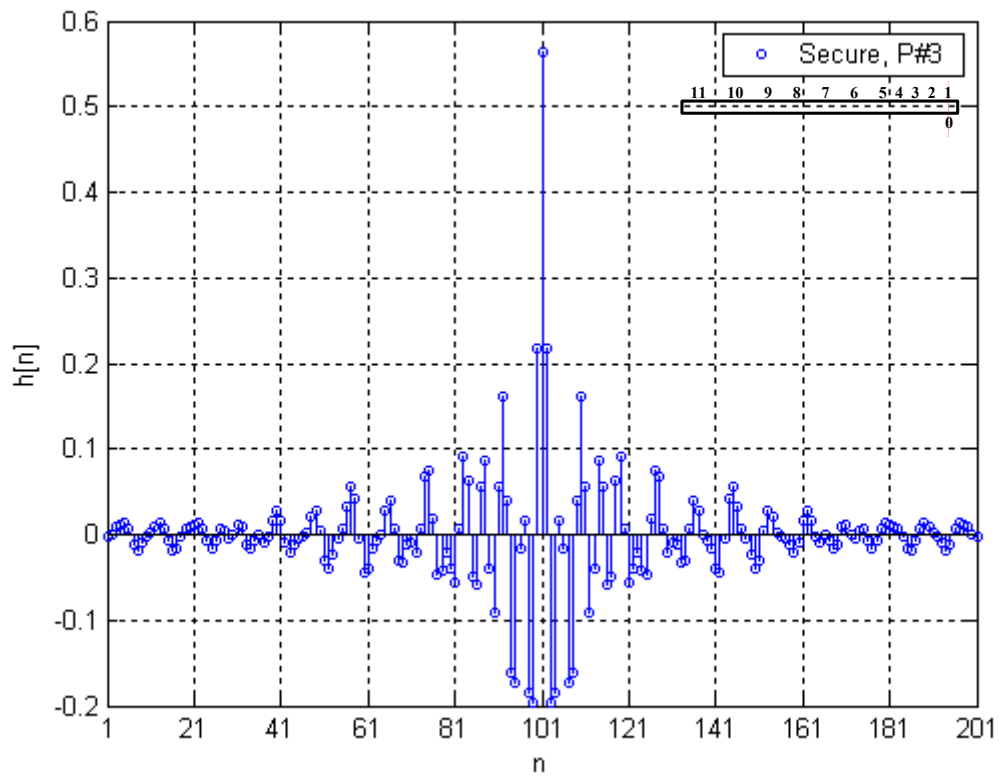
Fig.4.53　FIR-Filter coefficients before loosening for FRF_{30}.
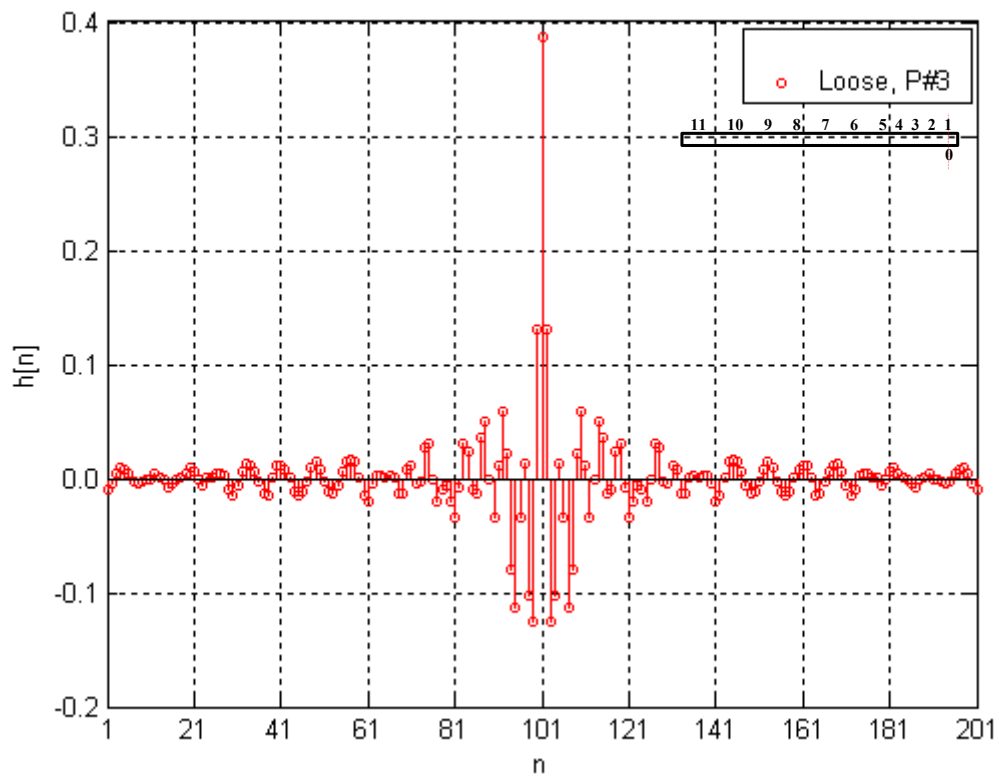
Fig.4.54　FIR-Filter coefficients after loosening for FRF_{30}.
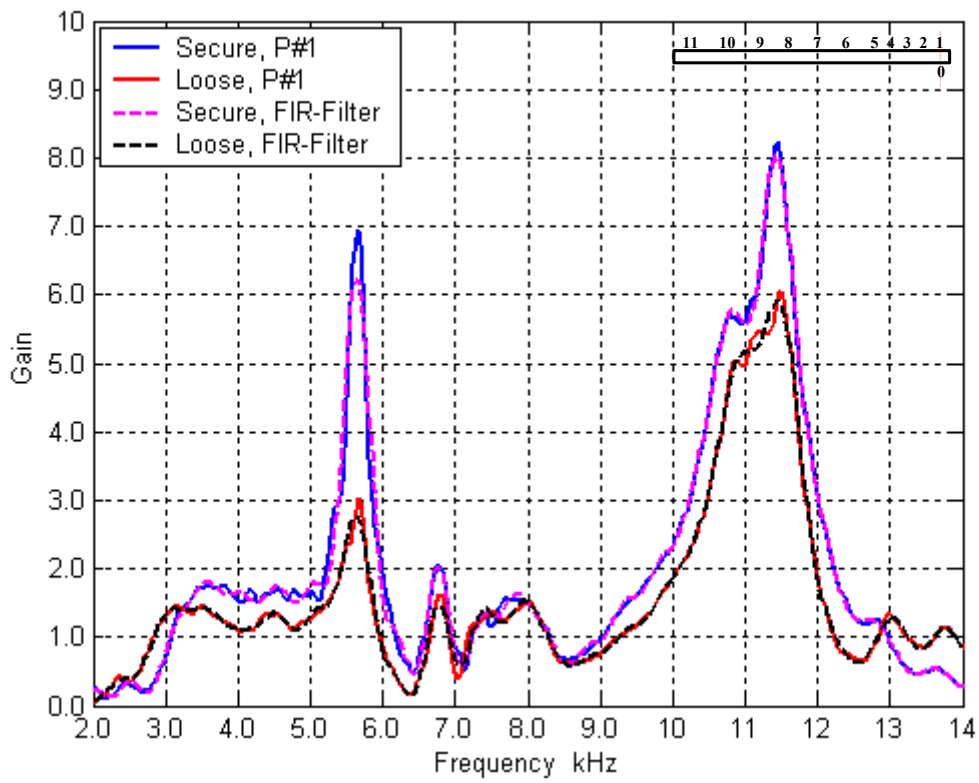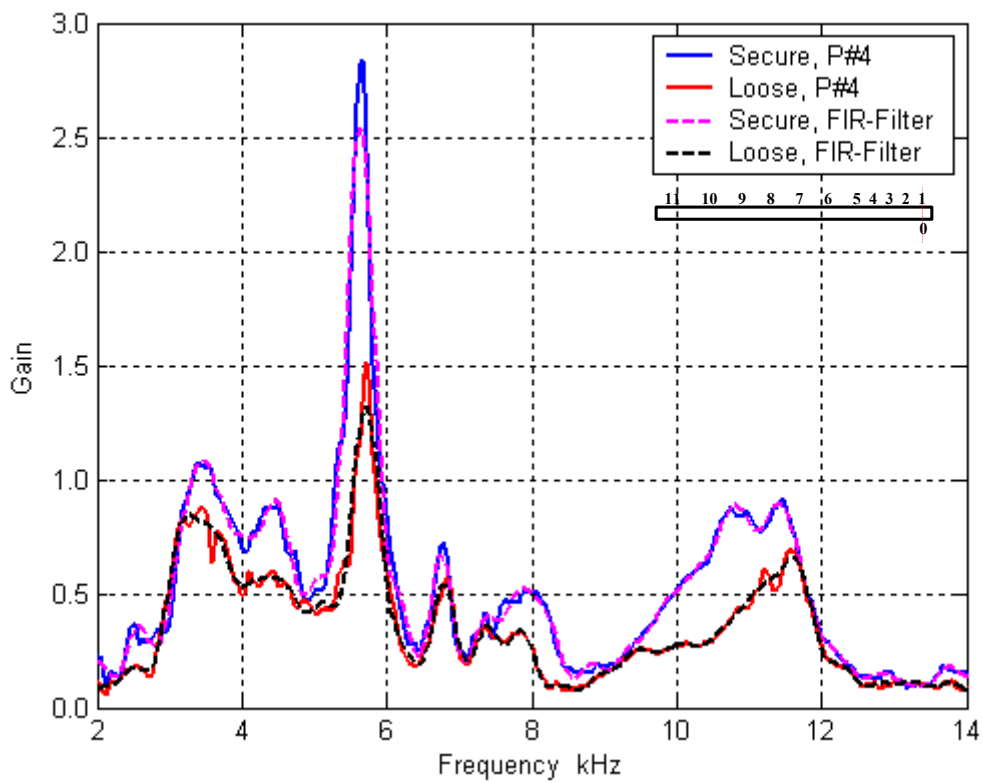
Fig. 4.55   Matching between the measured FRFs$_{40}$ and FIR-Filter FRFs$_{40}$.
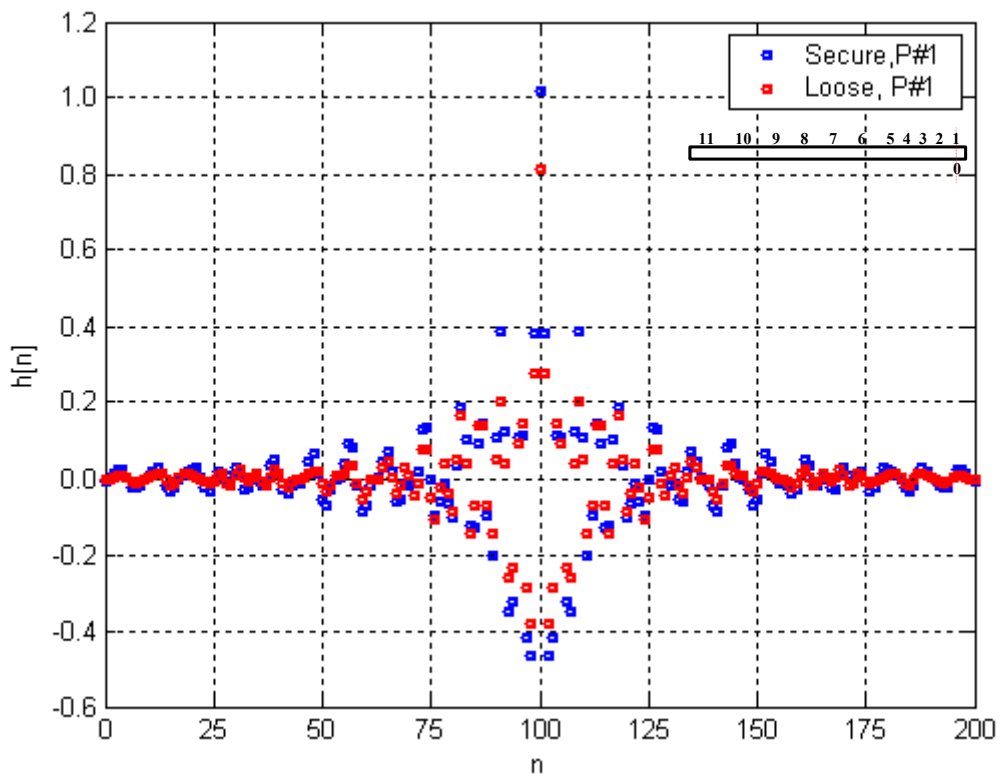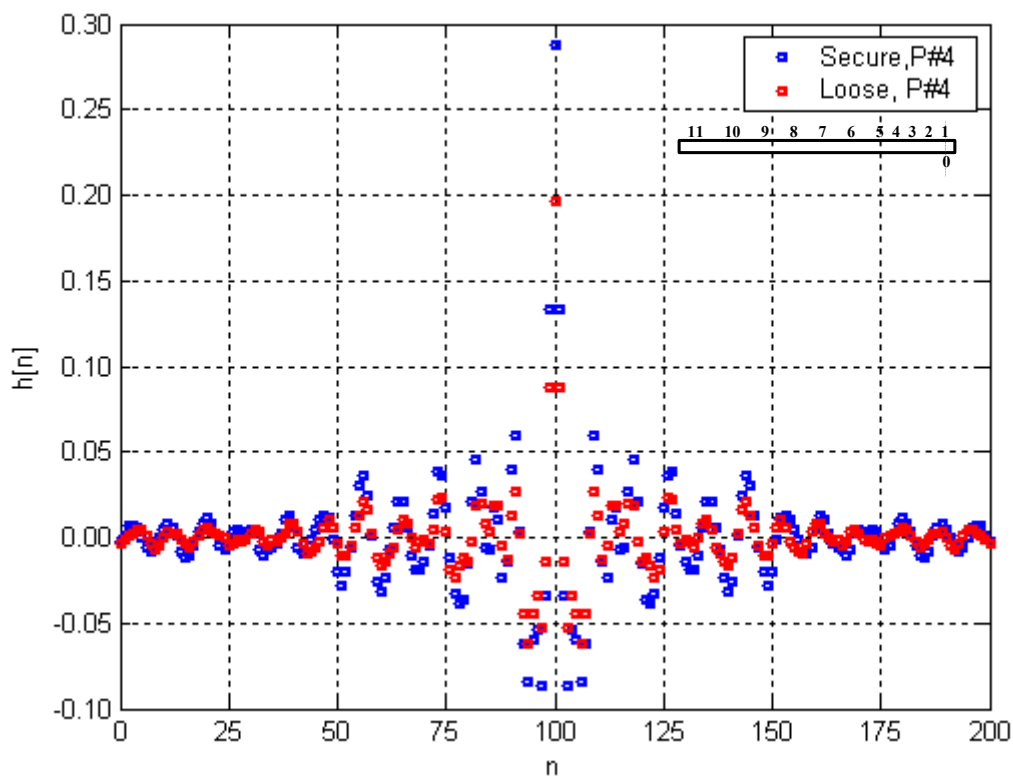

Fig. 4.56   FIR-Filter impulse response for FRF$_{40}$.
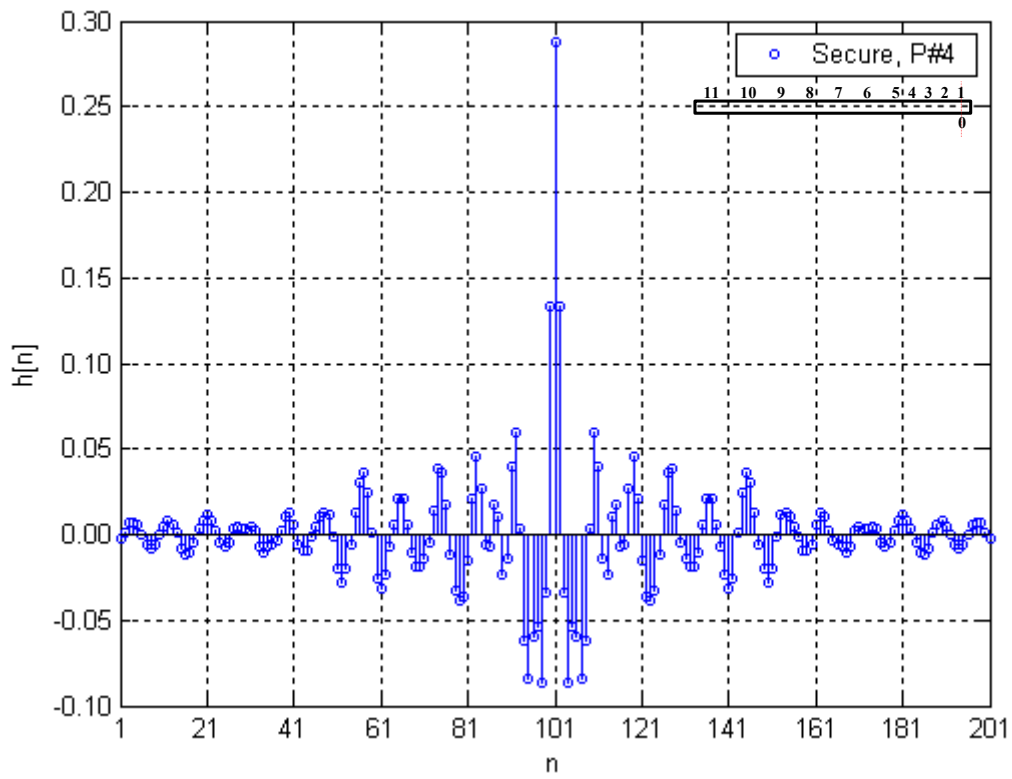
Fig.4.57 FIR-Filter coefficients before loosening for FRF_{40}.
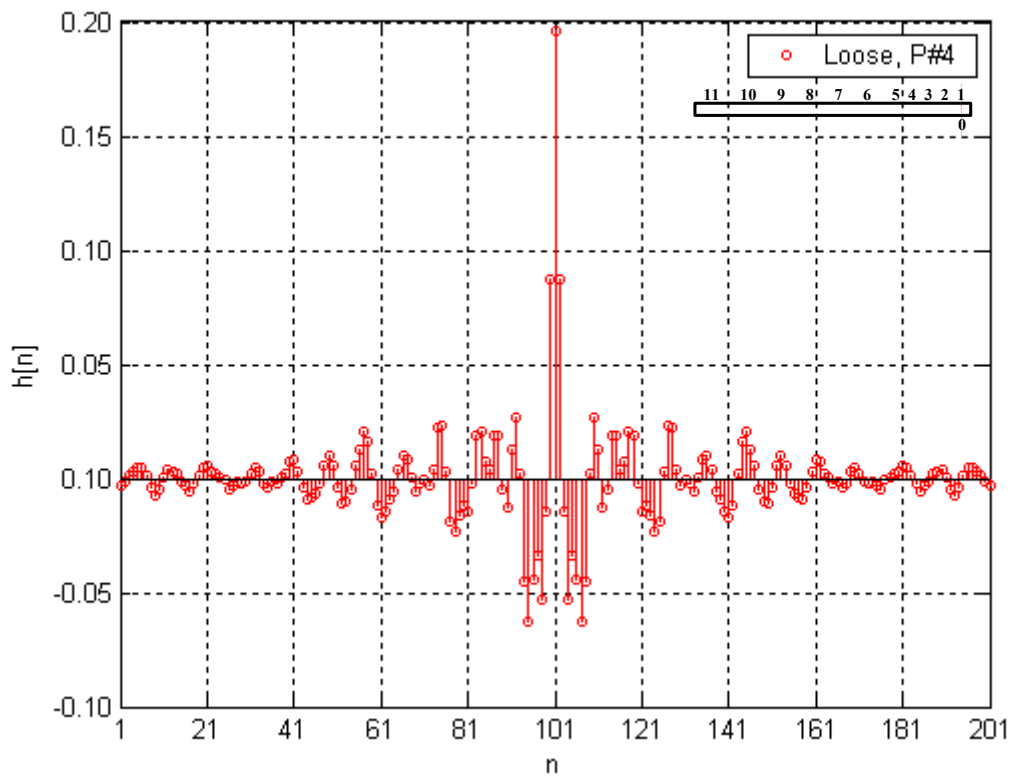
Fig.4.58 FIR-Filter coefficients after loosening for FRF_{40}.

102

4.5 Effect of Loosening Width

Surgeon consider the prosthesis is loosed if the radiolucent zone reaches 2 mm or more. The effect of loosening width on the dynamic characteristics of the system is investigated. The variation in loosening width is simulated by pushing the shaft for a certain distance to obtain a loosening width of 1.7 mm and 2.1 mm.

Figure 4.59 depicts the gain of the FRF_{10} for a loosening width of 0, 1.7 and 2.1 mm. Despite a new resonances are appeared, the shape of the curve is approximately unchanged. It is obvious that the 1st and the 2nd resonance are still lie at 5.6 kHz and 11.5 kHz, despite the changing in the width of loosening.

A new resonance are appeared at 5.4 kHz and 9.6 kHz for the loosening of 1.7 mm. An increase in the peaks of the 1st and the 2nd resonance is appeared.
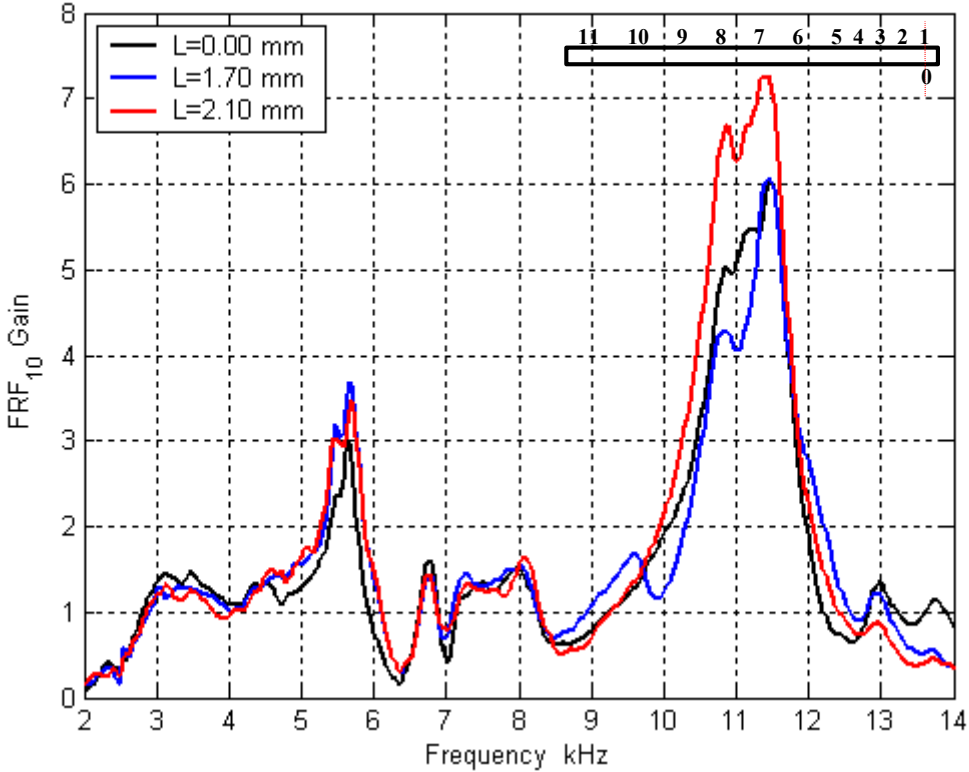
Fig. 4.59   Effect of loosening width on the dynamic characteristics of the system.

CHAPTER 5

CONCLUSIONS

The aim of the present research, is the development of a non-invasive analysis procedure based on a vibroacoustical techniques for extraction the loosening of the hip prosthesis. In this work the attention is focused on the experimental evaluation of the FRF, which can be used to study the system dynamic in secure and loose cases.

From the present work, the following conclusions can be abstracted:

1. The analysed results show that, the pulse excitation was in the considered frequency range.

2. Looking at the results, it is possible to state that the high frequency range is excited, even if the amplitude of the input decreases with the frequency.

3. It is clear that the loosening accelerate the decaying of the response of the system.

4. The choice of using the natural frequencies as a basis in the development of a non-invasive technique for hip prosthesis loosening is most attractive due to the fact that there is not a non-invasive method for detection the loosening of prostheses.

5. The magnitude of the results for the two analysis (secure & loose) are clearly different.

6. The loosening has its greatest influence on the resonance frequency of 5.6 kHz.

7. The loosening generates a new resonance peaks and consequently a new mode shape.

8. Nyquist plot is a very important diagnosis tool for the loosening.

9. A new method was developed to predict the loosening of the prosthesis with a FIR-Filter technique. The method calculates the filter coefficients in both intact (secure) and damage (loose) cases. The method calculate the FIR-Filter coefficients from the FRF of the real system.

10. The FRFs vectors are incorporation into a FIR-Filter framework for loosening detection problem.

11. The validity and capabilities of the FIR-Filter technique are demonstrated by in-vitro experiments.

12. It is useful to highlight that a novel algorithm (FIR-Filter) has good potential of applicability in experimental investigation of the loosening of the hip prosthesis.

13.   It has been shown that the loosening cause a significant changes in the FIR-Filter's coefficients.

14.   The methodology described here presents a new way to indirectly confirm the prosthesis loosening.

15.   FIR-Filter has been shown to have many potential advantages in prosthesis loosening.

16.   The achieved results by FIR-Filter are in complete agreement with other characterisation presented by FRF.

References

[1]   Egan, J. M. and Marsden, D. C., "A spring network model for the analysis of load transfer and tissue reactions in intra-medullary fixation," J. Clinical Biomechanics, Vol. 16, pp.71-79, 2001.

[2]   Pik Huiskes, "Biomechanics of Artificial-Joint Fixation," in Basic Orthopaedic Biomechanics, Van,C. M. and Wilson.C.H, New York, pp.375-442., 1991.

[3]   Grazier, K. L., Holbrook, T. L., Kelsey, J. L. and Stauffer, R. N., "The Frequency of occurrence, impact and cost of musculoskeletal conditions in the united states," chicago, AAOS Publ., 1984.

[4]   Concensus Development Panel, "Total hip replacement in the United State," Report of concensus conference, NIH, 1-3 March 1982, Bethesda, MD. JAMA, Vol. 248 No.15, pp.1817-1821, 1982.

[5]   http://www.nlm.nih.gov/medlineplus/ency/presentations/100006_1.htm

[6]   http://www.orthoassociates.com/Totalhip2.htm

[7]   Charnley, J., "Acrylic Cement in Orthopaedic Surgery," Edinburgh and London, E and S. Livingstone, 1970.

[8]   Charnley, J., "Low friction arthroplasty of the hip," New York Springer-Verlag 1978.

[9]   Walker, P. S., "Human joints and their artificial replacements," Spring field, III, Charles C. Thomas, 1977.

[10]   Geiman, L. M., Coleman, R. E. et al., "Radiography, Radionuclide Imaging and arthrography in the evaluation of total hip and knee replacement," J. Nucl. Med., Vol.128, pp.677-682, 1978.

[11]   Wirtz, D. Ch. Und Niethard, F. U., "Ursachen, Diagnostik und Therapie der aseptischen Hüftendoprothesenlockerung –eine Standortbestimmung," Z. Orthop., Band,153, Seiten,270-280, 1997.

[12]   Lewis, C. G., Jones, L. C. and Hungerford, D. S., " Effects of grafting on porous metal ingrowth. A canine model," J Arthroplasty, Vol.12, pp.451-460, 1997.

[13]   Dalton, J. E., Cook, S. D., et al., "The effect of operative fit and hydroxyapatite coating on the mechanical and biological response to porous implants," J. Bone and Joint Surg. Am, Vol.77, pp.97-110, 1995.

[14]   Davies, J.P. and Harris, W. H., "Tensile Bonding Strength of the Cement-Prosthesis interface," Orthopaedics, Vol.17, pp.171-173, 1994.

[15]   Keller, J. C., Lautenschlager, E.P., Marschall, G. W. and Mayer, P. R., "Factors Affecting Surgical Alloy/Bone Cement Interface Adhesion," J. Biomed. Mat. Res., Vol.14, pp.639-651, 1980.

[16]   Rabb, S., Ahmed, A. M. and Provan, J. W., "The quasitatic and fatigue performance of implant/bone cement interface," J. Biomed. Mat. Res., Vol.15, pp.159-182, 1981.

[17]   Currey, J. D., "Physical characteristics affecting the tensile failure properties of compact bone," J. Biomech, Vol.23, pp.837-844, 1990.

[18]   Eftekar, M. S., Doty, S. B., Johnston, A. D., and Parisien, M. V. 1985, "Prosthetic Synovitis," in, The Hip, R. H. Fitzgerald, ed., pp. 169-183. St. Louis, C. V. Mosby Co., 1985.

[19]   Goldring, S. R., Schiller, A. L., Roelke, M., Rourke, C. M., O'Neil, D. A., and Harris, W. H., "The synovial like membrane at the bone-cement interface in loose total hip replacements and its proposed role in bone lysis," J. Bone Joint Surg., 65A, pp. 575-583, 1983.

[20]   Moreland, J. R., "Mechanisms of failure in total knee arthroplasty," Clin. Orthp. Rel. Res., Vol.226, pp.49-57,.1988.

[21]   Radian, E. L., Rubin, C. T., Thransher, E. L., Lanyon, L. E., Crugnola, A. M., Schiller, A.S., Paul I.L., Rose, R. M., "Changes in the bone-cement interface after total hip replacement," J. Bone Joint Surg., Vol.64A, pp. 1188-1194, 1982.

[22]   Bos, I., Berner, J. und Löhrs, "Histologishe und morphometrische Untersuchungen an Femora mit stabilen Hüftgelenkendoprothesen. Eine autopsiestudie mit besonderer Berücksichtigung der zur Spätlockerung führenden Faktoren," Z. Orthop. Band. 133, S. 460-466, 1995.

[23]   Willert, H. G. Ludwig, J. and Semlitsch, M., "Reaction of bone to mythaacrylate after hip arthroplasty, a long-term gross, light microscopic, and scanning electron microscopy study," J. Bone Joint Surg., Vol.56-A, pp.1368-1382, 1974.

[24]   Ahmed, A. M., Raab, S., and Miller, J. E., "Metal-Cement Interface Strength in Cemented Stem Fixation," J. Orthop. Res., Vol.2, pp.105-118, 1984.

[25]   Gruen, T. A., McNeic, G. M., Amstutz, H. C., "Modes of Failure of Cemented Stem Type Femoral Components, A Radiographic Analysis of Loosening," Clin. Orthop. Rel. Res., Vol.141, pp.17-23, 1979

[26]   Johnston, R. C, "The Case for Cemented Hips," Iowa Orthop. J., No.6, pp. 60-64, 1987.

[27]   Krause, W. R., Krug, W., and Miller, J., "Strength of the Cement-Bone Interface," Clin. Orthop. Rel. Res. Vol.163, pp. 290-299, 1982.

[28]   Stauffer, R. N., "Ten-Year Follow-Up Study of Total Hip Replacement," J. Bone Joint Surg., Vol.64A, pp. 983-990, 1982

[29]   Perren, S. M., Ganz, R., and Rter, A., "oberflächliche Knochenresorption um Implantate," Med. Orthop. Tech., Vol.95, pp.6-10. 1975.

[30] Homsen, M., Görtz, A., et al., "Bending vibrations of femur and the oscillatory behavior of a cemented femoral hip endoprosthesis," J. Biomech. Engng., Vol. 122, Augst 2000.

[31] Ergmann, G., Graichen, F., and Rohlmann, A., "Hip loading during walking and running measured in two patients, " J. Biomech., Vol.26, pp. 969–990, 1993.

[32] Jörberg, B., Hansson, L. I., and Selvik, G., "Instability of total hip prostheses at rotational stress, " Acta Orthop. Scand., 55, pp. 504–506. 1984.

[33] Nägerl, H., Kubein-Meesenburg, D., Schäfer, W., Cotta, H., Thomson, M., v. Strachwitz, B., and Fanghänel, J., "Messung der räumlichen Mikrobewegung des Femurschaftes von Endoprothesen in Abhängigkeit des räumlichen Kraftsystems, " Z. Orthop., 134, pp. 99–110, 1996.

[32] Suguiyama, H., Whiteside, L. A., and Engh, C. A., "Torsional Fixation of the Femoral Component in Total Hip Arthroplasty, The Effect of Surgical Press-Fit Techniques, " Clin. Orthop. Relat. Res., 275, pp. 187–193. 1992.

[35] Schmalzried, T., Jasty, M. and Harris, W. H., "Preprosthetic bone loss in total hip arthroplasty. Polyethylene wear debris and the concept of the effective joint space," J. Bone Joint Surg., Vol.74-A, pp.849-863, 1992.

[36] Tallroth, K., Eskola, A. at al., "Aggressive granulomatous lesions after hip arthroplasty," J. Bone Joint Surg., Vol.71-B, pp.571-575, 1989.

[37] Vaes, G., "Ellular biology and biomechanical mechanism of bone resorption. A review of recent developments on the formation, activation, and mode of action of osteoclasts," Clin. Orthop. Vol.131, pp.239-271, 1988.

[38] Andrw, A. M. and Richard N. F., "Femoral component loosening after total hip arthroplasty," Clin. Orthp. Rel. Res., Vol.141, pp.66-70, 1979.

[39] Mjoberg, B., "Loosening of the cemented hip prosthesis, the importance of heat injury," Acta Orthop. Scand. Suppl. Vol.221, 1986.

[40] Willert, H.G., Ludwig, J., and Semlitsch, M., " Reaction of bone to methacrylate after hip arthroplasty," J. Bone Joint Surg., Vol.56A, pp.1368-1382, 1974.

[41] Wroblewski, B. M., "Wear and loosening of the socket in the charnely low-friction arthroplasty," Orthop. Clin. North Am., Vol.19, pp.627-630, 1988.

[42] Poss, R., Staehlin, P., and Larson, M, "Femoral expansion in the presence of total hip arthroplasty," J. Arthroplasty, Vol.2, pp.259-264, 1987.

[43] James SP., jasty, M., Davies J., Piehler H., Harris WH., "A fractographic investigation of PMMA bone cement focusing on the relationship between porosity reduction and increased fatigue life," J. Biomed. Mater. Res., Vol.26, pp. 651-662, 1992.

[44] Ahnfelt, L., Herberts, P., Malchau, H., and Andersson, G.B.J., "Prognosis of total hip replacement," Acta Orthop. Scand. Suppl., Vol.238, 1990.

[45]   Herberts, P., Ahnfelt, L., Malchau, H., Stromberg, C., and Andersson, G. B. J.,
       "Multicenter clinical trials and their value in assessing total joint arthroplasty," Clin.
       Orthop. Rel. Res. Vol.249, pp. 48-55. 1989.

[46]   Knutsen, K., Lindstrand, A., and Lidgern, L., "Survival of knee arthroplasties . A
       nation-wide multicentre," J. Bone Joint Surg., Vol.62B, pp.795-802, 1986

[47]   Kendall, G. M., Darby, S. C., Harries, S. U. and Rae, S., "A frequency srvey of
       radiological examination carried out in national health service hospitals in great
       britainin June 1977 for Dagnostic Purposes," NRPB eport, R 104, Idcot, Oxon,B,
       1980.

[48]   International Atomic Energy Agency, "International basic safety standard for
       protection against ionising radiation and for the safety of radiation sources," Intern
       publication, ienna, IAEA, 1994.

[49]   Anomohanran, O., Mokobia, C. E., Osakwa, R. A. O. and Wawe, M. O., "A Survey of
       X-ray diagnostic services in delta state, Nigeria 1991-1994," J. Radiol. Prot., Vol.22,
       No.1, pp.71-78, 2002.

[50]   Brian, R. J. W., Robert, E. M., Gwo-Jaw, W., Charles, W. M., Teates, C. D. and
       Sturat, T. B., "Radionuclide bone imaging as a means of differentiating loosening and
       infection in patients with a painful total hip prosthesis," J. Nuclear Medicine, Vol.133,
       Dec., pp.723-726, 1979.

[51]   Bauer, G. C. H, Lindberg, L., Naversten, Y., et al, "85Sr radionuclide scintimetry in
       infected total hip arthroplasty," Acta. Orthop. Scand., Vol.44, pp.439-450, 1973.

[52]   Creutzig, H, "Bone imaging after total replacement arthroplasty of the hip joint. A
       follow-up with different radiopharmaceuticals," Eur. J. Nucl. Med., Vol.1, pp.177-
       180, Aug.1976.

[53]   Feith, R., Slooff, T., Kazem, I., et al, "Strontium 87mSr bone scanning for the
       evaluation of total hip replacement," J. Bone Joint surg. [Br], Vol.58, pp.79-83,
       Feb.1976.

[54]   Campeau, R. J., Hall, M. F., Miale, A. Jr., " Detection of total hip arthroplasty
       complication with Tc-99m Pyrophosphate," J. Nucl. Med., Vol.17, pp.526, Jun. 1976.

[55]   Gelman, M. I., Coleman, R. E., Stevens, P. M., et al, " Radiography, radionuclide
       imaging, and arthrography in the evaluation of total hip and knee replacement,"
       Radiology, Vol.128, pp.677-682, Sept.1978.

[56]   Mclnerney, D. P., Hyde, I. D., "Technetium [99]Tcm pyrophosphate scaning in the
       assessment of the painful hip prosthesis," Clin. Radiol., Vol.29, pp.513-517, Sept.
       1978.

[57]   Williams, E. D., Tregonning, R. J., Hurley, P. J., "[99]Tcm –diphosphonate scanning as
       an aid to diagnosis of infection in total hip joint replacemens," Br. J. Radiol., Vol.50,
       pp.562-566, 1977.

[58] Weiss, P. E., Mall, J. C., Hoffer, P. B., Murray, W. R., Rodrigo, J. J. and Genant, H. K. "^{99m}Tc-Methylene Diphosphonate Imaging in the Evaluation of Total Hip Prostheses," J. Nuclear Medicine, Vol.133, December, pp.727-730, 1979.

[59] Richin, P. F., Harris, D. R. et al., "Differential bone scanning," Bull. Hosp. Joint Dis., Vol.37, pp. 149-158, 1976.

[60] Reing, M., Richin, P. F., et al., "Differential bone-scanning in the evaluation of a painful total joint replacement," J. Bone and Joint Surg., Vol.61-A, No.6, pp. 933-936, 1979.

[61] Eskridge, J. M, Becker, G. J., Rabe, F. H., Holden, R. W., Klatt, E. C., "Digital vascular imaging, practical aspects," Radiology, Vol.148, pp.703-705, 1983.

[62] Mistretta, C. A., Crummy, A. B., Strother, C. M., "Digital angiography, a perspective," Radiology, Vol.139, pp.273-276, 1981

[63] Newberg, A. H. and Wetzner, M. S., " Digital subtraction arthrography," J. Radiology, Vol.154, No.1, pp.238-239, 1985.

[64] Ginai, A.Z., Biezen, van F.C., Kint, P.A.M., Oei, H.Y., and Hop, W.C.J., "Digital subtraction arthrography in preoperative evaluation of painful total hip arthroplasty," Skeletal Radiol, Vol.25 No.4, pp. 25,357–363, 1996.

[65] Ghelman, B., Freiberger, R. H., "The adult hip," In: Freiberger R.H., Kaye JJ eds Arthrography. New York, Appleton-Century-Crofts, 1979, 189.

[66] Kilcoyne RF, Kaplan P., "The lateral approach for hip arthrography," Skeletal Radiol, Vol.21, pp. 239–240, 1992.

[67] De Lee JG, Charnley J., "Radiological demarcation of cemented sockets in total hip replacement," Clin Orthop, Vol.121, pp. 20–32, 1976.

[68] Lyons CW, Berquist TH, Lyons JC, Rand JA, Brown ML., "Evaluation of radiographic findings in painful hip arthroplasties," Clin Orthop, Vol.195, pp. 239–251, 1985.

[69] Johnston RC, Fitzgerald RH, Harris WH, Müller ME, Sledge CB., "Clinical and radiographic evaluation of total hip replacement," J Bone Joint Surg Am, Vol.72, pp.161–168, 1990.

[70] Hendrix RW, McAnderson T., "Arthrographic and radiologic evaluation of prosthetic joints," Radiol. Clin. North Am, Vol.2, pp. 349–364, 1981.

[71] Wejkner B, Wiege M., "Correlation between radiologic and clinical findings in Charnley total hip replacement," A 10-year follow-up study. Acta Radiol., Vol.28, pp. 607–613, 1987.

[72] Guercio N, Orsini G, Broggi S, Pasche-ro B., "Arthrography of the prosthesetized painful hip, the importance of imaging and functional testing," Ital J Ort-hop Traumatol, Vol.16, pp. 93–101, 1990.

[73]   Holder, L. E., "Radionuclide bone-imaging in the evaluation of bone pain," J Bone Joint Surg. Am, Vol.64, pp.1391–1396, 1982.

[74]   Freiberger RH., "Evaluation of hip prostheses by imaging methods," Semin Roentgenol, Vol. 21, pp. 20–28, 1986.

[75]   Jasty M, Maloney WJ, Bragdon CR, et al., "Histomorphological studies of the long-term skeletal responses to well fixed cemented femoral components," J Bone Joint Surg., 72, 1220–1225, 1990.

[76]   Apple JS, Robers L, Gamba J, Marti-nez S, Khoury M, Ford K., "Digital subtraction arthrography of the prosthetic hip," South Med. J., Vol.79, pp. 808–810, 1986.

[77]   Davies, J.P., Tse, M-K and Harris, W. H., "In vitro evaluation of bonding of the cement-metal interface of a total hip femoral component using ultrasound," J. Orthop. Res., Vol.13, No.3, pp. 335-338, 1995.

[78]   O`Neill, D. A. and Harris, W. H, "Failed Total Hip Replacement, Assessment by Plain Radiographs, Arthrograms, and Aspiration of the Hip Joint," J. Bone Joint Surg., Vol.66-A, No.4, pp.540-546, 1984.

[79]   Kühen, von J. H., Wirth, C. J., Refior, H. J., Moser, E. und Hergeth, K., "Szintigraphische Verläufe und röntgenologische Befunde nach zementfreier Implantation des PM-Schaftes im Rahmen der Hüftgelenksalloarthroplastik," Z. Forschr. Röntgenstr., Band: 153, Heft: 4, Seiten: 442-450, 1990.

[80]   Bettin, D. und Katthagen, B.-D., "Die DGOT-Klassifikation von Knochendefekten bei Hüfttotalendoprothesen-Revisionsoperationen," Z. Orthop., Band: 135, Seiten: 281-284, 1997.

[81]   J.Krautkramer and H.Krautkramer, Ultrasonic Testing of materials, G.Allen &Unwin, 1969.

[82]   Halmshaw, R. "Non-destructive testing" London, Edward Arnold, 1987

[83]   Graff, K. F. "Wave motion in elastic solid". Dover Publications Inc., New York, 1973.

[84]   Achenbach, J. D. "Wave propagation in elastic solid" North Holland, Amsterdam, 1973

[85]   Brehovskikh, L.M. " Waves in layered medial". 2 nd edition, Translated by Robert, T. Beyer, Academic Press Inc., 1980.

[86]   Cawley, P. and Lowe, M. J. S "The application of plane wave techniques for inspection of adhesive and diffusion bonded joints" Non-destructive evaluation, Vol.13, pp.185-199, 1994.

[87]   Tucker, D. G. and Gazey, B. K. " Applied underwater acoustics". Pergamon Press, 1965.

[88]   Thomson, W.T. " Transmission of elastic wave through a stratified solid medium". J. Applied Physics, Vol. 21, pp.89-93, 1960.

[89]   Thomson, W.T. " The equivalent circuit for the transmission of plane elastic waves through a pate at oblique incidence". Applied Physics, Vol. 21, pp.1215-1217, 1950.

[90]   Mayer, W. G. " Mode conversion of ultrasonic wave at flat boundaries". IEEE Trans. On Sonics and Ultrasonics, SU-11, pp. 1-3, 1964.

[91]   Kendal and Tabor, An ultrasonic study of the contact between stationary and sliding surfaces, Proceeding of the royal Society, Vol.A323, pp.321-340, 1971.

[92]   Tattersall, H. G., The ultrasonic pulse-ecoh technique as applied to adhesion testing, J.of Applied Physics D, Vol.6, pp.819-832, 1973.

[93]   Baik, J. M. and R. B. Thompson, Ultrasonic Scattering from imperfect surfaces: a quasi-static model, J. non-destructive Evaluation, Vol.4, pp.177-196, 1984.

[94]   Abdalla, M., Grigoriadis, K.M., Zimmerman, D.C. " Enhanced damaged detection using linear matrix inequalities", Proceedings of the 16th International Modal Analysis Conference, Santa Barbara, CA, pp. 144–150. , 1998.

[95]   Pandey, A.K. and Biswas, M. "Damage detection in structures using changes in flexibility ". *Journal of Sound and Vibration* 169 (1994), pp. 3–17.

[96]   Hajela, P. and Soeiro, F.J. " Structural damage detection based on static and modal analysis". *American Institute of Aeronautics and Astronautics Journal* 28 6, pp. 1110–1115, 1990.

[97]   Smith, S.W. " Iterative matrix approximation for model updating ". *Mechanical Systems and Signal Processing* 12, No.1, pp. 187–201, 1998.

[98]   Lew, J.S. " Using transfer function parameter changes for damage detection of structures". *American Institute of Aeronautics and Astronautics Journal,* Vol.33, No.11, pp. 2189–2193, 1995.

[99]   Li, D., Zheng, Z., He, K. and Wang, B. " Damage detection in offshore structures by the FRF method". Proceedings of the International Offshore Mechanics and Arctic Engineering, Calgary, Vol. 1, Part B, pp. 601–604, 1992.

[100]   Hwang, H.Y. and Kim, C. "Damage detection in structures using a few frequency response measurements". J. Sound and Vibration, Vol.270, pp. 1-14,2004.

[101]   Jahn, H.A. " Improvement of an approximate set of latent roots and modal columns of a matrix by methods akin to those of classical perturbation theory". *Quarterly Journal of Mechanics and Applied Mathematics*, Vol. 1, pp. 132–144, 1948.

[102]   Fox, R.L. and Kapoor, M.P. " Rates of change of eigenvalues and eigenvectors". *American Institute of Aeronautics and Astronautics Journal*, Vol. 6, pp. 426–2429, 1968.

[103]   Lin, R.M. and Lim, M.K. " Derivation of structural design sensitivities from vibration test data". *Journal of Sound and Vibration*, Vol. 201, pp. 613–631, 1997.

[104] Vanhonacker, P. " Differential and difference sensitivities of natural frequencies and mode shapes of mechanical structures". *American Institute of Aeronautics and Astronautics Journal*, Vol. 18, pp. 1511–1514, 1980.

[105] Belle, H.V. " Higher order sensitivities in structural systems". *American Institute of Aeronautics and Astronautics Journal*, Vol. 20, pp. 286–288, 1982.

[106] Liu, A.Q., Lim, S.P. and Liew, K.M. " Sensitivity analysis of complex dynamic system modelling". *JSME*, Vol. 36, pp. 209–213, 1993.

[107] Qu, Z.-Q. " Hybrid expansion method for frequency responses and their sensitivities, Part I: Undamped systems". *Journal of Sound and Vibration*, Vol. 231, pp. 175–193, 2000.

[108] Qu, Z.-Q. and Selvam, R.P. " Hybrid expansion method for frequency responses and their sensitivities, Part II: Viscously damped systems". *Journal of Sound and Vibration*, Vol. 238, pp. 369–388, 2000.

[109] Yang, C., Adams, D.E., Yoo, S.-W and Kim, H.-J. An embedded sensitivity approach for diagnosing system-level vibration problems. J. Sound and Vibration V269, pp. 1063-1081, 2004.

[110] Dale W. Fitting and Laszlo Adler, Ultrasonic spectral analysis for nondestructive evaluation. plenum press, New York, ISBN 0-306-40484-2, 1981.

[111] Ewins, D.J."*Modal Testing: Theory and Practice*". Research Studies Press, Letchworth, Hertfordshire, England. 1984.

[112] Senf, B. und Strobel, H., Verfahren zur Bestimmung von Übertragungsfunktionen linearer Systeme aus gemessenen Werten des Frequenzgangs, Zmsr, Band.4, H.10, S. 411-420, 1961.

[113] Dudnikow, E. E., Bestimmung der Koeffizienten von Übertragungsfunktionen linearer System aus dem Anfangsabschnitt gemessener Frequenzgänge. (Russ) Avtomatika i Tele-mechanika, Vol.20, No.5, pp. 576-582, 1959.

[114] Strobel, H., Zur Frage des Wesentlichen Frequenzbereiches bei der Approximation gemessener Frequenzgänge, Zmsr, Band.7, H.1, S. 19-23, 1964.

[115] Ward Heylen, Stefan Lammens and Paul Sas, Modal Analysis Theory and Testing, Katholieke Universiteit Leuven, © 1997.

[116] Nuno Maia, Julio Silva, Theoretical and Experimental Modal Analysis, Research Studies Press LTD., ©1997.

[117] Steve Goldman, Vibration spectrum analysis: A practical approach, Industrial Press Inc., © 1991.

[118] Steven W. Smith Digital processing A practical guide for engineers and scientists, EIsevier, 2003.

[119] Maurice Bellanger, Digital processing of signals: theory and practice, 2nd edition, Wiley & Sons, 1984.

[120] Dietrich Schlichthärle, Digital filters basic and design, Springer-Verlag, 2000

[121] Roland Best, Digitale Signalverarbeitung und-Simulation, Band 2, AT Verlag Aarau, 1991.

[122] DIN EN 61212 (VDE 0319).

Lebenslauf

Persönliche Daten

Name	Ayman El-Sayed Eshra
Geburtsdatum	4 Juli 1967
Geburtsort	El-Zarka, Damiette - Ägypten
Staatsangehörigkeit	Ägypter
Familienstand	Verheiratet mit 3 Kindern

Schulischer Werdegang

1972-1978	Grundschule in El-Zarka
1978-1981	Vorschule in El-Zarka
1981-1984	Gymnasium in El-Zarka
1984	Abitur in El-Zarka

Studium

1984-1989	Maschinenbau an der Universität Minia-Ägypten Studienschwerpunkt Design –und Konstruktionstechnik

Studienabschluss

1989	B. Sc. Maschinenbau an der Universität Minia
1995	M. Sc. Maschinenbau an der Universität Minia
1989-1990	Wehrdienst

Praktika

1985	Werkstatt Training, Maschinenbau an der Universität Minia
1986	Technische Zeichen, Maschinenbau an der Universität Minia
1987	El-Zarka Reis Fabrik

Berufstätigkeit

1990-1999	Wissenschaftlicher Mitarbeiter an der Universität Minia-Ägypten
1999-2000	Als Stipendiat am Institut für Biomedizinische Technik und Krankenhaustechnik, Medizinische Hochschule Hannover
seit 02.2000	Als Stipendiat am Institut für Mess– und Regelungstechnik an der Universität Hannover